ABSTRACT

Title of Dissertation: SURFACE ENHANCED RAMAN SPECTROSCOPY TECHNOLOGIES AND TECHNIQUES FOR ON-SITE QUANTIFICATION OF CHEMICAL AND BIOLOGICAL ANALYTES

Stephen M Restaino
Doctor of Philosophy, 2017

Dissertation directed by: Professor Ian M White
Department of Bioengineering

The rapid advancement in mobile devices has illustrated the widening technological gap in health and environmental sensing. Unfortunately, the time and financial burdens imposed by the current central lab model prohibit regular sensing of crucial biological and ecological elements, which can lead to delayed responses and exacerbated conditions. Current portable diagnostic solutions lack the necessary sensitivity or multiplexing potential to address the ever-expanding library of biomarkers. An emerging solution known as surface enhanced Raman spectroscopy (SERS) can provide the sensitivity of current techniques, but with drastically improved multiplexing density. Many existing SERS applications however, require multiple processing steps to introduce samples to the enhancement surface. Practical application of SERS to diagnostics and environmental samples requires more convenient materials and methods to support the broad array of conditions in on-site sensing. In this work, three new

methods to apply SERS to portable sensing systems are developed. Specifically, a new SERS diagnostic is presented that details the first implementation of SERS for real-time PCR; we accomplished multiplexed detection of MRSA genes to specifically identify species and drug resistance. Second, we developed a new flexible SERS sponge based on PDMS that provides unprecedented control over sample handling and can readily concentration organic analytes. Finally, we present a novel raster scanning protocol to address the persistent reproducibility issues that has slowed commercialization of new SERS devices. Together, these three techniques advance the development SERS as a practical and portable solution for on-site diagnostics and environmental sensing.

DEVELOPMENT OF IMPROVED SURFACE ENHANCED RAMAN SPECTROSCOPY TECHNOLOGIES AND TECHNIQUES FOR PORTABLE BIOSENSING

Stephen Mario Restaino

Dissertation submitted to the Faculty of the Graduate School of the
University of Maryland, College Park in partial fulfillment
of the requirements for the degree of
Doctor of Philosophy
2017

Advisory Committee

Professor Ian M White, Committee Chair

Professor Jason Kahn
Professor Zhihong Nie
Professor Gregory Payne
Professor Srinivasa Raghavan

© Copywrite by
Stephen M Restaino
2017

Acknowledgements

This effort was supported by a number of people, without whom none of this work would have been possible.

Adam Berger provided immeasurable support to this process. He provided text, experiments, figures, and ideas to Chapters 3-5. This work would certainly not have been possible without his unmatched work ethic and unending supply of terrible puns.

The current graduate students of the White Lab John Goertz, Imaly Nanayakkara, Hieu Nguyen, Alessandra Zimmermann, provided thoughts, ideas, and support throughout this work. They each provided text and ideas to Chapter 2, for which I am incredibly grateful. I would especially like to thank Imaly and Alessandra for their dedicated support on experiments that, unfortunately, did not make it into this work.

Former graduate students of the White lab, Kunal Pandit, Eric Hoppmann, Veemoon Yu, Soroush Yazdi, Sean Virgile laid the foundation for this work. Especially the SERS work by Veemoon, Eric, and Soroush.

Current and former undergraduate students of the White Lab provided thoughts, ideas, and experimental support. I would especially like to thank Adriel Sumathipala for the discussions on science and SERS that inspired Chapter 5.

My advisor Ian White, provided thoughts, ideas, and guidance throughout every step of this work. I am eternally grateful for your patience and dedication. My approach in critically evaluating science and life will be forever shaped through our discussions.

My committee who generously agreed to spend precious time providing feedback to improve my ideas, experiments, and scientific understanding. I would especially like to acknowledge Dr. Jason Kahn for his ideas and discussions on Chapter 3.

My family and friends, provided the love and support that were the foundation that enabled this effort. I especially need to acknowledge my wife, Lauren, whose love and unending patience enabled the long days and late nights spent in the lab. I would not have made it through this difficult process without you. I love you.

Finally, I would be remiss if I did not acknowledge the sources of funding that drove this work. In particular, the National Science Foundation, Diagnostic AnSERS, and the Intelligence Advanced Research Projects Agency for their financial support.

Table of Contents

List of Figures vi
List of Tables xii
List of Abbreviations xiii
Chapter 1. Introduction 1
Chapter 2. Molecular diagnostics and Raman spectroscopy 5
2.1 Molecular diagnostics 5
2.2 Classical molecular amplification 6
2.3 Isothermal nucleic acid amplification 9
2.3.1 Loop-mediated isothermal amplification (LAMP) 10
2.3.2 Nuclease driven amplification 11
2.3.3 Protein guided duplex opening 13
2.4 Raman spectroscopy 15
2.4.1 Raman scattering 15
2.4.2 Surface enhancement 18
2.4.3 SERS sensors 21
2.4.3.1 Colloidal SERS 21
2.4.3.2 Rigid SERS Sensors 23
2.4.3.3 Flexible SERS Sensors 25
2.4.3.4 Variance and ambiguity in SERS data 28
2.5 SERS in molecular diagnostics 30
Chapter 3. Real-time PCR using Surface Enhanced Raman Spectroscopy in a thermoplastic chip 34
3.1 Introduction 34
3.2 Materials and Methods 37
3.2.1 Materials 37
3.2.2 Device Fabrication 38
3.2.3 Nanoparticle synthesis 39
3.2.4 Experimental setup 40

3.2.5 Thermodynamic Modelling 42
3.2.6 PCR Reactions 43
3.3 Results 45
3.4 Discussion 53
3.5 Conclusion 57
Chapter 4. Integrated concentration, handling, and detection of organic analytes in a sponge-like PDMS matrix with Surface Enhanced Raman Spectroscopy 58
4.1 Introduction 58
4.2 Materials and Methods 62
4.2.1 Materials 62
4.2.2 Nanoparticle Synthesis 63
4.2.3 PDMS Sponge Fabrication 63
4.2.4 Selective Absorption Characterization 65
4.2.5 PDMS Sponge Decoration for SERS 65
4.2.6 SERS Measurements 66
4.2.7 SERS data analysis 68
4.2.8 Concentrating of organic analytes with PDMS Sponges 69
4.3 Results 71
4.4 Discussion 78
4.5 Conclusion 83
Chapter 5. Addressing variance and ambiguity in SERS through optimized sampling methods 84
5.1 Introduction 84
5.2 Materials and Methods 88
5.2.1 Materials 88
5.2.2 Sensor Fabrication 89
5.2.3 Raman spectrometry 90
5.3 Results 93
5.3.1 Number of Spots 94

5.3.2 Spot selection criteria 96
5.3.3 Langmuir Fit 99
5.4 Discussion 101
5.5 Conclusion 104
Chapter 6. Conclusion 106
6.1 Summary of findings 106
6.2 Contributions to the field and potential impact 109
6.3 Future work 112
Bibliography 117

List of Figures

Figure 2.1: Illustration of an Enzyme Linked Immunoassay (ELISA). A: Presentation antibody binding sites immobilized on a surface. B: Specific analyte binding to antibodies and subsequent washing to remove other sample components. C: Binding of a detection antibody to a second epitope on the analyte, subsequent steps wash unbound detection antibodies and introduce a chromophore that is acted upon by the attached enzyme. 7

Figure 2.2: Illustration of PCR amplification mechanism. A: Amplification steps beginning with hybridized template or amplicons melted at high temperatures, rapid transition to low temperatures allows small primers to bind and be extended by TAQ polymerase. B: Illustration of the exponential product formation rate (2^n) in PCR. 8

Figure 2.3: Jablonski energy diagram. A: Energy transfer for Rayleigh (elastic) scattering. B: Energy loss (hv_v) in Raman (inelastic) scattering. C: Electronic transition and energy loss in resonance Raman scattering. 16

Figure 2.4: Raman (surface enhanced) spectrum of R6G and attributions of peak intensities to individual and cooperative molecular structures.[38] 17

Figure 2.5: Nanoscale shape dependence of electromagnetic enhancement intensity. (Reproduced from Haes et al.[50]) 20

Figure 2.6: Nanotriangles and nanostars are a representative subset of the possible complex shapes available in colloidal SERS. (Reproduced from Abalde-Cela et al.[71]) 23

Figure 2.7: Shape complexity and regularity in rigid SERS sensors.(Reproduced from Cinel et al.[92]) 25

Figure 2.8: Nanoparticle distribution and functional properties of paper based SERS sensors. (Reproduced from Left: Yu and White 2010[104]; Right: Yu and White 2013[109]) 27

Figure 2.9: Variation in shape, size, and enhancement factor of deposited nanoparticle aggregates. (Reproduced from Laurence et al.[120]) 29

Figure 2.10: Demonstration of the potential for SERS to enable highly multiplexed molecular assays. (Reproduced from Cao et al.[132]) 31

Figure 2.11: Example of PCR product separation and SERS analysis. (Reproduced from Hoppmann et al.[108]) 32

Figure 3.1: Photograph and Illustration of Dialysis driven SERS-PCR device. A: Photograph of device taken shows AgNP colloid above a PCR solution. Chip is pictured after thermocycling. B: Schematic of device function during a probe based qPCR assay, in which a dye is liberated and passes through pores to the AgNP colloid for SERS detection. 36

Figure 3.2: Schematic of device construction and use. A: Fabrication pathway of SERS-PCR devices. Laser cutting (i) is used to prepare device layers that are thermally bonded(ii) with a dialysis membrane between the bottom and middle layers; the device is sealed (iii) with an adhesive polymer film. B: Device preparation for PCR involves a simple three step process of adding the sample and nanoparticles to the respective inlet (i), sealing the device with an optically clear adhesive film (ii) and finally thermocycling under a portable Raman probe. 39

Figure 3.3: Illustration of device setup and estimated thermal profile during PCR. A: PCR/Raman control system including a surface mounted thermocouple that feeds data to a microcontroller connected to a LabVIEW interface to synchronize temperature and spectrometer control. B: Thermal profile estimated through a COMSOL FEM model. Three points were chosen to highlight the produced temperature gradient. (A) (B) and (C) represent the bottom, middle and top of the PCR well respectively. 42

Figure 3.4: Evaluation of potential PCR inhibitors. A: PCR run off-chip to evaluate inhibition by the dialysis membrane (n=3 for samples with and without the membrane). B: Spermine inhibition of PCR at concentrations only above the on-chip assay concentration of 1mM (n=1 for each concentration). C: PAGE separation of PCR reactants (i) and products (ii & iii) in the presence of the dialysis membrane. Diminishing intensity of the probe band (d) indicates successful digestion during amplification. 46

Figure 3.5: SERS spectra collected from pre-cycled PCR samples added to the SERS-PCR chip. A: Cy3 signal development over time from diffusion of the pre-amplified FemA gene. B: Blank signal from FemA PCR mixture without pre-cycling and with no added MRSA genome. C: R6G signal development over time from diffusion of the pre-amplified MecA gene. B and C: I_{1400} and I_{1515} represent the intensity of the peak for quantification of signal intensity from Cy3 and R6G respectively. D: Overlapped spectra from degraded FemA (Cy3) and MecA (R6G) highlighting distinct peaks..... 49

Figure 3.6: Temperature dependent diffusion rate of degraded MecA probe (R6G) into the SERS well. A: Average (n=3) signal generation profile of dye transfer across the embedded dialysis membrane at 95°C (red), 67°C (green), and 55°C (cyan). B: Calculated diffusion rate (linear fit slope) plotted versus temperature..... 50

Figure 3.7: Real-time and quantitative data for SERS-PCR. A: Averaged data for increasing concentration of MRSA genome amplified in a PCR reaction on chip and quantified with SERS. Concentrations tested were $5x10^7$ (n=3), $5x10^6$ (n=4), $5x10^5$ (n=5), and a negative (0 copy) control (n=3). B: Cycle threshold (Ct) calculated as the first intensity value to surpass the calculated noise level defined as the mean plus the ten times the standard deviation of the first 15 cycles. C: Peak height from A (I_{1515}) normalized to a control point (I_{1400}). D: Ct values calculated from normalized data in C; threshold was defined as a ratio of 1.0. 51

Figure 3.8: Multiplexed detection of MecA and FemA MRSA genes with SERS. A: Peak ratio for identification of R6G (MecA). B: Peak ratio for identification of Cy3 (FemA). A & B: light, medium, and dark grey indicate MecA primers only, MecA & FemB primers only, and FemA primers only..... 52

Figure 4.1: Photograph of SERS sponge fabrication process and flexibility. A: fabrication of SERS sponge beginning with the sugar cube template, curing and removal of sugar to form the PMS sponge, and finally decoration with nanoparticles to produce the final SERS sponge sensor. B: Compression of SERS sponge with forceps to illustrate high flexibility and shape conformability of SERS sponges..... 61

Figure 4.2: Illustration of stepwise SERS sponge fabrication process. A: Process of PDMS sponge fabrication: PDMS preparation, vacuum aided PDMS perfusion of sugar cube pores, heat curing of PDMS, bisection and cylindrical coring for the final sensor shape. B: Process of nanoparticle decoration from a concentration AgNP colloid: surfactant treatment and two nanoparticle submersion steps each separated by a heated dry. 64

Figure 4.3: Illustration of data collection and analysis process. A: Raster pattern with highlighted movement path (Red) in a predefined spiral path (blue). B: Heat map demonstrating Raman intensity across a sensor surface based on a sample R6G concentration (10 μM); pixels are colored based on the intensity visible in plot C. C: Full spectra for data visible in plot B. D: Isolation of peak value at 1515cm^{-1}, used for quantification of R6G concentration. 68

Figure 4.4: Photographs of phase preference for modified and unmodified sponges. A,B,&E: Specific uptake of organic phase (decanol, yellow) over aqueous phases (blue) in an unmodified PDMS sponge. C&D: Mixed and individual uptake of both organic and aqueous phases in a surfactant modified PDMS sponge. F: Ejection of absorbed liquid via sponge compression..... 72

Figure 4.5: Extraction of an organic analyte (R6G) with a PDMS sponge. A: Image of sponge within a 1mL syringe. B: Images of sponges through which an increasing volume of R6G was forced through with a syringe. C: Background subtracted red channel of the image in B. D: Quantified pixel intensity as the average of the sponge area in C. 74

Figure 4.6: Illustration and data of phase based separation of organic analytes with PDMS sponges. A: Illustration of concentration process: decanol is loaded into sponges, which are then added to a sample solution containing either R6G (100 nM) or cPyrene (1 μM), after 90 minutes sponges are removed from the sample and fluorescence was recorded through UV transillumination. B: Quantified fluorescence intensity of dyes concentrated into sponges (Sample) and related concentrations of dyes. 75

Figure 4.7: Scanning electron micrographs of nanoparticle decoration on SERS sponges. A: View (80x) of SERS sponges with lighter areas indicating silver nanoparticle deposits. B-C: Views (320x) of SERS sponges. D: EDS data superimposed on image C. Red color represents the presence of silver. These confirm the lighter areas as AgNPs. E: Photograph of nanoparticle decorated SERS sponge. 77

Figure 4.8: SERS sponge data summarizes detection and quantification of three model analytes: R6G, Malachite green, and Pyrene. A-C: SERS data collected via Raster scanning of sponge surfaces. Various concentrations were tested for each analyte. (i) Average spectra for 3 sensors at all tested concentrations. Blue highlighted area represents the peak chosen for quantification of signal intensity. I_{1515} for R6G, I_{1125} for MG, and I_{1245} for cPyrene. (ii) Zoomed view of data from (i). (iii) Concentration vs. Intensity plot based showing mean and standard deviation of the calculated mean peak intensity for each dye. A: Data collected from R6G samples, spectra labeled a-h represent averaged data from 10, 5, 1, 0.5, 0.1, 0.05, 0.01 and 0 μM R6G respectively. B: Data collected from MG samples, spectra labeled as a-g represent averaged data from 10, 5, 1, 0.5, 0.1, 0.025, and 0 μM respectively. C: Data collected from cPyrene samples, spectra labeled as a-e represent averaged data from 100, 50, 25, 5, and 0 μM respectively. 78

Figure 5.1: Illustration of Raster data collection and spot selection. A: Raster process in which motors are actuated in a cartesian coordinate system to move the Raman probe and SERS sensor independently, forming a spiral pattern. B: Example of 3 out 6 spot selection methods. Top, middle, and bottom, represent RS, RSS, and LSS respectively. 92

Figure 5.2: Data summary for 200 spots obtained from each of 3 sensors over 8 R6G concentrations. A & B: colors represent each of 3 sensors. Horizontal colored lines of each color represent the intra-sensor mean intensity for each sensor. Horizontal black and grey lines represent inter-sensor mean and standard deviation respectively. A: Peak intensity (Raman Shift: 1515cm^{-1}) values for background subtracted spectra plotted on a log scale. B: Peak intensity normalized to the inter-sensor mean for each concentration. 93

Figure 5.3: Change in concentration dependent Raman intensities based on number of spots selected via RS (random) sampling. A: Signal change over 200 independent spot selection sets, with sample spot numbers increasing from 1-200 respectively.. B: Signal variability over 50 indpendent spot selection sets with spot numbers increasing from 1 to 50 respectively. Subplots i-iv represent additional variability through additional test sets over the same spot numbers. 95

Figure 5.4: Standard error calculated as an average error over all 8 concentrations using RS (random) sampling of 1-200 spots. Subplots i-iv show four collections of independent sample sets, with each subset being an independent randomly sampled set from each sensor..... 96

Figure 5.5: Concentration dependent signal intensities collected from an increasing sample size with 6 spot selection criteria. SS: Sequential sampling; RSS: Reverse sequential sampling; LSS: Linearly spaced sampling; RS: Random sampling; HIS: Maximum intensity sampling; LIS: Minimum intensity sampling 97

Figure 5.6: Standard error calculated as an average error over all 8 concentrations using 6 sampling criteria to generate sets of 1-200 spots. 98

Figure 5.7: Langmuir fit to concentration dependent data from an increasing number of randomly selected points. Each of the four plots represents an independent, randomly (RS) sampled set of 1, 5, 50, or 200 spots. Both x- and y-axes are logarithmic. 100

Figure 5.8: Quality of Langmuir fit calculated for an increasing number of points chosen through 6 sampling methods. Fit quality is defined as the coefficient of determination (R^2). Subplots represent a shifted y-axis representation of the parent plot. 100

List of Tables

Table 1: Sequences used for PCR targetting the Methicillin resistance gene MecA and the Staphylococcus Aureus gene FemA 44

Table 2: Distribution of SERS enhancement factors between tightly packed silver nanoparticles. (Reproduced from Fang et al.[6]) 86

List of Abbreviations

POC: Point-of-care
RDT: Rapid diagnostic test
PCR: Polymerase chain reaction
SERS: Surface Enhanced Raman Spectroscopy
ELISA: Enzyme linked immunosorbent assay
HRP: Horseradish peroxidase
DNA: Deoxyribonucleic acid
RNA: Ribonucleic acid
LAMP: Loop-mediated Amplification
SDA: Strand displacement amplification
EXPAR: Exponential amplification reaction
NASBA: Nucleic acid sequence based amplification
T7-RP: T7 RNA polymerase
RPA: Recombinase polymerase amplification
HDA: Helicase dependent amplification
R6G: Rhodamine 6G
LSPR: Localized surface plasmon resonance
PDMS: Polydimethyl Siloxane
FRET: Forster resonance energy transfer
MRSA: Methicillin resistant staphylococcus aureus
PMMA: Polymethyl methacrylate
PVP40: Polyvinyl pyrrolidinone 40KDa
PAGE: Polyacrylamide gel electrophoresis
Ct: Cycle threshold
PAH: Polyaromatic hydrocarbon
SEM: Scanning electron micrograph
EDS: Energy-dispersive X-Ray spectroscopy
MG: Malachite Green
DMSO: Dimethyl Sulfoxide
SS: Sequential sampling
RSS: Reverse sequential sampling
LSS: Linearly spaced sampling
RS: Random sampling
HIS: Maximum (High) intensity sampling
LSS: Minimum (Low) intensity sampling

Chapter 1. Introduction

With the push towards precision medicine, the need for patient specific diagnostic information has grown. Unfortunately, the existing central lab model concentrates diagnostic assays into facilities detached from the point-of-care (POC) and imposes large time and financial costs on diagnostic testing. The inhibitory cost of central labs places an undue burden on physicians to accurately diagnose and treat patients with little information. A new model for distributed sensing is expanding with advances in POC sensor technologies.[1,2] POC systems provide clinicians the ability to rapidly identify diseases and immediately begin targeted treatments to improve patient outcomes.[2,3]

Portable biosensing solutions have been a common element in the current medical system for many years. Specifically, glucose meters and pregnancy tests represent the standard for rapid diagnostic technologies (RDTs). These types of low sensitivity RDT's have recently been expanded to infectious diseases, but they are applicable only in advanced disease conditions and can be unreliable.[4] Further, diseases are targeted by independent devices and require independent techniques; these limited technologies cannot address the needs of a patient centric testing environment and the expanding library of treatable disease conditions.[5–7] Enabling clinicians to diagnose these new conditions will require

advanced sensors and assay mechanisms that can simultaneously, rapidly, and cheaply detect and identify multiple disease biomarkers.

As a perpetually relevant example, overuse of broad spectrum antibiotics is leading to an ever-shrinking library of effective antibiotic treatments. One obvious solution is the careful prescription of targeted antibiotics.[8] Unfortunately, rapid identification of infectious agents in clinics and remote settings is currently available for only a few conditions and each requires an independent test. Further, these tests are limited to a single bacterial resistance gene of the many that exist for each species.[2] Resistance testing requires time-consuming culture based assays to concentrate samples before species and resistances can be specifically determined. These methods are highly inefficient and infeasible for regular on-site use.

Amplified molecular diagnostic assays, such as the polymerase chain reaction (PCR), provide rapid amplification of virtually any biomarker at nearly any concentration. Though amplified assays are highly sensitive, they are currently unable to easily and cheaply provide the multiplexing needed for on-site identification of multiple biomarkers. Multiplexing potential of any assay is generally limited by the sample processing or transduction mechanism. The fluorescent mechanisms commonly used for PCR are especially difficult to multiplex in portable devices as they rely on mechanical actuation of expensive

filter sets for each additional target. Though it is possible to accomplish parallel transduction of PCR with a single dye in a divided sample, sufficiently large samples may not exist in the necessarily small sample volume acquired through non-invasive methods on-site.

Improving the multiplexing density in portable biosensing technologies may be simplest with a complete replacement of conventional methods (e.g. fluorescence). Instead, a method is required that can discriminate multiple molecules simultaneously with simple, portable hardware. Surface enhanced Raman spectroscopy (SERS) provides one of the most promising methods to address the limitations in portable assay transduction. Based on the molecule dependent effect called Raman scattering detailed in Chapter 2, SERS provides the potential for simultaneous quantification of many biomarkers with no additional hardware. SERS has been applied broadly to chemical and diagnostic sensing, and advancements continue to increase the portability of SERS substrates. Unfortunately, convenient solutions have yet to be developed that can easily integrate SERS with amplified assay mechanisms.

Toward the goal of truly portable molecular diagnostic systems, this work develops technologies to simplify the use of SERS sensors for POC sensing. Specifically, chapter 3 details the development of the first integrated device for real-time monitoring of multiplexed PCR reactions with SERS. This device is

used to simultaneously identify *Staphylococcus aureus* and the presence of methicillin resistance. Chapter 4 expands the library of portable, flexible SERS sensors with SERS sponges that enable new sample acquisition and processing capabilities for harmful organic compounds. Finally, Chapter 5 addresses common concerns with reproducibility in flexible SERS substrates and recommends simple methods for acquiring data and improving inter and intra-sensor variance.

Chapter 2. Molecular diagnostics and Raman spectroscopy

As medical care transitions to a patient centered approach with universal access to quality care, the need for improved POC devices is growing rapidly. New technologies are needed to enable the transition of multifunctional diagnostic technologies out of the central laboratory and into the hands of medical providers. Two major factors inhibiting portabilizing existing technologies are sensitivity and multiplexing density. This chapter will detail the strategies and recent advancements in molecular amplification methods to improve diagnostic assay sensitivity and the mechanisms enabling SERS to allow unprecedented multiplexed assay transduction.

2.1 Molecular diagnostics

Molecular diagnostics have become an integral tool in the diagnostic process and represent the logical solution to address current limitations in POC devices. The technologies behind molecular diagnostics have a diverse set of underlying mechanisms governing the recognition of biomarkers, production of a signal, and transduction to a meaningful answer. Of particular interest to the field of POC diagnostics is improvement of the sensitivity and detection limit of portable technologies. While traditional systems utilize large and expensive equipment to improve the quality of signal detection systems, assay sensitivity can be more

practically improved through novel assay developments that increase signal production rates. Traditionally, the signal generation paradigm produces a signal intensity directly proportional to the number of analytes present. This section will detail the developments of assay mechanisms capable of exponentially amplifying a signal from analyte concentrations as low as a single molecule.

2.2 Classical molecular amplification

Molecular amplification has defined the most well-known and commonly used assays in diagnostics and research settings. By far the most common and recognizable molecular amplification technique is the immunoassay, or more specifically the enzyme linked immusorbent assay (ELISA). Illustrated in Figure 2.1, a typical ELISA begins with antibodies immobilized onto a surface, to which the sample is added. The analyte of interest is then specifically bound by an antibody and prevented from release during subsequent rinsing steps that eliminate contaminants. After rinsing, a detection antibody is added to introduce a signal generating enzyme (i.e. HRP); this detection antibody specifically binds the analyte and is maintained through another series of washes to remove unbound enzymes. A chromogen is then added to produce a signal, which is produced at a constant rate dictated by the number of bound enzymes and effectively indicating the analyte concentration. This proportional amplification technique provides sufficient sensitivity for many laboratory techniques, but is

incapable of reaching detection limits necessary for many unconcentrated or impure POC samples.

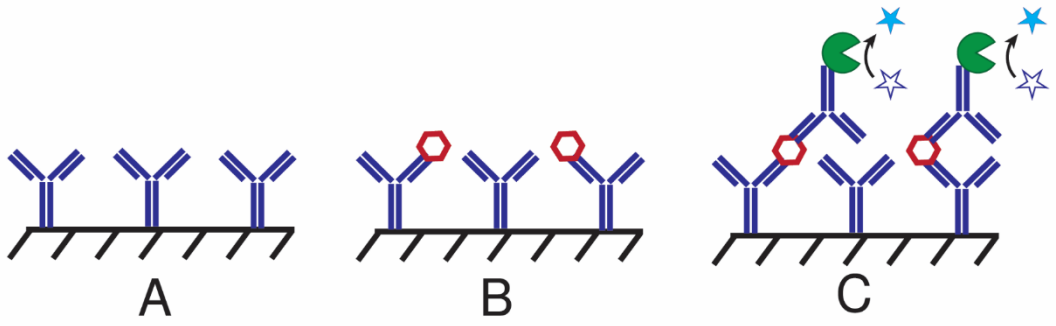

Figure 2.1: Illustration of an Enzyme Linked Immunoassay (ELISA). A: Antibodies present analyte binding sites immobilized on a surface. B: Specific analyte binding to antibodies and subsequent washing to remove other sample components. C: Binding of a detection antibody to a second epitope on the analyte, subsequent steps wash unbound detection antibodies and introduce a chromophore that is acted upon by the attached enzyme.

PCR is the classical exponential amplification technique, commonly used in both diagnostics and research for genetic sequence identification. In PCR (Figure 2.2), a polymerase amplifies short gene-specific sequences of DNA through repeated copying of the sequence. After the double-stranded template has been melted into single strands, DNA primers (typically 18-25 bases) specifically hybridize to the template to mark the locations for the polymerase to begin copying. Following each cycle, the number of targeted sequence doubles, and then the initial sequences and the copies (amplicons) are available for replication in the next cycle (i.e., exponential amplification with positive feedback).

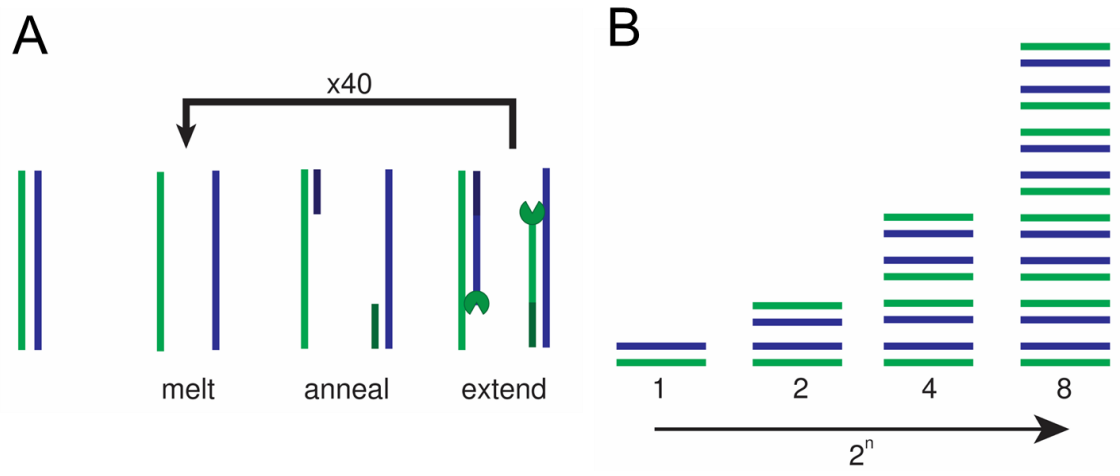

Figure 2.2: Illustration of PCR amplification mechanism. A: Amplification steps beginning with hybridized template or amplicons melted at high temperatures, rapid transition to low temperatures allows small primers to bind and be extended by TAQ polymerase. B: Illustration of the exponential product formation rate (2^n) in PCR.

Though PCR is typically used only for nucleic acid biomarkers, it can also be used as a tool to drastically improve the detection limit of traditional immunoassays. In this method, termed immuno-PCR, the detection antibody of the immunoassay is linked to an amplifiable DNA sequence. Once the antibody is specifically bound to a surface or a particle, PCR reagents are added and signal develops exponentially.[1–3] Implementations of this technique have led to detection limits down to a single molecule, which represents an improvement of up to 5 orders of magnitude over traditional immunoassays.[1,4] This technique has been expanded with the use of DNA and RNA sequences that can specifically bind non-nucleic acid targets. These sequences, called aptamers, can act as both the recognition element –replacing the antibody– and the amplification template, further simplifying the assay.[5,6]

As a result, PCR is not only pervasive in the detection of nucleic acid sequences, but can also be viewed as a generic signal amplification methodology for a range of biomarkers. Unfortunately, even as the standard amplification mechanism, the increasing body of work seeking to deliver PCR assays to the field has yet to produce a practical solution.[7–10] The temperature control and fluorescence quantification hardware have remained inherent limitations. The following sections highlight both existing alternatives and future directions in the replacement of PCR for POC molecular diagnostics.

2.3 Isothermal nucleic acid amplification

Since the invention of PCR, new polymerase-dependent DNA replication schemes have been continuously developed to address the hardware and energy requirements associated with thermal cycling. In particular, eliminating the requirement of heat denaturation used in PCR has been the primary unifying alteration desired in polymerase-driven nucleic acid amplification mechanisms. The goal of heat denaturation is to enable binding of the primer sequence and replication of the amplicon. This section will illustrate the many potential alterative mechanisms to promote primer annealing, but also highlight the compromissary limitations introduced in these methodologies.

2.3.1 Loop-mediated isothermal amplification (LAMP)

The most commonly studied PCR alternative is Loop-mediated isothermal amplification.[19–21] In this technique, initiating primers insert looping modifications to the gene of interest. Loops are produced through addition of a primer sequence that is bookended by self-complementary regions that form a loop. A primer is then able to bind and be extended from the loop region; at the same time, the loop itself can prime replication. Primer extension then generates a cyclic see-saw like process, where extension of a primer displaces the existing hybrid promoting formation of the opposing loop. Note that much like PCR, LAMP's DNA replication capability can also serve as the label amplification method for immunoassays.[22–24]

Despite the advantages of LAMP, this amplification scheme requires a constant temperature of 65°C, and therefore requires more power than amplification systems that operate at 37°C or below. Furthermore, four to six primers are required, making a multiplex assay highly complex to design and potentially susceptible to non-specific amplification. Thus, simpler assays without the heating requirements and complexity of LAMP may be more attractive for POC diagnostics.

2.3.2 Nuclease driven amplification

Nucleases, or enzymes that cleave nucleic acids, have been utilized in multiple PCR alternatives to promote annealing and generate new primers. The original nuclease based method is strand displacement amplification (SDA).[17,18] SDA utilizes a specialized restriction endonuclease to insert a single-stranded "nick" into DNA duplexes, thus allowing binding and replication by a polymerase at moderate temperatures (37°C). Similar to LAMP, a DNA-displacing polymerase is utilized to copy DNA (starting at the nick site) while displacing hybridized DNA, thereby eliminating the need for a high temperature melt step. The displaced strand is then capable of binding the anti-sense primer continuing the amplification as the amplicon. For genomic targets, SDA typically requires addition of a second set of primers (bump primers), that allow displacement of the initial amplicon without action of the nicking enzyme; this eliminates the need to locate a genomic region with a particular restriction sequence.[26,27] SDA has also been applied to proteins[28] and microRNA[29].

Another isothermal amplification technique built from the concepts of SDA is the exponential amplification reaction (EXPAR).[30] EXPAR utilizes a nicking enzyme to lower the thermal stability of newly-polymerized amplicons. The EXPAR reaction differs from SDA in that the nicking enzyme acts at the center of the amplicon instead of towards the end of the sequence. Bisecting the

amplicon allows for simple thermal destabilization an elevated temperature around 60°C. Once denatured, the bisected sections are capable of priming extension on single stranded templates and continuing the reaction, leading to exponential cycling. Initially, EXPAR was designed as an alternative to current isothermal amplification technologies for genomic DNA targets. Unlike SDA however, EXPAR's requirement for a centrally located restriction site requires the site to be present in the gene of interest and therefore cannot be avoided with a bump primer. EXPAR has been used as a secondary amplification mechanism for alternative sequence identification mechanisms such as SDA.[28] When applied outside genomic targets, the simple mechanism behind the EXPAR system allows for a convenient platform for expansion beyond nucleic acid diagnostics and has been shown to be effective for amplification after recognition with enzymes[31], aptamers[28], and whole cells[32].

As an alternative to sequence specific nucleases, RNA has been utilized in a number of methods to act as a specific target for nucleases to open primer binding sites. The original method, which was nearly simultaneously reported by two groups[25,26], is based on the use of transcription enzymes to produce RNA transcripts from a DNA template. As a class, these methods are called transcription mediated amplification (TMA); nucleic acid sequence based amplification (NASBA) is the most common implementation, and is used for

RNA sequence detection. In NASBA, an RNA template acts as a primer binding and extension site for a primer containing the T7 RNA polymerase (T7-RP) promoter sequence. Extension of the primer by a reverse transcriptase produces a complementary DNA (cDNA) transcript containing the T7-RP promotor sequence. The RNA is then removed from the duplex by an RNA-specific nuclease (RNase-H), leaving the cDNA open to annealing of the secondary primer. Extension of the secondary primer produces the double stranded promotor sequence allowing for production of a single stranded RNA template by T7-RP to restart the cycle. Unlike many nucleic acid amplification schemes, NASBA was initially developed for amplification of genomic RNA sequences from viral sources. Outside of genomic RNA, NASBA is most easily applied to alternative RNA applications such as mRNA[27–29], tmRNA[30], miRNA[31], immunoassays[32].

2.3.3 Protein guided duplex opening

Biological mechanisms for DNA replication use neither thermal denaturation or nucleases to open DNA duplexes. Some isothermal methods have taken advantage of natural DNA binding proteins to open duplexes for primer annealing steps. Recombinase polymerase amplification (RPA) and helicase-dependent amplification (HDA) both utilize specialized enzymes that open

double stranded oligomers to insert primers, in some cases stabilizing the opening with single strand binding proteins.

In many organisms, the helicase enzyme opens double-stranded DNA to enable primer binding and DNA duplication. The helicase unwinds the duplex, which is then stabilized through single-stranded DNA binding proteins while a primer hybridizes and is extended by a polymerase. Since the initial report[33], several HDA variations have been reported. HDA has not been widely applied to many targets, but has been successfully applied to a commercial lateral flow device for viral genomic RNA[42].

RPA utilizes a primer-recombinase complex to scan the DNA in the sample and perform strand exchange at a homologous sequence within the target.[35] This inserts the primer and recruits proteins, specifically gp32, to stabilize the loop opening of the target DNA. A polymerase then extends the primer along the target, generating a new double-stranded DNA amplicon. This new double stranded copy is subsequently targeted by recombinase, which inserts a primer to initiate another round of duplication. RPA has been successfully applied to highly sensitive detection of both DNA[35] and RNA[36] genomes. Some work has applied RPA to protein detection through aptamer binding and amplification, but results show only ELISA-like detection limits[37].

2.4 Raman spectroscopy

2.4.1 Raman scattering

When light contacts a molecular structure, the energy is temporarily absorbed exciting the bonds within the molecule. Frequently, the excited state of the molecule is an unstable and rapidly decays through radiative relaxation back to the ground state. The energy of the radiated photon is commonly of equal energy to the adsorbed photon; this elastic scattering process is known as Rayleigh scattering. Alternatively, certain highly polarizable molecular structures can lead to the existence of a virtual energy state composed of temporarily stable vibrational modes. Illustrated in Figure 2.3, an excited molecule can relax into a virtual state leading to energy loss corresponding to the energy lost through vibrational relaxation to the ground state. This inelastic scattering process is known as Raman scattering, named for C.V. Raman who discovered the phenomenon in 1928.

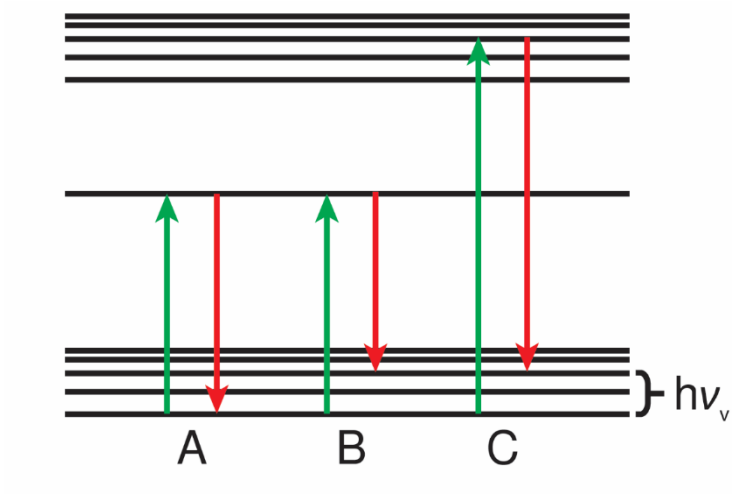

Figure 2.3: Jablonski energy diagram. A: Energy transfer for Rayleigh (elastic) scattering. B: Energy loss ($h\nu_v$) in Raman (inelastic) scattering. C: Electronic transition and energy loss in resonance Raman scattering.

The vibrational modes induced during Raman scattering are specific to the bonds and their arrangement within the excited molecule. Further, the tendency for particular molecular structures to enter virtual states leads to relative differences in the tendencies for molecules to emit photons of a particular energy. Together, the specific energy and intensity of photons emitted by an excited molecule produces a spectroscopic profile of the molecular structure. When utilizing a monochromatic light source, such as a laser, it is possible to excite and isolate Raman scattered photons from the Rayleigh scattered light from the source frequency. Figure 2.4 illustrates the spectrum of Raman scattered photons of a common dye, Rhodamine 6G, excited by a diode laser at 785 nm. The spectrum illustrates the bond specific peaks, that together, uniquely represent the structure of R6G.

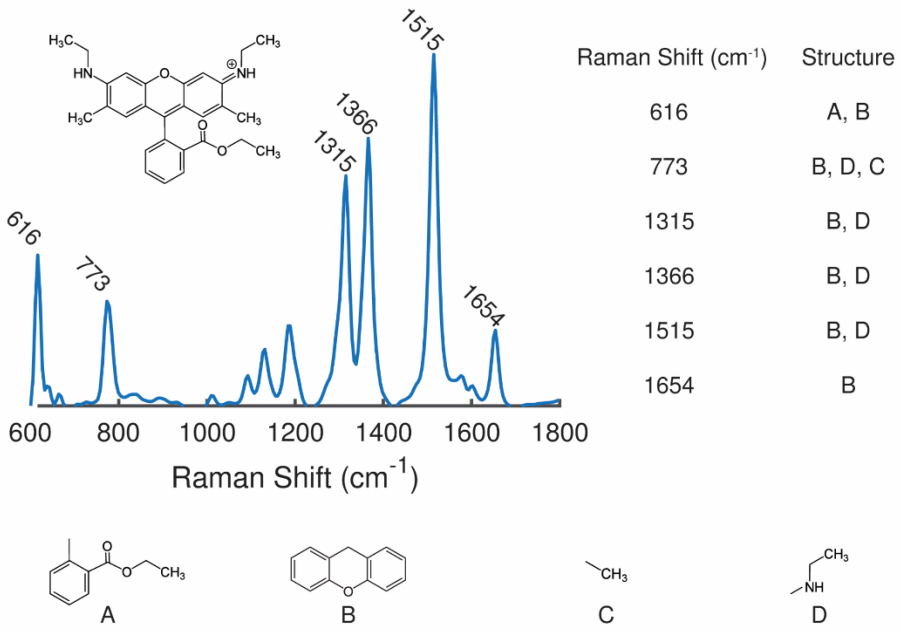

Figure 2.4: Raman (surface enhanced) spectrum of R6G and attributions of peak intensities to individual and cooperative molecular structures.[38]

While Raman intensity has a similar wavelength dependence for scattering intensity as Rayleigh scattering ($I \propto \frac{1}{\lambda^4}$), certain molecules exhibit wavelength dependent intensities that correspond to their absorption spectrum. Near the absorption peak, molecules such as fluorophores undergo an electronic transition to a stable energetic state that can increase the Raman scattering intensity by a factor of 10^4; this effect is known as resonance Raman scattering (Figure 2.3C).

The molecular specificity of Raman scattering has allowed its use as an analytical technique in fields as diverse as astronomy and forensics. In many of the current applications utilizing Raman spectroscopy, analytes are most easily

identified when they are pure or represent a dominant portion of the excited area and recorded spectrum. However, when approaching applications with samples that contain optically active components or low analyte concentrations, specific signals are easily obscured. In these cases, Raman spectroscopy requires increased sensitivity and robustness.

2.4.2 Surface enhancement

The low intensity of Raman scattering signals inherently limits its use to relatively pure or highly concentrated analytes. Over the last 50 years, significant work has led to drastic improvements in the sensitivity of Raman spectroscopy through the use of conductive surfaces that greatly increase the rate of Raman scattering; improvements in Raman scattering efficiency can be induced from 10^6-10^{10}.[39–41]

Discovered in the 1970's, a number of early groups identified unexpectedly intense Raman scattering from the surface of roughened silver electrodes.[42–45] Over the next couple decades, these early reports led to steady academic development of the technique with little translational growth. Then in the 1990's, reports of single molecule detection generated compounding interest and exponential growth that has lasted through the present.[54,55]

Enhancement of Raman scattering intensity is primarily attributed to two distinct but cooperative mechanisms: electromagnetic enhancement and

chemical enhancement. Briefly, electromagnetic enhancement is generated by an increase in the local electromagnetic field strength, while chemical enhancement is the molecule dependent effect of direct bond coordination with the enhancement surface.

The largest portion of the Raman enhancement factors (10^4-10^8) generated through surface enhancement, is attributed to electromagnetic effects. This mechanism is based on coupling of the incident light into oscillations of the conducting band electrons generating the effect called localized surface plasmon resonances (LSPR).[48] Within the produced high intensity local fields, shifted electromagnetic oscillations within the molecule can couple back into the local plasmon oscillations leading to amplified scattering intensities of both the incident and shifted frequencies. The extent of Raman signal enhancement is dependent on the geometry of the conductive surface and interaction distance of the molecule with the surface. Figure 2.5 illustrates the relative local field enhancements created by various metal shapes, each with features necessarily on the nanoscale. Figure 2.5 can also serve to illustrate the distance dependent effects of surface enhancement, which is subject to a sharp drop-off rate as the separation distance grows away from the nanoparticle surface. For spherical particles[49] the distance (d) dependence is on the order of $\left(\frac{1}{d}\right)^{12}$. The severe distance dependence of SERS defines one of the most limiting factors of the

technique: efficient enhancement requires spontaneous or forced immobilization of the analyte within 1-2 nanometers of the surface.

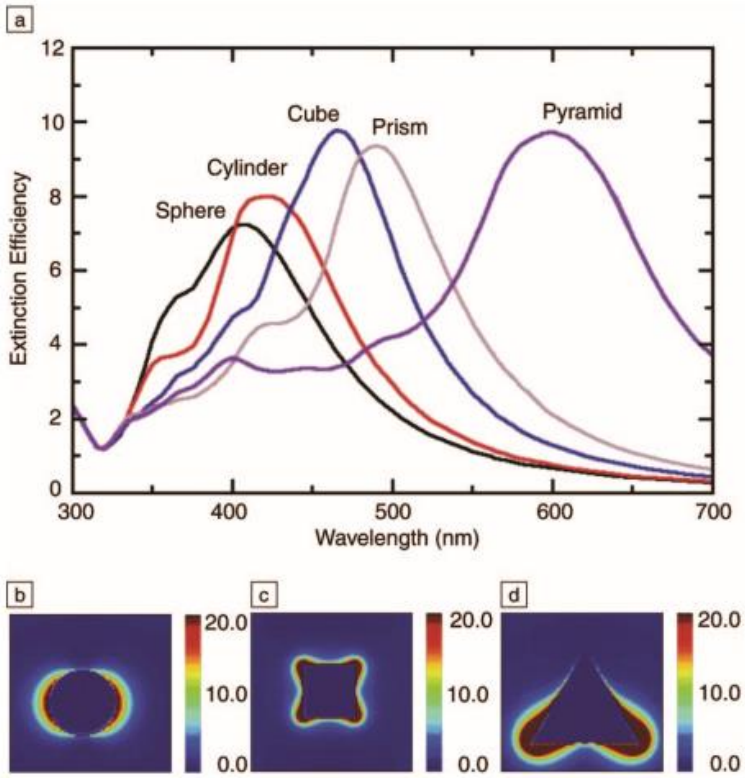

Figure 2.5: Nanoscale shape and size dependence of electromagnetic enhancement intensity. (Reproduced with permission, Haes et al.[50])

Chemical enhancement is possible when analytes adsorb directly onto the enhancement surface, where charge transfer complexes are formed between the surface and the molecule in a coordinate-covalent state.[51] This coupling leads to enhancement factors on the order of 10^2, is somewhat geometry dependent, and has strong dependencies on molecular structure.[52–54]

When combined, electromagnetic and chemical enhancement of Raman scattering allowed detection of a single molecule, a feat impossible for most

analytical chemistry methods. The impressive potential implied by detection of a single dye molecule has driven a surge in interest for SERS as a label-free biosensing technique with unprecedented sensitivity and multiplexing density.

2.4.3 SERS sensors

The high potential for SERS to enable new assays and replace existing mechanisms like fluorescence continues to inspire developments in methods to generate and utilize SERS sensor surfaces. Though the library of sensing substrates for SERS analyses is diverse, it can most simply be divided into three broad categories: colloidal, rigid, and flexible.

2.4.3.1 Colloidal SERS

While colloidal methods do not meet the visible classification of a "sensor" and cannot said to be contained within a "substrate", the advances around their use in single molecule SERS[54,55] as well as assays deserve appropriate attention. Use of colloidal particles for SERS hinges on the spontaneous interaction of the analyte with the nanoparticles, which are then commonly aggregated to produce the nanostructures required for Raman enhancement. Colloidal SERS has been broadly applied to various assays and commonly exhibits enhancement factors around 10^5.[41] However, analyte-nanoparticle interactions and aggregation represent fundamental challenges for colloidal SERS versus substrate based methods.[55–57]

As nanoparticles inherently have an effectively high surface energy, stabilizing agents are required to stabilize their interactions with the solvent, usually water. These capping agents can prevent the adsorption of analytes to the surface of nanoparticles and, therefore, prevent the development of a signal. Poor analyte adsorption has been addressed through various nanoparticle modifications to promote ionic interactions, van der waals forces, and hydrophobic interactions.[58–62]

The spherical particles commonly used for colloidal SERS require aggregation to produce the necessary nanostructures for sufficient enhancement. The process of aggregation can lead to non-uniform aggregates and produce inconsistent enhancement.[55,56,63] Significant effort has been spent attempting to produce nanoparticles that are uniform and inherently SERS active. These particles often require complex fabrication procedures leading to complex shapes that can produce sufficient enhancement with minimal need for aggregating agents.[72–78]

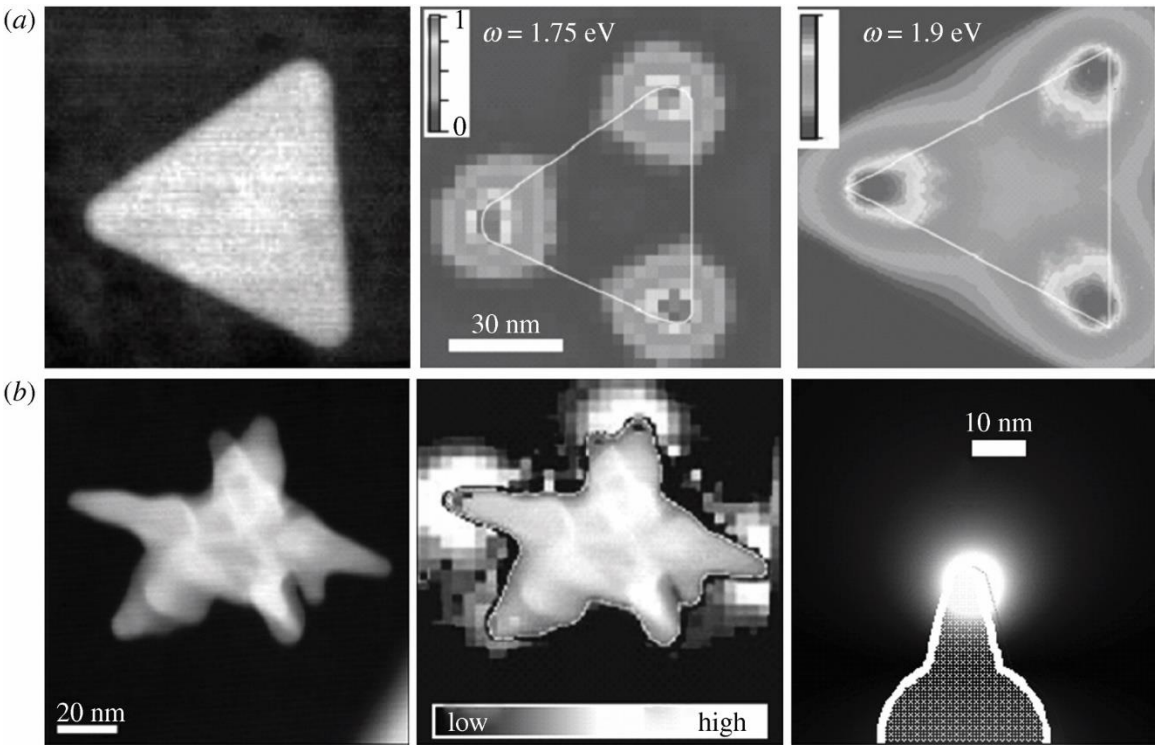

Figure 2.6: Nanotriangles and nanostars are a representative subset of the possible complex shapes available in colloidal SERS. (Reproduced with permission, Abalde-Cela et al.[71])

2.4.3.2 Rigid SERS Sensors

Rigid SERS substrates illustrate a continuous line of improvements from the initial reports of SERS on roughened silver electrodes.[42,44] These technologies have been invaluable in studying the SERS mechanisms and achieving single molecule detection. Rigid, carefully fabricated devices have consistently high enhancement factors (10^6-10^8) and represent the standard for surface and signal reproducibility.[80–84] Methods began with unpatterned roughened surfaces and rapidly evolved to controlled deposition of nanoparticles. As study of the Raman mechanism has advanced, control over the nanostructures has considerably improved. Modern methods include deposition or ablation of materials in highly

uniform array patterns such as nano- triangles[73,85,86], cubes[86–88], holes[81–84], domes[85–87], voids[88–90], etc[72–74,91]. The high performance of these complex shapes is acquired at significant cost and manufacturing difficulty through non-scalable methods. The rigid, 2-dimensional nature of these devices provides little inherent assay processing functionality beyond transduction, and therefore requires peripheral devices and technical intervention. Ultimately, these devices represent an important research platform, but cannot accommodate the necessary functions required for practical sensing of real-world samples, especially for on-site applications.

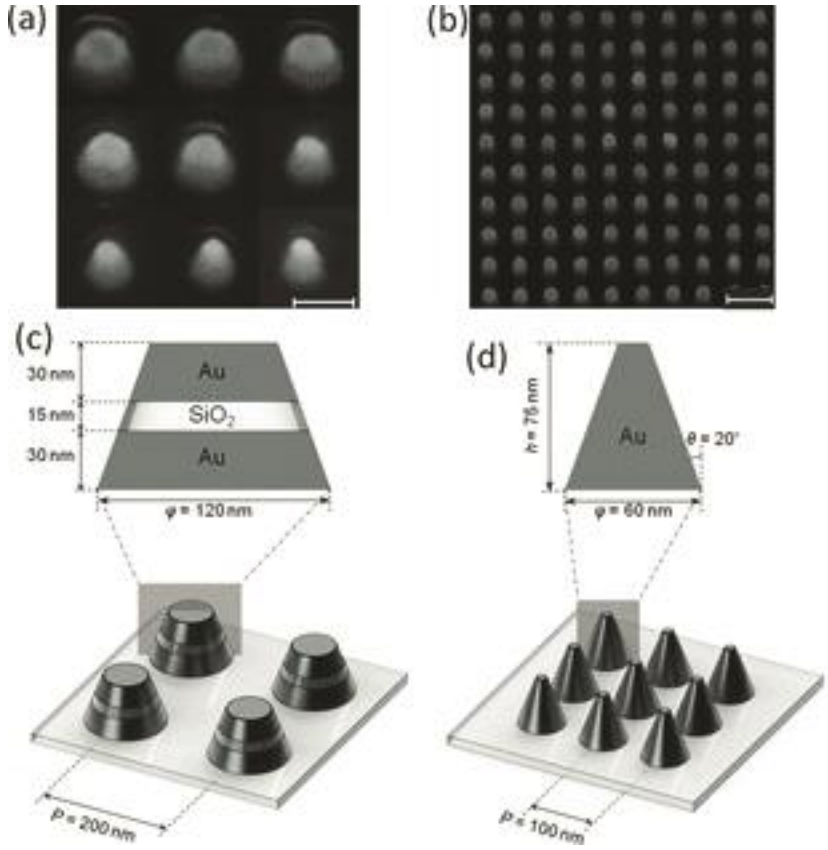

Figure 2.7: Shape complexity and regularity in rigid SERS sensors.(Reproduced with permission, Cinel et al.[92])

2.4.3.3 Flexible SERS Sensors

In the drive to enable practical use of SERS as an analytical technique, flexible SERS substrates have been developed to provide inherent or modular sample processing features. While flexible substrates have seen constant development and attention over the last decade, deposition of silver nanoparticles into flexible cellulose filter paper was first reported in 1984.[93] Continuous development of SERS in cellulose derivatives persisted through the following decades, but interest and expansion of the technique was minimal. Recently, advances in

simplified fabrication methods and lower cost spectrometers have invigorated interest in portablizing SERS.

By far the most common material adapted for flexible SERS substrate remains cellulose filter paper. Methods of functionalizing cellulose –similarly used materials include nitrocellulose and polyvinylidene difluoride (PVDF)– include various mechanisms for both in-situ nanoparticle growth and for deposition of colloidal particles. Deposition of colloidal particles include simple, non-specific methods such as soaking[94] as well as scalable and customizable ink deposition methods such as pens[95], sprays[96,97], screen printing[106–108], and ink-jet printing[101–104]. Growth of nanoparticles within the paper includes methods that include deposition of nanoparticle seeds and growth on chemically modified surfaces[105–107]. Paper based devices are capable of augmenting the transduction benefits of SERS with fluidic handling properties and surface interactions that include sample transfer, purification, and concentration.[94,103,108,109]

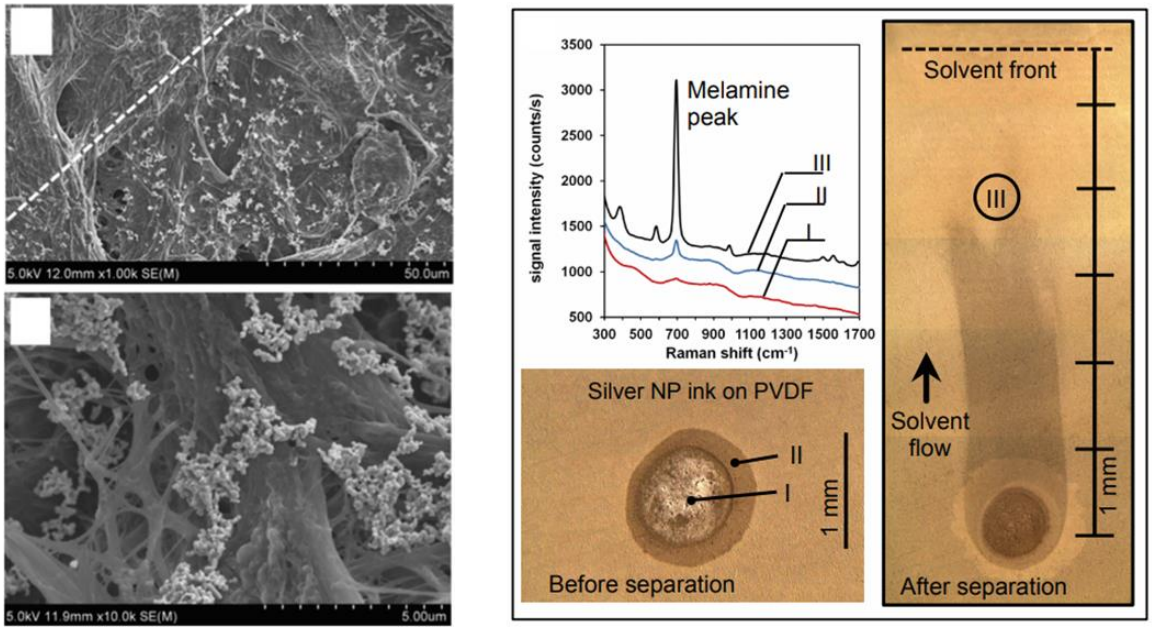

Figure 2.8: Nanoparticle distribution and functional properties of paper based SERS sensors. (Reproduced with permission, Left: Yu and White 2010[112]; Right: Yu and White 2013[109])

Though fibrous paper is the most common substrate, other materials have been explored to broaden the functional capabilities of flexible sensors. Adhesives have been proposed as materials capable of utilizing adhesion to retain nanoparticles and extract trace analytes from complex surfaces.[118] Recently, polydimethyl siloxane (PDMS), the material most commonly used for soft lithography of microfluidic devices, has been applied as a method to provide a highly customizable surface for enhanced plasmonic properties.[111–115] These PDMS substrates also provide convenient flexibility and adhesive properties to aid in acquiring samples.

Chapter 4 builds on the existing work with PDMS SERS sensors to produce a 3-dimensional fluid handling matrix replicating sponge-like materials. When

functionalized with nanoparticles, these hydrophobic sponges can specifically intake organic solvents and organic molecules to concentrate organic molecules from aqueous samples.

2.4.3.4 Variance and ambiguity in SERS data

The drive towards portable SERS technologies has led to rapid expansion in the number of substrate materials and types used to house the metal nanostructures necessary for Raman enhancement. These sensors have been shown to be highly sensitive and specific for analytes in a number of applications. However, the departure from highly ordered nanostructures introduces the potential for a distribution of non-uniform enhancement factors and therefore signal intensity.[63,71,108,124,125] Indeed, it is commonly acknowledged that SERS signals from aggregated nanoparticles, a common feature of low-cost substrates, show large contributions from relatively few enhancement sites and therefore proportionally few analyte molecules.[63] On top of heterogenous nanostructures, flexible substrates are subject to additional criticisms[118] from factors such as nanoparticle distributions, environmental factors[119], as well as sample concentration and addition methods[56,119].

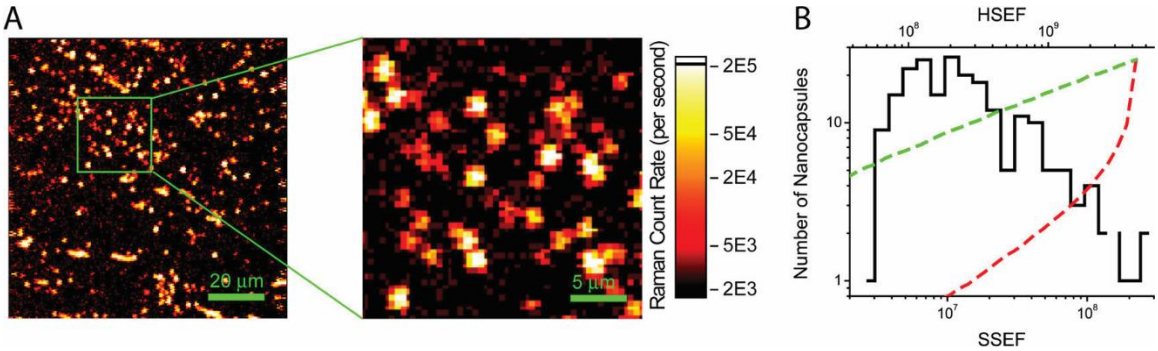

Figure 2.9: Variation in shape, size, and enhancement factor of deposited nanoparticle aggregates. (Reproduced with permission, Laurence et al.[120])

Empirical evidence, however, suggests that flexible SERS substrates are indeed capable of highly sensitive and robust measurements across a practical dynamic range. When sampled across the sensor surface, these surfaces can provide both high enhancement factors and reproducible intensities.[107,108,110,129,130] However, the extent to which locality impacts signal intensity and intra- and inter-sensor signal variance are rarely addressed in demonstrations of novel SERS sensors. Incomplete and unclear methodologies are commonly reported in the literature and occasionally include questionable intensities, spectra, and conclusions. As a result, skepticism and misunderstanding will persist until standard methods are defined and followed to ensure sufficient surface sampling and explicit spot definition.

Toward the goal of robustness in SERS methodologies, Chapter 5 details proposed techniques for algorithmically sampling and processing data across a sample surface.

2.5 SERS in molecular diagnostics

As assay mechanisms are evolving to enable portable use, diagnoses are becoming increasingly complex and reliant on multiple biomarkers to improve diagnostic precision. The spectroscopic nature and sensitivity of SERS provides a promising platform for POC diagnostics. SERS is commonly studied method for a variety of both direct and reaction dependent detection of nearly every type of biomarker including small molecules[122–124], nucleic acids[133], proteins[126], and even whole cells[127,128].

Alone, SERS does not have the capability to provide sufficient sensitivity to identify and quantify complex biomacromolecules in a portable setting. As discussed in Chapter 1, the move to portable diagnostics will require advanced techniques to improve assay sensitivities and eliminate lab based processing steps. Combined with the multiplexing capability of SERS, amplified assays have the potential to provide portable diagnostic devices that can simultaneously provide complex diagnostic information from relatively simple hardware. One early proposal by Cao et al. highlights (Figure 2.10) the potential for SERS to simplify multiplexed detection of DNA targets. This technique and many developed since that time utilize a dye labelled oligonucleotide probe. The dye is able to provide high intensity SERS signals through a large Raman cross-section not inherent to most biomacromolecules. The use of Raman labels on

oligonucleotide probes has allowed SERS to replace monoplex transduction mechanisms in amplified assays such as PCR and its derivatives.[108,128–131]

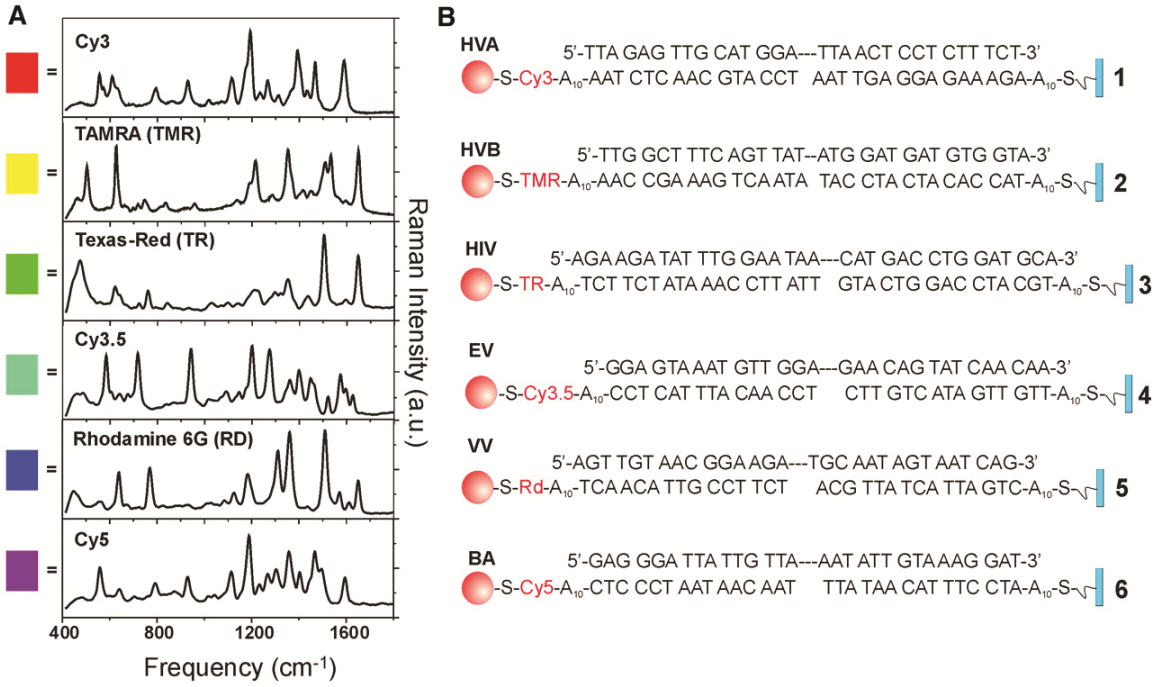

Figure 2.10: Demonstration of the potential for SERS to enable highly multiplexed molecular assays. (Reproduced with permission, Cao et al.[132])

As Raman requires the adsorption of a dye on a surface, the product of the reaction must specifically adsorb to the surface, away from any unreacted probe. This is often accomplished either through the use of DNA digesting enzymes[116,139,141] or physical separation.[128,129,134] The most common of these assay mechanisms is the TAQ-MAN PCR assay. Originally developed as a fluorescence method based on FRET, a dye labeled TAQ-MAN probe is degraded by TAQ polymerase when specifically hybridized to the produced amplicon. For SERS, the digestion of the probe enables simple separation from

the intact probe through a variety of methods, such as simple chromatography or magnetic separation.[108,131]

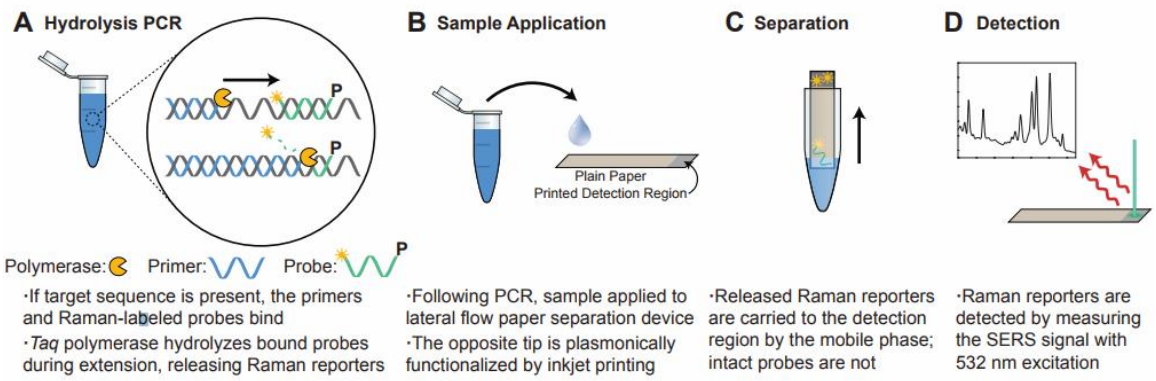

Figure 2.11: Example of PCR product separation and SERS analysis. (Reproduced with permission, Hoppmann et al.[108])

Despite the success of these methods in applying SERS to amplified assays, the added steps required to separate the intact probe from the digested product increase the technical requirements of completing the assay. Few methods include a fully integrated solution that is capable of being applied to the point of care. Microfluidics offer promising multistep assay integration with SERS[143–145], but complex microfluidic devices remain practical largely as research tools. Together, all existing SERS solutions enable only endpoint analysis of PCR samples and are therefore subject to the specificity limits of exponential assays.

Ultimately, new techniques are needed to apply SERS to POC implementations of amplified assays like PCR. A new approach using real-time filtration is detailed in Chapter 3 that can, for the first time, accomplish real time

PCR with SERS. Further, the simple to use device is easily constructed via laser cutting and thermal bonding of a low-cost thermoplastic.

Chapter 3. Real-time PCR using Surface Enhanced Raman Spectroscopy in a thermoplastic chip

3.1 Introduction

The trend towards precision medicine has introduced the benefits of on-site diagnostic systems that can rapidly detect and identify disease conditions and causative agents. Rapid diagnostic information can improve healthcare outcomes[2,3] and provide necessary, widespread monitoring of diseases and drug resistances[3,4]. The primary development path for portable diagnostic sensor technologies has been miniaturization of existing laboratory systems to produce mobile versions for identical use away from the traditional central lab environment.[2,5] However, the existing technologies are largely dependent on inherently expensive hardware and technically difficult procedures that do not easily translate to the size, power, and cost needs of point-of-care (POC) devices.

For common bioassays such as the polymerase chain reaction (PCR), fluorescence is the gold standard to quantify the amplified gene copies and specifically identify them as the product of interest. Because fluorescence requires specific filter sets, it is expensive and mechanically difficult to allow simultaneous and specific detection of multiple targets, which is commonly needed in diagnostic assays. With difficulties in spectral multiplexing, spatial

multiplexing is commonly used as an alternative that allows multiple independent wells or droplets to use one fluorophore to identify different targets.[6] Devices and procedures designed around multiple wells typically require increased sample volumes, complex and expensive fabrication, and difficult, multistep fluid transfers. All of these requirements place existing solutions beyond the limitations of the POC.

Surface enhanced Raman spectroscopy (SERS) has emerged as a promising alternative to fluorescence and other established methods to improve the hardware cost and simplify assay schemes.[108,117,118] As a spectroscopic method, SERS is able to provide molecule specific information and can be utilized for chemical analytics in many applications.[113,117,118,149,150] In diagnostics, SERS has been applied as a method for direct detection and identification of a variety of targets from small molecules[7,13,14], proteins[15], and even phenotypic cell identification[16,17]. In biochemical assays, SERS has been broadly applied to replace monoplex transduction mechanisms like colorimetry and fluorimetry in assays like ELISA and PCR.[18–21]

The most common format for implementation of PCR with SERS is based on derivatives of the TAQ-MAN assay in which a hybridization event between a DNA target and a labelled probe exposes the probe to digestion by a polymerase. In the TAQ-MAN assay, the fluorescent label is liberated from a

quencher to specifically distinguish the degraded probe from the intact probe. In SERS adaptations, a secondary step is necessary to accomplish the same signal specificity. Multiple elegant methods have been described to only expose the SERS surface to only the free fluorophore, including paper chromatography[18] and affinity separation on microparticles[21,22]. These methods successfully highlight the sensitivity and multiplexing capabilities of SERS with PCR. Unfortunately, these methods impose additional technical and time burdens not imposed by fluorescence and therefore encumber the portable implementation of PCR.

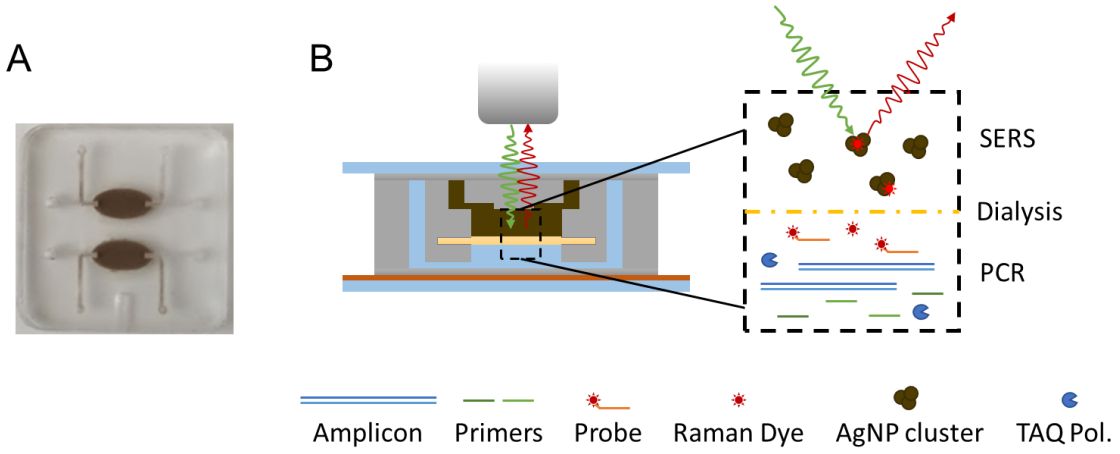

Figure 3.1: Photograph and Illustration of Dialysis driven SERS-PCR device. A: Photograph of device taken shows AgNP colloid above a PCR solution. Chip is pictured after thermocycling. B: Schematic of device function during a probe based qPCR assay, in which a dye is liberated and passes through pores to the AgNP colloid for SERS detection.

In this work, we demonstrate a technique that is capable of eliminating post-processing steps and demonstrates, for the first time, real-time PCR with SERS. Using a dialysis membrane to isolate a silver colloid from the PCR reaction, target

specific digestion of the labelled probe leads to sufficient molecular weight change to allow passage across the membrane and into the colloid. At the high temperatures in PCR, diffusion across the membrane is fast enough to enable the high sensitivity of SERS to rapidly detect the buildup of free fluorophores. Further, the reaction is housed in a laser cut thermoplastic chip that allows low-cost, scalable construction. With this technique, we show quantitative and specific detection of two genes for Methicillin resistant *Staphylococcus aureus* (MRSA) through probe based PCR and simultaneous quantification of two genes necessary for identifying MRSA and the presence of methicillin resistance.

3.2 Materials and Methods

3.2.1 Materials

Devices were fabricated from 1 mm thick polymethyl methacrylate (PMMA) obtained from Inventables (Chicago, IL) through laser ablation. All drawings sent to the laser cutter were generated in Adobe Illustrator (San Jose, CA). Biotechnology grade dialysis membranes with a MWCO of 20 kDa (part no. 133336) were obtained from Spectrum Laboratories (Rancho Dominguez, CA). Fabricated chips were sealed on the top and bottom with PCR grade sealing foils (part no. 04729757001) from Roche Molecular Systems (Indianapolis, IN). Nanoparticle colloids were synthesized from $AgNO_3$ (SKU 209139), sodium citrate tribasic (SKU S4641), spermine tetrahydrochloride (SKU S1141), and

polyvinyl pyrrolidinone (SKU PVP40) all obtained from Sigma Aldrich (St. Louis MO). PCR reactions were performed with primers and labelled probes obtained from either IDT (Coralville, IA) or BioSearch (Petaluma, CA). Reaction mixes were purchased as a master mix from IDT (PrimeTime master mix) and augmented with BSA and dNTPs from NEB (Ipswich, MA). MRSA genomes (MCH70) were obtained through BEI Resources (Manassas, VA).

3.2.2 Device Fabrication

SERS-PCR chips were fabricated through laser ablation and thermal bonding (Figure 3.1). Laser cutting is a well-established technique for PCR grade thermoplastic devices.[23,24] In this work, the design was drawn and sent to the laser cutter (Fusion M2, Epilog Laser Golden, CO) through Adobe Illustrator. Channels were etched partially into the PMMA at 50% power and 50% speed. Wells, inlets, and outlets were cut using 15% power and 10% speed. The manufacturer applied adhesive backing remained during cutting and was removed just prior to bonding to reveal a clean surface. Bonding was performed with each of the three layers aligned with the cut dialysis membrane (1 cm X 1 cm) between the bottom and middle layers. The stacked layers were then clamped between two pieces of glass (2x2x0.2 cm) and placed in an oven at the glass transition temperature of PMMA (105 °C) for 1 hour.[23,24] After bonding, the chips were unclamped and allowed to cool to room temperature. An adhesive

polypropylene film was cut to size and applied as the bottom layer of the device; these films simplify fabrication and provide minimal thermal resistance.

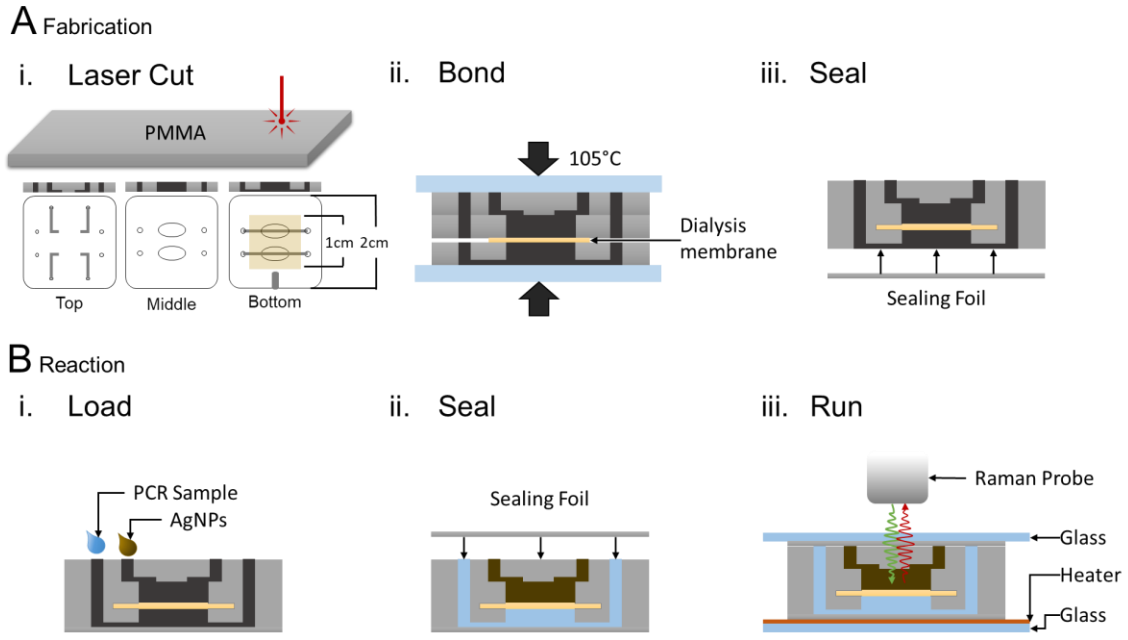

Figure 3.2: Schematic of device construction and use. A: Fabrication pathway of SERS-PCR devices. Laser cutting (i) is used to prepare device layers that are thermally bonded(ii) with a dialysis membrane between the bottom and middle layers; the device is sealed (iii) with an adhesive polymer film. B: Device preparation for PCR involves a simple three step process of adding the sample and nanoparticles to the respective inlet (i), sealing the device with an optically clear adhesive film (ii) and finally thermocycling under a portable Raman probe.

3.2.3 Nanoparticle synthesis

Nanoparticle colloids used as the enhancement surface for SERS were synthesized using a concentrated solution of aggregated citrate capped silver nanoparticles fabricated through the Lee-Miesel method.[25] First, 72 mg of $AgNO_3$ was added to 400 mL deionized water and brought to a boil under vigorous stirring. Sodium citrate (80 mg) was then added and the reaction was allowed to progress for 10 minutes before being removed from heat to cool and

stored at 4 °C. Stocks of 100x concentrated colloid were produced through centrifugation of the original nanoparticle solution at 12000 g for 20 minutes. After centrifugation, the 99 % of the supernatant was removed leaving a 100x concentrated colloid; the concentrated stock was also stored at 4 °C.

Prior to each reaction, solution stable aggregates were produced through an optimized mixture of a stabilizing agent (PVP40) and a positively charged aggregating agent (spermine). The spermine promotes both nanoparticle aggregation and ionic DNA binding.[26,27] PVP prevents total aggregation and precipitation of the nanoparticles from the spermine and the salts required for PCR. In detail, 50 μL of 100x AgNP's were added to 50 μL of 1 mM PVP40. Next, 10 μL of 10 mM Spermine and 10 μL 10x Standard TAQ Buffer (NEB) were added. The solution was then vortexed and briefly sonicated for 30 seconds.

3.2.4 Experimental setup

On-chip experiments were accomplished through a custom thermocycler and spectrometer control system illustrated in Figure 3.3. Briefly, a 10 W polyimide film heater (Omega, Norwalk CT) was attached to a glass microscope slide and positioned under a portable 532 nm Raman Spectrometer (StellarNet Tampa, FL). Temperatures within the device were controlled through feedback from a thermocouple on the heater surface, near the reaction well. An Arduino Uno microcontroller was used to independently control cycle temperatures through

activation of the heater and a cooling fan. Thermal cycles and spectrometer readings were synchronized through a custom LabVIEW interface.

SERS data was collected at the end of every reaction cycle from 6 independent readings with 1 second exposure times. All six spectra were averaged and the background was subtracted through a sextic fit. Signal intensity was measured as the peak height of one dye specific peak (R6G: 1515 cm^{-1}; Cy3: 1400 cm^{-1}). Real-time PCR progression could then be monitored in LabVIEW with the increase in peak heights versus cycles. All post-processing was accomplished with custom MATLAB scripts.

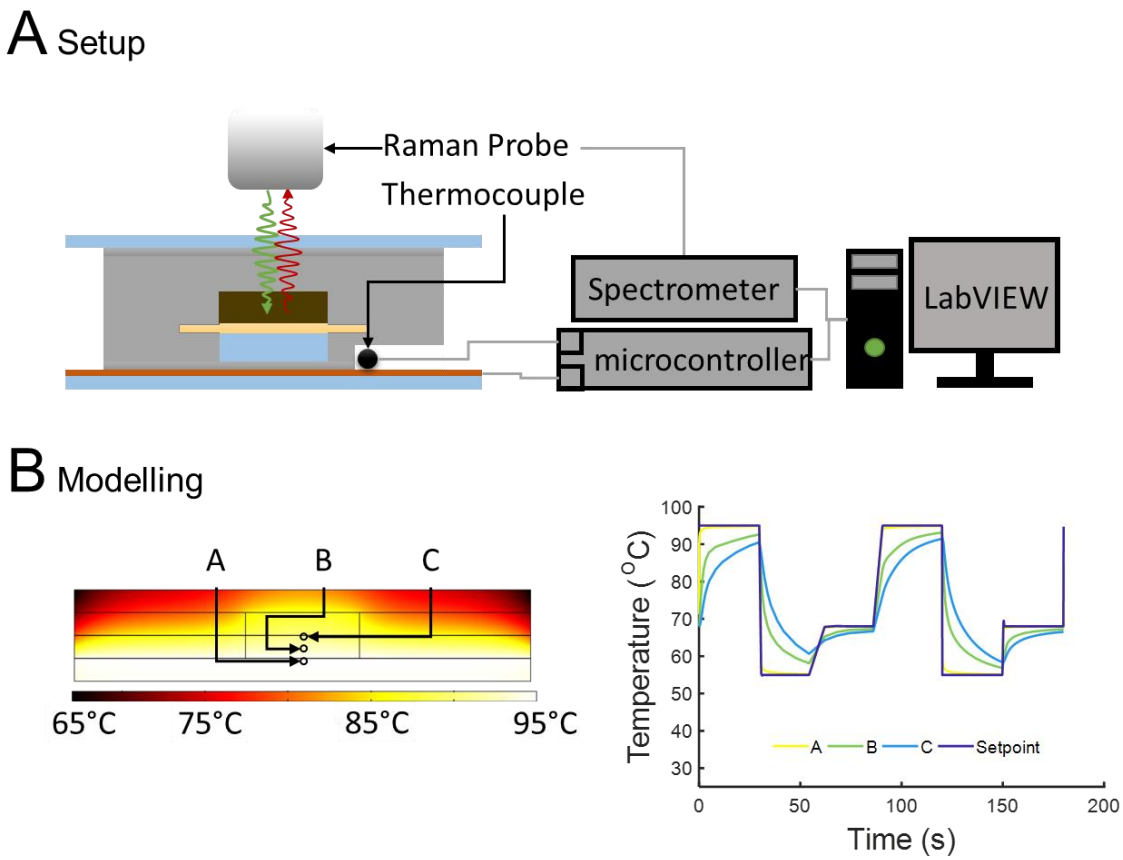

Figure 3.3: Illustration of device setup and estimated thermal profile during PCR. A: PCR/Raman control system including a surface mounted thermocouple that feeds data to a microcontroller connected to a LabVIEW interface to synchronize temperature and spectrometer control. B: Thermal profile estimated through a COMSOL FEM model. Three points were chosen to highlight the produced temperature gradient. (A) (B) and (C) represent the bottom, middle and top of the PCR well respectively.

3.2.5 Thermodynamic Modelling

The difficulty of monitoring temperatures within the sample wells was alleviated through monitoring of surface temperatures near the well. However, it was important to ensure reliable temperature control in the presence of the membrane and nanoparticle well. Toward that end, a finite element model was constructed in COMSOL (Burlington, MA). A multiphysics simulation was run

with combined thermodynamic and pressure driven fluid dynamic models to allow thermal mixing. Temperature conditions similar to PCR reactions discussed below were applied to a thin heater below the simplified chip geometry Figure 3.3.

3.2.6 PCR Reactions

As PCR in thermoplastic chips is well established, the untested aspects of this assay that require validation with PCR are the presence of spermine and the dialysis membrane. These factors were tested off-chip independently using an established TAQ-Man assay for the FemB MRSA gene.[18] These reactions were run as published on a Miniopticon thermocycler (Biorad Hercules, CA) with a ZEN double quenched probe and PrimeTime master mix from IDT. A typical 20 μL reaction contained 10 μL PrimeTime master mix, 5 μL 1 μM probe and primers, 2 μL template, and 3 μL of DI H_2O. To test the impact of the membrane on PCR efficiency, small pieces of dialysis membrane were cut and added to prepared PCR reactions; reactions were run alongside membrane free conditions. Next, the impact of spermine was evaluated through reactions prepared with an increasing concentration (1 – 4 mM) of spermine.

On-chip reactions were performed with an augmented mastermix to prevent non-specific reagent loss. A typical 20 μL reaction contained 10 μL PrimeTime master mix, 0.2 μL 100 ug/mL BSA, 0.4 μL 10mM dNTP's, 5 μL 1 μM probe

and primers, 2 μL template, and 2.4 μL of DI H_2O. Two primer sets for the MecA and FemA MRSA genes were used to illustrate the potential for multiplexed SERS-PCR. The primer set for MecA was used as published previously[18], while the FemA primers and probe were generated through primer blast. All sequences are listed in Table 3.1.

Table 3.1: Sequences used for PCR targetting the Methicillin resistance gene MecA and the Staphylococcus Aureus gene FemA

	Sequence	**Dye**
Mec A		
Forward primer	CAA ACT ACG GTA ACA TTG ATC GC	
Reverse primer	GCT TTG GTC TTT CTG CAT TCC	
Probe	AGA AGA TGG TAT GTG GAA GTT AGA TTG GGA	cR6G
Fem A		
Forward primer	ACA CTT TCA TAA CAG GTA CAG CA	
Reverse primer	CCA TAC AGT CAT TTC ACG CAA AC	
Probe	GCT GCA AT GAC CTC GTT ATT ATT GTT TTT T	Cy3

All on-chip reactions were setup in a rapid three step process illustrated in Figure 3.2B. First, finished chips were loaded via pipette with 20 μL of sample per PCR well. Next, 20 μL of fresh aggregated colloid was added to each upper well. The top surface was then wiped with a cotton swab dipped in methanol to remove and sample or nanoparticle residue. Finally, the chips were sealed with another polypropylene foil and placed in the custom thermocycler. Cycle settings were set to 30 seconds each for the melt, anneal, and extension steps that were held at 95, 55, and 67°C respectively. PCR amplification is commonly quantified

by the cycle at which the signal surpasses a noise threshold. In this work, cycle threshold (Ct) was calculated as the first cycle at which the signal surpassed the mean of the first 15 cycles plus 10 times the standard deviation over those cycles.

Diffusion rate experiments were performed with PCR "samples" that were pre-run off-chip then spiked into the reaction well as stated above. The thermocycler was then set to maintain 55, 67, or 95 °C for 1 hour with readings taken every 1 minute.

3.3 Results

To address common limitations in current SERS adaptations of PCR assays, a novel, low-cost thermoplastic chip was constructed to enable simultaneous reaction and product separation during PCR. Devices were fabricated with the rapid, scalable combination of laser ablation and thermal bonding. The dialysis membrane is readily embedded in the chip during boding through softening of the PMMA at its glass transition temperature (105 °C). Indention of the PMMA surface around the dialysis membrane forms a tight seal around the membrane preventing leakage around the edges. Even at temperatures at and above 95 °C, no evidence indicated leakage around the membrane edges, leaving the dialysis pores as the only mass transfer path between the reaction and SERS wells.

The small dialysis pores prevented any significant reagent or DNA loss to the SERS well which can be qualitatively assessed by the amplicon intensities visible

in the PAGE gel (Figure 3.4) comparing on and off chip PCR reactions. The membrane also completely isolated the large nanoparticle clusters from passing through to the reaction well; nanoparticles were assumed to be absent from reaction well, as they showed no increase in opacity at the end of any reaction.

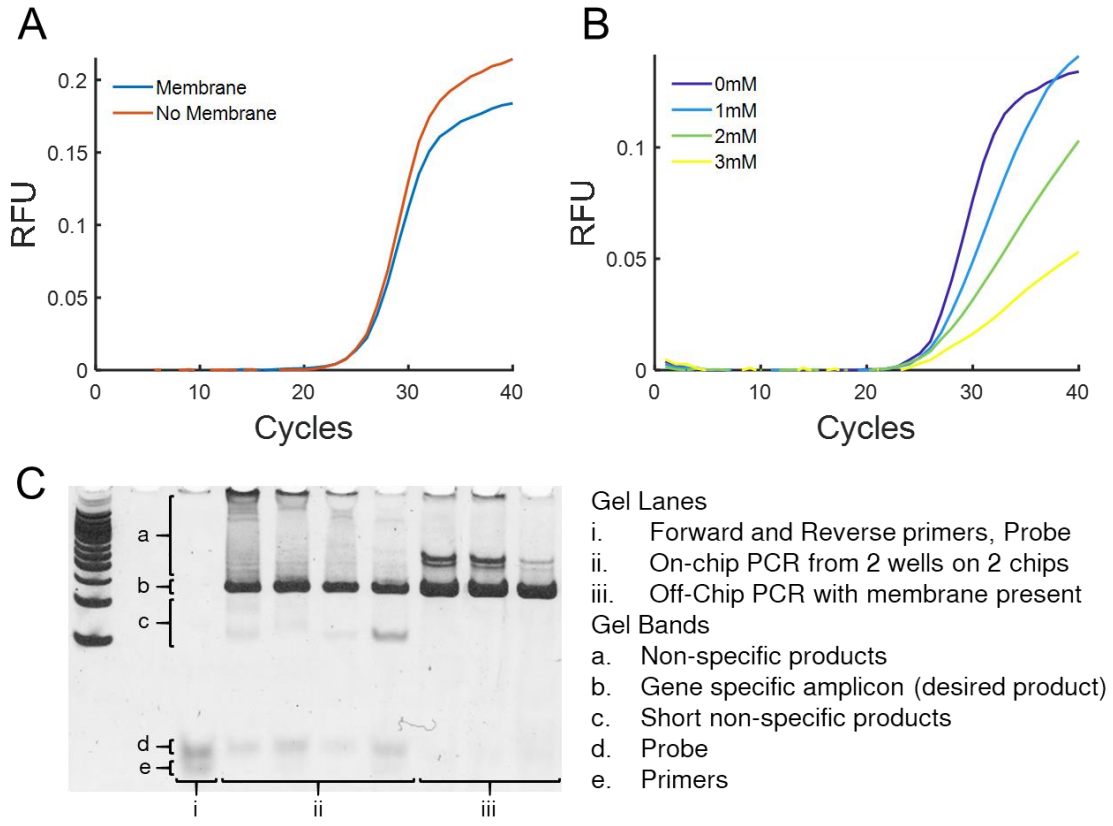

Figure 3.4: Evaluation of potential PCR inhibitors. A: PCR run off-chip to evaluate inhibition by the dialysis membrane (n=3 for samples with and without the membrane). B: Spermine inhibition of PCR at concentrations only above the on-chip assay concentration of 1mM (n=1 for each concentration). C: PAGE separation of PCR reactants (i) and products (ii & iii) in the presence of the dialysis membrane. Diminishing intensity of the probe band (d) indicates successful digestion during amplification.

Temperature accuracy for PCR on chip was first validated through a finite element model in COMSOL. Figure 3.3 illustrates the estimated temperature

distribution throughout the reaction well at each PCR phase over two full cycles. The combined thermal mass of the PMMA and the additional liquid in the SERS well serve to insulate the reaction well. Heating and cooling rates decrease towards the middle of the chip, creating gradients of up to 5 °C initially, though these seem to decrease to less than 3 °C over the course of additional cycles. While precise temperature control is ideal, these gradients are within the optimal range for these primers (data not shown) and do not appear to significantly impact reaction efficiency.

Prior to on-chip assays, the impact of two potentially inhibiting chip conditions were evaluated independently off chip to ensure uninhibited PCR reactions. First, the membrane presents an untested surface for PCR reagents that may irreversibly adsorb onto the membrane. Figure 3.4 shows no change in signal development throughout the assay. Spermine however, does lead to a concentration dependent impact on the PCR signal. The spermine appears to primarily effect the endpoint signal amplitude without much shift in cycle threshold until 3 mM spermine is present. Fortunately, the 1 mM concentration introduced to the nanoparticles for SERS appears to have only a minor effect on signal development. PAGE results highlight successful amplification of the desired products in the presence of the membrane both on- (ii) and off-chip (iii); though band intensity differences may imply a small drop in reaction efficiency

on-chip. Intensity results can also indicate the expected degradation of the dye labelled probe (band d), suggesting successful liberation of a dye required for SERS.

To validate the potential for real-time analysis of diffusion across the dialysis membrane, qPCR probes were degraded in an off-chip PCR reaction, then spiked into sample wells of the chip. During thermal cycling the dyes rapidly accumulate in the SERS well and can be distinguished from the background within 1-2 cycles. Conversely, when a fresh PCR mixture is loaded into the chip without a template to amplify, little to no signal develops throughout the 41 cycles displayed in Figure 3.5B. Notably, a background signal from the inherent Raman activity present in the PMMA structure is present in all spectra collected Figure 3.5. However, with the Raman probe focused within the colloid, even the most intense PMMA peak around 1450 cm^{-1} is consistently only 400 counts and therefore not enough to obscure either the R6G or the Cy3 spectra.

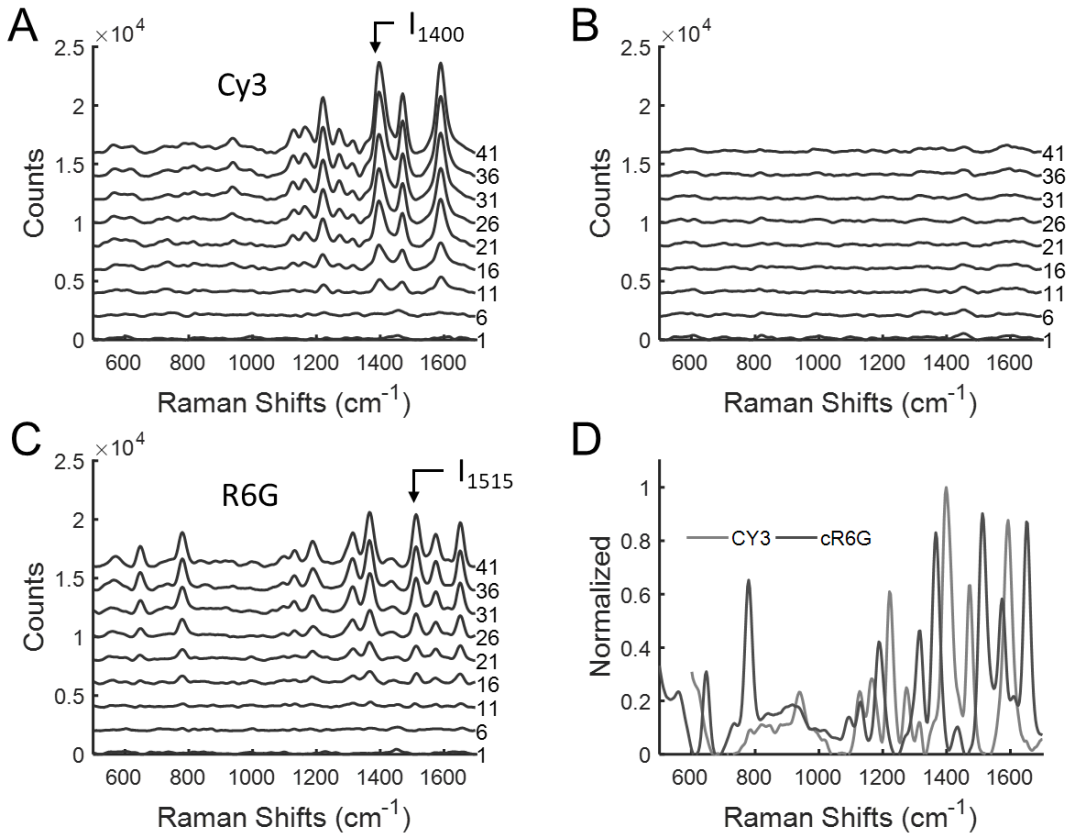

Figure 3.5: SERS spectra collected from pre-cycled PCR samples added to the SERS-PCR chip. A: Cy3 signal development over time from diffusion of the pre-amplified FemA gene. B: Blank signal from FemA PCR mixture without pre-cycling and with no added MRSA genome. C: R6G signal development over time from diffusion of the pre-amplified MecA gene. B and C: I_{1400} and I_{1515} represent the intensity of the peak for quantification of signal intensity from Cy3 and R6G respectively. D: Overlapped spectra from degraded FemA (Cy3) and MecA (R6G) highlighting distinct peaks.

To test the impact of each PCR phase on the diffusion of dyes across the membrane, pre-amplified samples were spiked into SERS-PCR chips and held at either the melt temperature (95°C), the extension temperature (67°C), or the anneal temperature (55°C). These data (Figure 3.6) show an expected increase in diffusion rate with an increase in temperature; however, the apparent diffusivity appears to plateau starting above 67°C.

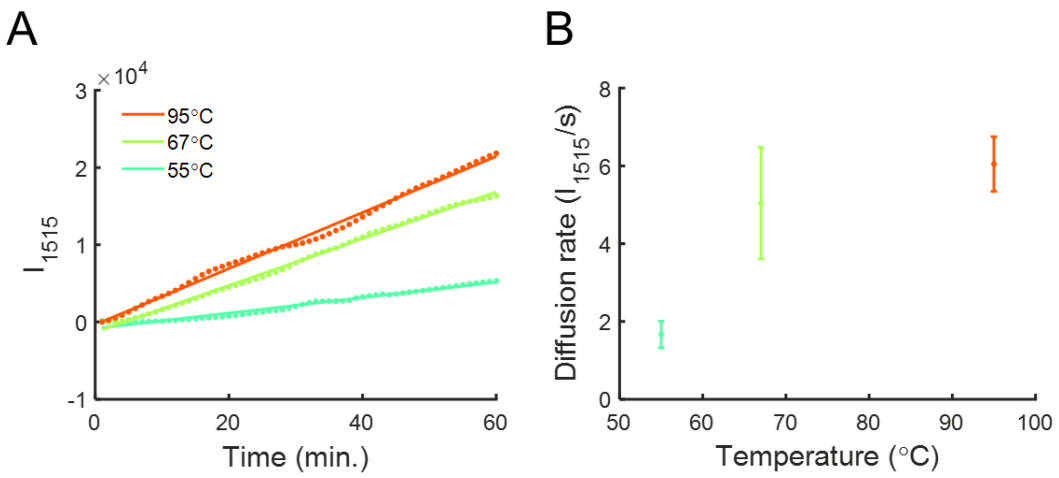

Figure 3.6: Temperature dependent diffusion rate of degraded MecA probe (R6G) into the SERS well. A: Average (n=3) signal generation profile of dye transfer across the embedded dialysis membrane at 95°C (red), 67°C (green), and 55°C (cyan). B: Calculated diffusion rate (linear fit slope) plotted versus temperature.

The real-time Raman signal growth as the dye accumulates in the SERS well can allow the differentiation of template concentrations. Figure 3.7 illustrates the concentration dependent signals from an increasing concentration of MRSA genome from $5x10^5$ copies through $5x10^7$ copies. Figure 3.7A shows real-time signals generated from the PCR reactions. These curves show signals increasing at a rate dependent on the starting concentration, though it is clear that there are non-linear effects that dampen signal generation as the starting template concentration decreases from 10^6 to 10^5 copies/μL. As absolute signal intensities appear to decrease rapidly with concentration, cycle threshold calculations for each dye were calculated independently for each run. Cycle thresholds were calculated as the cycle at which the signal intensity surpassed the background signal detailed in the methods. Ct values were calculated to be 22.33 ± 2.5, 24.5

± 1.9, 37 ± 2.7, and 53 ± 7.6 cycles for 10^5, 10^6,10^7, and the NTC respectively. Though there is a distinctly non-linear trend, the calculated Ct's exhibit a clear concentration dependence.

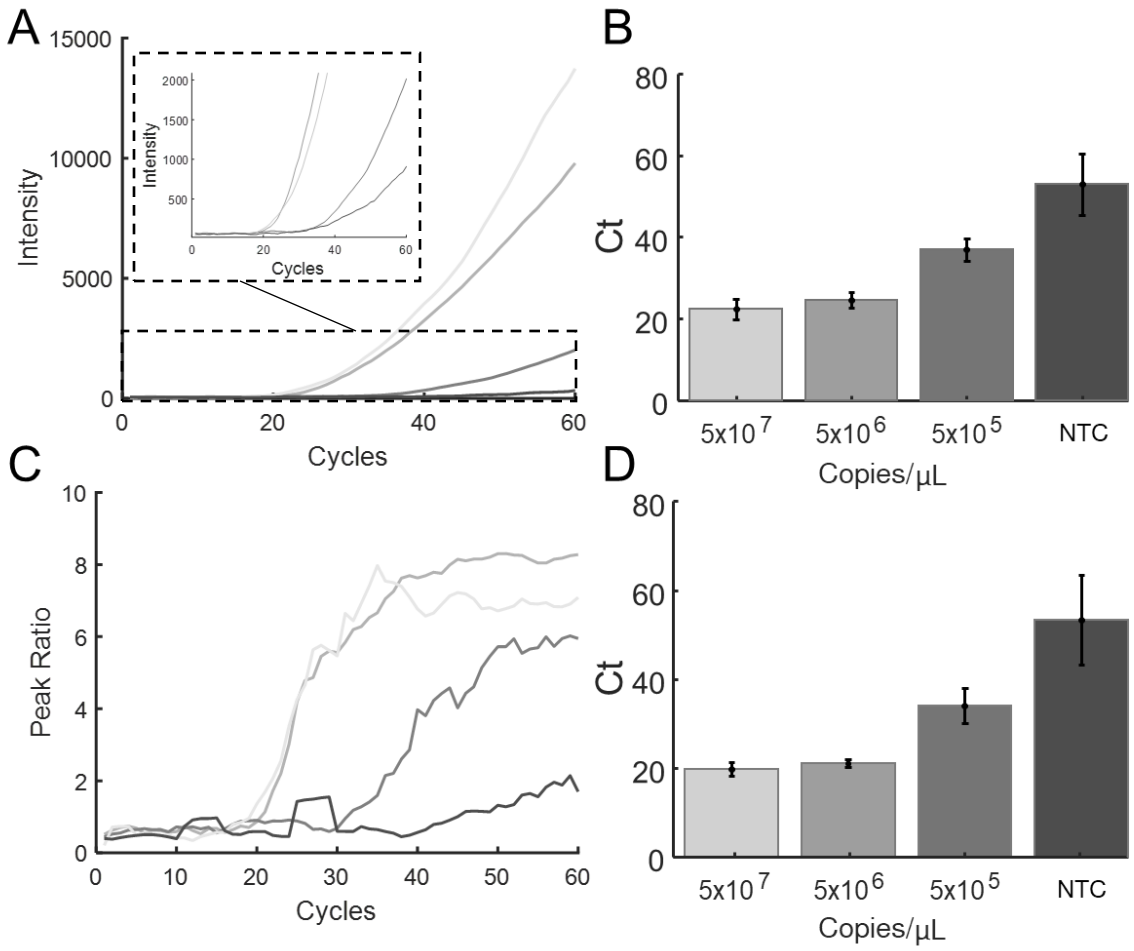

Figure 3.7: Real-time and quantitative data for SERS-PCR. A: Averaged data for increasing concentration of MRSA genome amplified in a PCR reaction on chip and quantified with SERS. Concentrations tested were $5x10^7$ (n=3), $5x10^6$ (n=4), $5x10^5$ (n=5), and an NTC (no-template control, 0 copies) (n=3). B: Cycle threshold (Ct) calculated as the first intensity value to surpass the calculated noise level defined as the mean plus the ten times the standard deviation of the first 15 cycles. C: Peak height from A (I_{1515}) normalized to a control point (I_{1400}). D: Ct values calculated from normalized data in C; threshold was defined as a ratio of 1.0. A-D: Line colors in A and C darken with decreasing concentration and correspond with colors and concentrations in B and D respectively.

In Raman spectra, relative intensities of various locations in a spectrum should be relatively consistent in a given set of conditions, it is possible to normalize peak heights to intensities at other wavenumber values. For instance, Figure 3.7 shows simpler signal discrimination and sharper reaction transitions when the I_{1515} is normalized to intensity at 1400 cm^{-1}. With this method, a sample-independent threshold of 1.0 can be used to calculate nearly identical Cts.

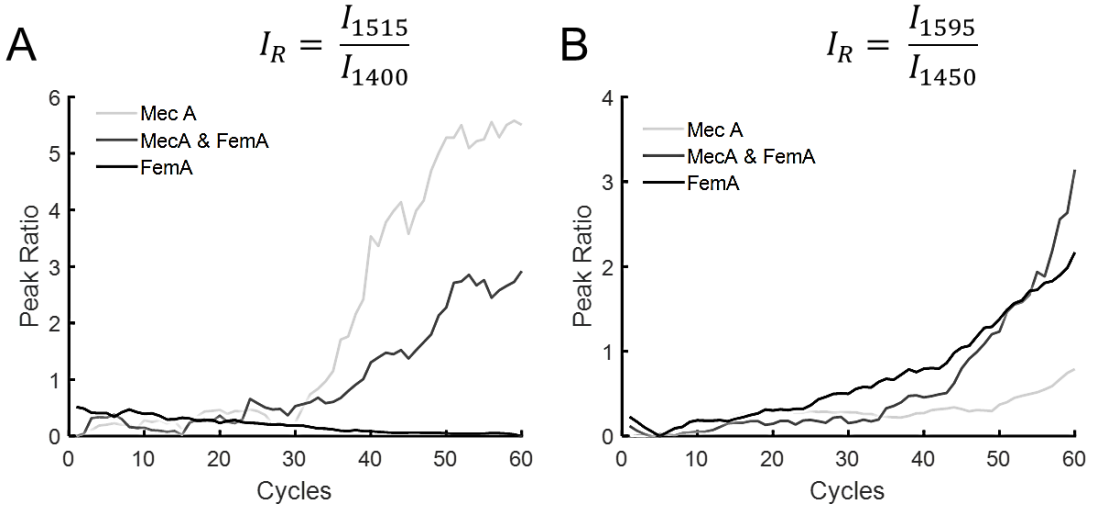

Figure 3.8: Multiplexed detection of MecA and FemA MRSA genes with SERS. A: Peak ratio for identification of R6G (MecA). B: Peak ratio for identification of Cy3 (FemA). A & B: light, medium, and dark grey indicate MecA primers only, MecA & FemB primers only, and FemA primers only.

Finally, achieving a multiplexed reaction requires simultaneous detection of both the FemA and MecA genes. To accomplish this, FemA and MecA primer sets were loaded into a single reaction on chip allows amplification and identification of both genes from a single well. Figure 3.8 shows a similar peak ratio method to isolate MecA (R6G) and FemA (Cy3) signals from an overlapping signal. The R6G ratio used (I_{1515}/I_{1400}) shows a slight decrease when

FemA is present as 1400 cm^{-1} is also a peak in FemA, but as the R6G signal dominates the signal ultimately follows a similar trend. Detection of Cy3 is possible with the ratio: I_{1590}/I_{1450}. The FemA signal alone shows a drifting background, but ultimately similar amplification profile as the signal with MecA and FemA primers combined. In both cases, only when the appropriate dyes are present, does the desired signal appear in from each ratio.

3.4 Discussion

Presented here is a novel approach to PCR assays that utilizes a low-cost fluidic device to enable real-time readout using SERS for the first time. Portable diagnostic devices require low-cost implementations of highly sensitive assays with high multiplexing density. SERS has long been presented as a potential solution for portabilizing PCR, but required new procedures on top of existing protocols. SERS-PCR devices are fabricated using simple and scalable techniques based on laser ablation and thermal bonding. The combination of these methods provides a platform to rapidly produce devices without the requirement of any liquid reagents. Further, the use of thermal bonding allows direct impregnation of a dialysis membrane between bonded device layers, producing a permanent, leak free seal at temperatures above 95°C. Dialysis membranes have been embedded in microfluidic systems before[28,29]; however our device is significantly

simpler to use and integrate with existing assays and quantification methods like SERS.

Thermodynamic modelling was used to estimate the temperature profile within the PCR well through each phase of a PCR cycle. Results show the existence of a temperature gradient throughout the well. Fortunately, the extent of the gradient at each of the three phases is within traditional PCR parameters and should not significantly impact PCR efficiency. Though 1 mm thick PMMA presented a simple development platform, thinner layers may help to reduce thermal gradients in the future through reduced thermal mass around a smaller reaction volume.

Publications have detailed inhibition of PCR through reagent contact with various materials.[30,31] As a result, BSA was added to the PCR mixture to passivate the PMMA and the impact of the membrane on PCR efficiency was tested off-chip. Shown in Figure 3.4, tests suggest that the dialysis membrane presents a relatively inert surface for the PCR reaction. Above the membrane, the nanoparticle solution contains three primary components: AgNP's, PVP40, and spermine. The AgNP's and the PVP are both relatively large and unlikely to pass through the pores of the membrane, that have a MWCO of 20 kDa. Spermine, however, is relatively small molecule (MW 202.34 Da) and can readily diffuse across the membrane. Further, as a cationic polymer spermine has the potential

to inhibit PCR at high concentrations through complexation with primers and genomes. The impact of spermine on PCR was tested at and above the concentration introduced to the nanoparticles, 1 mM. Figure 3.4 shows slight alteration in the amplification profile for 1 mM spermine, but no significant alteration in the Ct or endpoint signal intensity. Though higher concentrations may have an effect, practical diffusion limits reduce the equilibrium concentration to 0.5 mM at most, while the expected concentration is likely much lower due to adsorption of the spermine onto the nanoparticles.

Quantification of the assay progression relies on the specific transfer of dyes liberated through the assay process and retention of intact probes. Figure 3.5 shows signals developed over the course of assays containing only degraded or intact probes. Specifically, the Cy3 signal growth seen in Figure 3.5A contrasted with the lack of signal developed in Figure 3.5B demonstrates successful passage of digested probes and effectively full exclusion of unreacted probes.

The thermal impact on diffusion was tested to explore the impact of high temperatures on diffusion rates across the dialysis membrane. Results show a large increase in diffusion rate between 55°C and 67°C with a plateau of the between 67°C and 95°C. These results suggest, at least, that diffusion and signal production are not drastically hindered by high temperature effects on the

membrane or nanoparticles. However, a complex temperature dependent mechanism is present and will be explored in future studies.

PCR reactions performed on-chip show successful generation of a liberated dye and a quantifiable accumulation of the dye on the SERS side of the membrane. The signal development rate in on-chip reactions (Figure 3.7) is distinct from that of signals from pre-run samples (Figure 3.6). Specifically, on-chip reactions exhibit an exponential growth pattern, unlike the linear growth pattern expected and found in predegraded probe. An exponential signal is indicative of an increasing concentration gradient generated through dye liberation throughout the course of the assay, while a linear signal is easily explained by a constant gradient. All concentrations tested are distinct from the negative control. Further, average Ct values calculated for each concentration indicate a concentration dependent signal development rate. Discrimination between concentrations is difficult at high concentrations, but non-linear effects increase separation as the concentration decreases towards the negative control. Future work will explore this delayed amplification rate and seek to improve amplification efficiency.

Finally, with this work we successfully show multiplexed PCR through amplification of two MRSA genes MecA and FemA. Figure 3.8 shows that that signals from each primer set can be independently identified with a distinct peak

ratio chosen for each dye. When the primer sets were combined, both dyes can simultaneously be identified in signals calculated with both ratios. While this early demonstration detects a single pair of genes, the spectroscopic benefits of SERS are often used for many dyes simultaneously.[11,22,32,33] In theory, this work requires little effort to expand across a much wider library of genes and dyes.

3.5 Conclusion

In this work, we demonstrate the first real-time, multiplexed PCR assay with SERS. Based on high temperature dialysis in a novel and low-cost thermoplastic device, we are able to separate digested PCR probe dyes from a TAQ-Man like reaction from an ongoing assay. Dialysis enables elimination of post-processing steps through isolation of the SERS colloid from the PCR reaction. With this system, we show a thermodynamic model to validate precise temperature control and controlled, temperature dependent diffusion of dyes into a SERS colloid. PCR reactions were successfully run on chip allowing simple, real-time identification of both the MecA and FemA MRSA genes. Finally, we show simultaneous, multiplexed detection of these genes in a single SERS-PCR reaction and from a single well.

Chapter 4. Integrated concentration, handling, and detection of organic analytes in a sponge-like PDMS matrix with Surface Enhanced Raman Spectroscopy

4.1 Introduction

Raman spectroscopy and the more sensitive surface enhanced Raman spectroscopy (SERS) have long been hailed as promising techniques, whose sensitivity and specificity could rival entrenched methods such as IR spectroscopy and fluorescence. However, since the discovery of surface enhancement by noble metal nanostructures[1–4], the field of SERS sensing has relied on complex, expensive, and non-scalable fabrication techniques to produce the metal nanostructures necessary for enhancement.

Traditional nanostructured SERS devices on rigid silicon substrates provide no capabilities for acquiring and processing complex samples, and consequently require laboratory techniques to prepare samples for SERS analysis. The combined impacts of inefficient fabrication and the absence of integrated assay techniques has restricted SERS to academic laboratories and hindered expansion to industrial applications.

Recent work, however, has considered the application of SERS from a systems approach intended to augment SERS sensors with integrated sample

processing techniques. This reimagining of the traditional, rigid SERS substrate has led to new flexible substrates and fabrication methods that are simple and scalable as well as sensors that have integrated functionality to facilitate sample handling away from a laboratory.

Fabrication of the noble metal nanostructures within these sensors is commonly simple and low cost with varying degrees of scalability from in-situ generation of particles[5–7] and soaking, to customizable spot deposition methods such as ink-jet[8,9] and screen printing[108,164]. These methods have been applied to a diverse set of materials, including various flexible membranes[108,111,113,114,164], rigid filters[12], cotton swabs[166,167], adhesives[118], and elastomers[16–18]. Functionally, these materials provide application specific sample processing from sample acquisition with swabs[102,111,166,167], dipsticks[9] and adhesive extraction[118,168], to analyte isolation through filtration[12,20,21], chromatography[22,23], and analyte concentration[20,22].

The existing library of techniques and applications for SERS has highlighted the many advantages of flexible, porous substrates for sample processing. Despite the benefits of wicking in fibrous papers, sample control remains entirely passive, leading to limited sample transfer ability, low sample volumes, and complex multi-step concentration methods. Moving forward, newer and more customizable solutions are necessary to address the limitless conditions throughout the portable application space. In particular, development of a SERS

sensor based on a flexible, 3-dimensional, and porous matrix could allow for a higher sample processing volume and provide active fluid handling methods leading to a more dynamic sensor system for field use.

A 2011 paper by Choi et al introduced the concept of mesoporous sponges from polydimethylsiloxane (PDMS), in order to provide selective processing of organic phases from aqueous samples.[170] The authors demonstrated a simple fabrication method using a sugar cube as a sacrificial template to produce a highly porous, deformable PDMS sponges. The sponges were shown to selectively absorb oil from water, owing to their hydrophobic nature, opening the door for a new domain of simplified sample processing for SERS substrates.

Herein, we present SERS sponges based on flexible, mesoporous, and fully customizable PDMS constructs that improve upon the current limitations inherent in the 2-dimensional nature membrane based devices. This novel sensor substrate is capable of simple customizability through control of the shape of the sacrificial sugar template; nearly any shape can be developed and tailored to the requirements of a particular application. Further, the high flexibility and void volume of the PDMS sponge structure allow for even simple shapes to be reversibly molded to fit necessary application surfaces or voids.

To illustrate use for organic molecules, PDMS sponges are characterized to show the selective uptake of organic solutions and hydrophobic molecules from

aqueous solutions. Two demonstrations are presented. First, an aqueous sample is loaded into a syringe holding a custom fit sponge. The solution then passes through the pores, while the dye is extracted onto the PDMS surface. Second, we demonstrate the potential for controlled organic phase extraction of an analyte in which a sponge saturated with an organic solvent extracts and concentrates organic molecules.

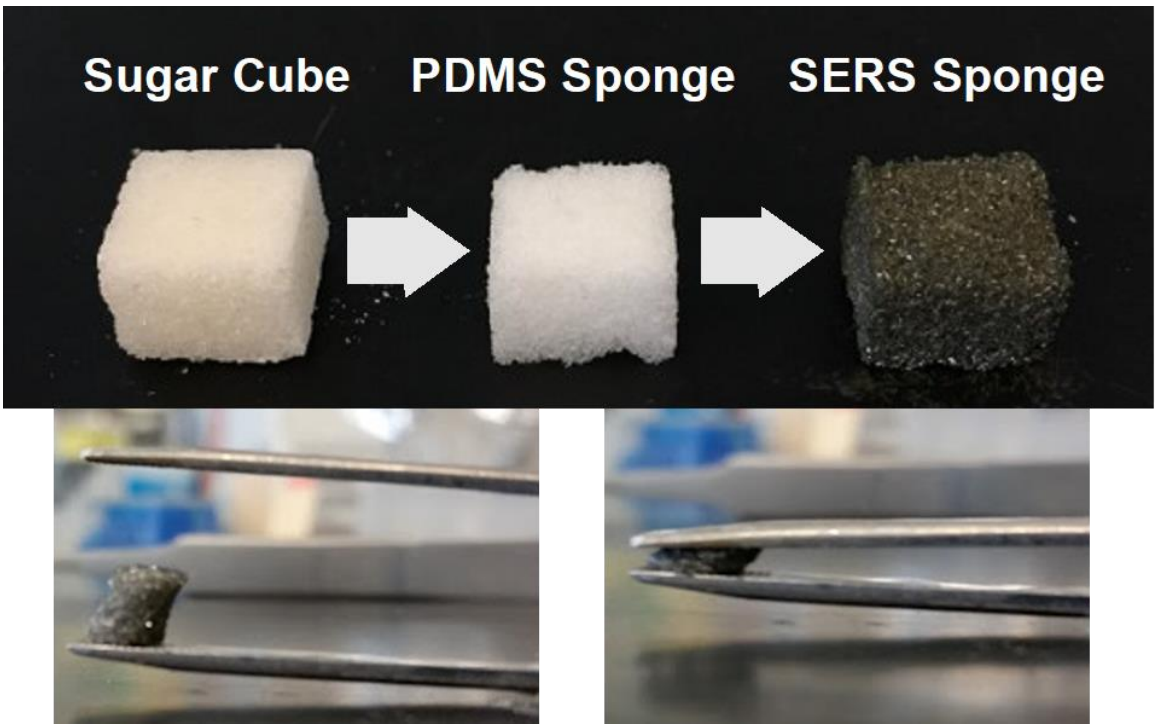

Figure 4.1: Photograph of SERS sponge fabrication process and flexibility. A: fabrication of SERS sponge beginning with the sugar cube template, curing and removal of sugar to form the PMS sponge, and finally decoration with nanoparticles to produce the final SERS sponge sensor. B: Compression of SERS sponge with forceps to illustrate high flexibility and shape conformability of SERS sponges.

Finally, we demonstrate the ability to generate SERS-active PDMS sponges through an adsorption-based nanoparticle decoration procedure. We characterize these sponges both on the macroscale and on the microscale,

demonstrating the detection of three molecules, two of which have direct applications in the field for environmental monitoring. We detect: (i) Rhodamine 6G (R6G), a commonly used Raman dye, (ii) Malachite Green (MG), a common toxic fungicide used in aquaculture, and (iii) Pyrene carboxylic acid (cPyrene), a model polyaromatic hydrocarbon (PAH), which are a class of potentially carcinogenic byproducts of burning fossil fuels.[25–29]

4.2 Materials and Methods

4.2.1 Materials

Sylgard 184 polydimethylsiloxane kit was purchased from Dow Corning (Midland, MI). Half teaspoon sized compressed sugar cubes were obtained from Domino Sugar (Baltimore, MD). Ethanol, methanol, and isopropyl alcohol were purchased from Pharmco-Aaper (Brookfield, CT). Malachite green oxylate salt (MG), sodium citrate tribasic dihydrate, silver nitrate, 1-pyrenecarboxylic acid, and Triton X-100 were from Sigma-Aldrich (St. Louis, MO). 1-decanol was purchased from Alfa Aesar (Haverhill, MA). Rhodamine 6G (R6G, Rhodamine 590) was purchased as a chloride salt from Exciton (West Chester, OH). Dimethyl sulfoxide (DMSO) was obtained from Fisher Scientific (Waltham, MA). All reagents were used according to their safety data sheet.

4.2.2 Nanoparticle Synthesis

Silver nanoparticles were synthesized with a modified Lee-Meisel method, as we have described before.[8,30] Briefly, the 72 mg of silver nitrate was added to 400 mL of boiling water in an Erlenmeyer flask. A stir bar was set such that the vortex touched the bottom of the flask, and 80 mg of sodium citrate tribasic dihydrate was added. After 10 minutes, the solution was removed from heat, cooled, and verified with UV-Vis spectroscopy. The nanoparticles can be stored after this step for months at 4°C. Alternatively, they can be concentrated right away. The nanoparticles are concentrated about 50 times using a centrifuge at 12000g and 4°C for 20 minutes. They can be stored for a shorter amount of time at 4°C.

4.2.3 PDMS Sponge Fabrication

PDMS sponges were fabricated based on a method adapted from Choi et al.[170] Briefly, PDMS was made by mixing 5 g of the base with 0.5 g of the curing agent by weight. Six sugar cubes were placed into the PDMS and the whole setup placed under vacuum for one hour. The sponges were then removed from the vacuum and baked in an oven at about 80°C for an hour. The cubes were cut away from any excess PDMS in the tray. To remove the sugar cube template, the sponges were placed in a hot water bath and sonicated until the sugar dissolved. Once the sugar is removed, the sponges rapidly become hydrophobic and maintain little to no water within the pores. In order to remove any residual sugar,

solvents that can penetrate the hydrophobic pores, such as ethanol or isopropanol, were used for subsequent washes. The sponges were cut in half at the plane parallel to the side that was initially placed in the PDMS. A 5 mm biopsy punch created sponges with consistent diameters. A schematic is shown in Figure 4.2.

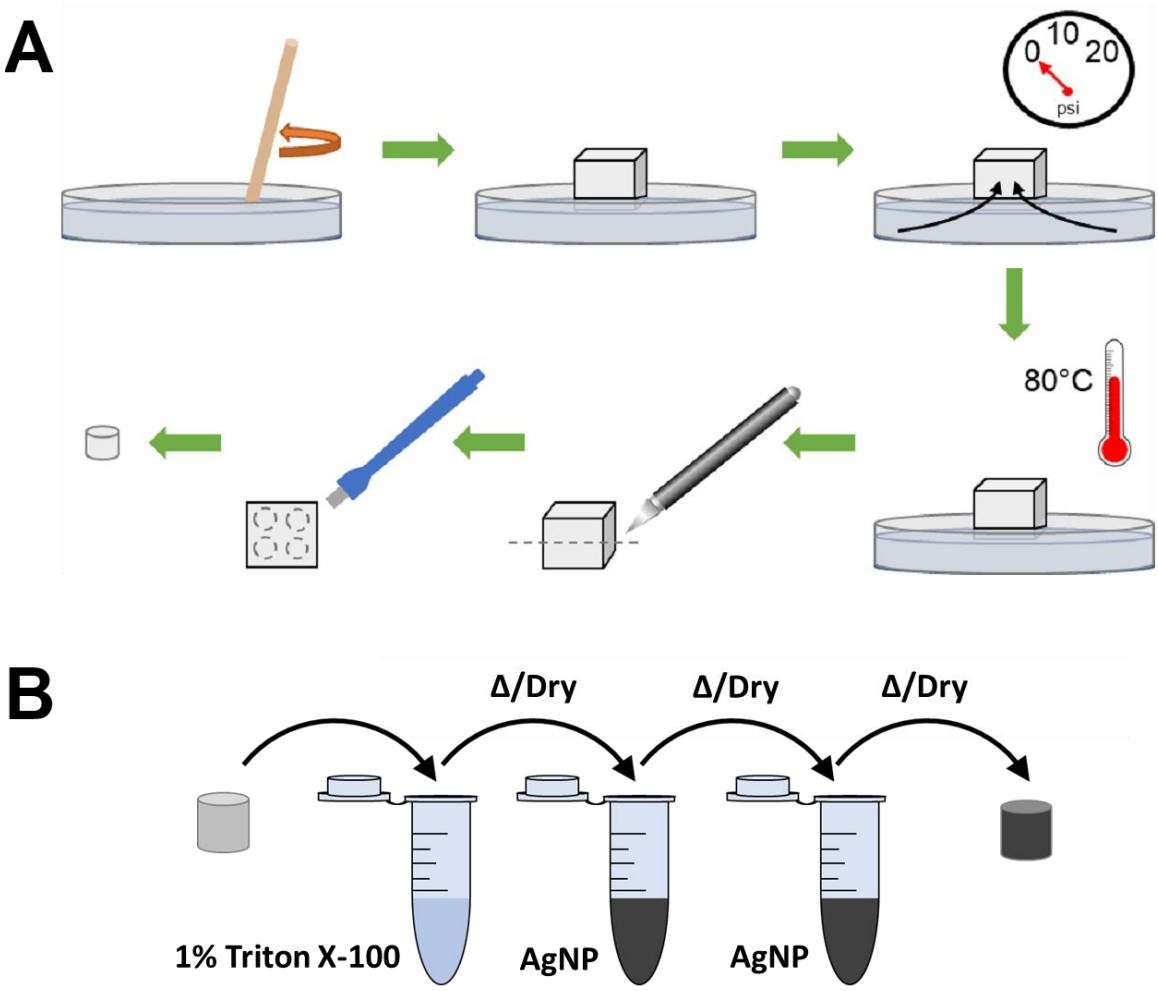

Figure 4.2: Illustration of stepwise SERS sponge fabrication process. A: Process of PDMS sponge fabrication: PDMS preparation, vacuum aided PDMS perfusion of sugar cube pores, heat curing of PDMS, bisection and cylindrical coring for the final sensor shape. B: Process of nanoparticle decoration from a concentration AgNP colloid: surfactant treatment and two nanoparticle submersion steps each separated by a heated dry.

4.2.4 Selective Absorption Characterization

To demonstrate the selective absorption characteristics of the PDMS sponges, a qualitative experiment was performed. Solutions of malachite green in water R6G in decanol were formed. 100 μL of the two solutions were placed next to one another on a glass slide. PDMS sponges both with and without Triton treatment were placed at the interface of the two to observe which solvent was selectively absorbed. Sponges were also placed directly into the solvents to observe which one absorbed into the sponges. Finally, an untreated sponge was placed in the aqueous solution. Forceps were used to squeeze and release the sponge repeatedly to demonstrate that force could be used to absorb aqueous solution into the hydrophobic untreated sponges. Pictures were taken for qualitative analysis.

4.2.5 PDMS Sponge Decoration for SERS

Sponges were treated with Triton prior to adsorption of nanoparticles onto their surface, by incubating them on a nutating mixer for 5 minutes in a 1% v/v solution in ethanol. Triton improves wettability of the sponge and thus allows penetration and direct interaction of the nanoparticle colloid with the surface. They were then centrifuged in a table top centrifuge to fill all pores of the sponge. The sponges were dried in the oven at 80°C for 20 minutes and then incubated in 50 times concentrated nanoparticles for 5 minutes on a nutating mixer.

Following a second centrifugation step, the sponges were removed from the nanoparticle suspension and dried in the oven at 80°C for 20 minutes. This procedure was repeated once more to increase the density of nanoparticles on the sponge surface. The sponges are dried for two hours at 80°C to ensure no residual water is left. Figure 4.2 shows a schematic of this procedure. Sponges were imaged using a S-3400 Variable Pressure SEM (Hitachi, Schaumburg, IL). The accelerating voltage was set between 5 and 10 kV and current to 67 to 74 μA in order to get the best image. EDS mapping was performed on the surface of the sponges to confirm the presence of silver using the SEM system and its associated detector (Bruker, Billerica, MA). For EDS, the accelerating voltage was set to 10 kV and the current to about 65-70 μA.

4.2.6 SERS Measurements

For the creation of standard curves with R6G in water, R6G in decanol, malachite green in water, and cPyrene in water, spectra were taken for three sponges. Stock solutions of R6G and MG were at 2 mM and 1.36 mM, respectively, and then diluted to the appropriate concentration. A stock of 2 mM R6G in decanol was also made and diluted. cPyrene was dissolved as a 5 mM solution in DMSO. It was then diluted in water. To collect spectra, 10 μL 2% HCl was dropped on the surface for R6G and MG. For cPyrene, 10 μL water

was dropped on the surface to keep the total volume applied constant. 20 μL of the R6G, MG, or cPyrene was then pipetted onto the surface of the sponge.

Spectra were obtained using a QE65000 portable Raman spectrometer (Ocean Optics, Dunedin, FL) with a 785 nm diode laser and fiber optic probe (Integrated Photonic Solutions, Monmouth Junction, NJ). The laser power was set at about 15 mW. A custom raster pattern collects 200 predetermined points in the shape of a 3.5 mm diameter spiral on the surface of the sponge. Automated control of the raster pattern was programmed in LabView 2016 (National Instruments, Austin, TX). Spectral acquisition was set to 1 second exposures with 1 accumulation.

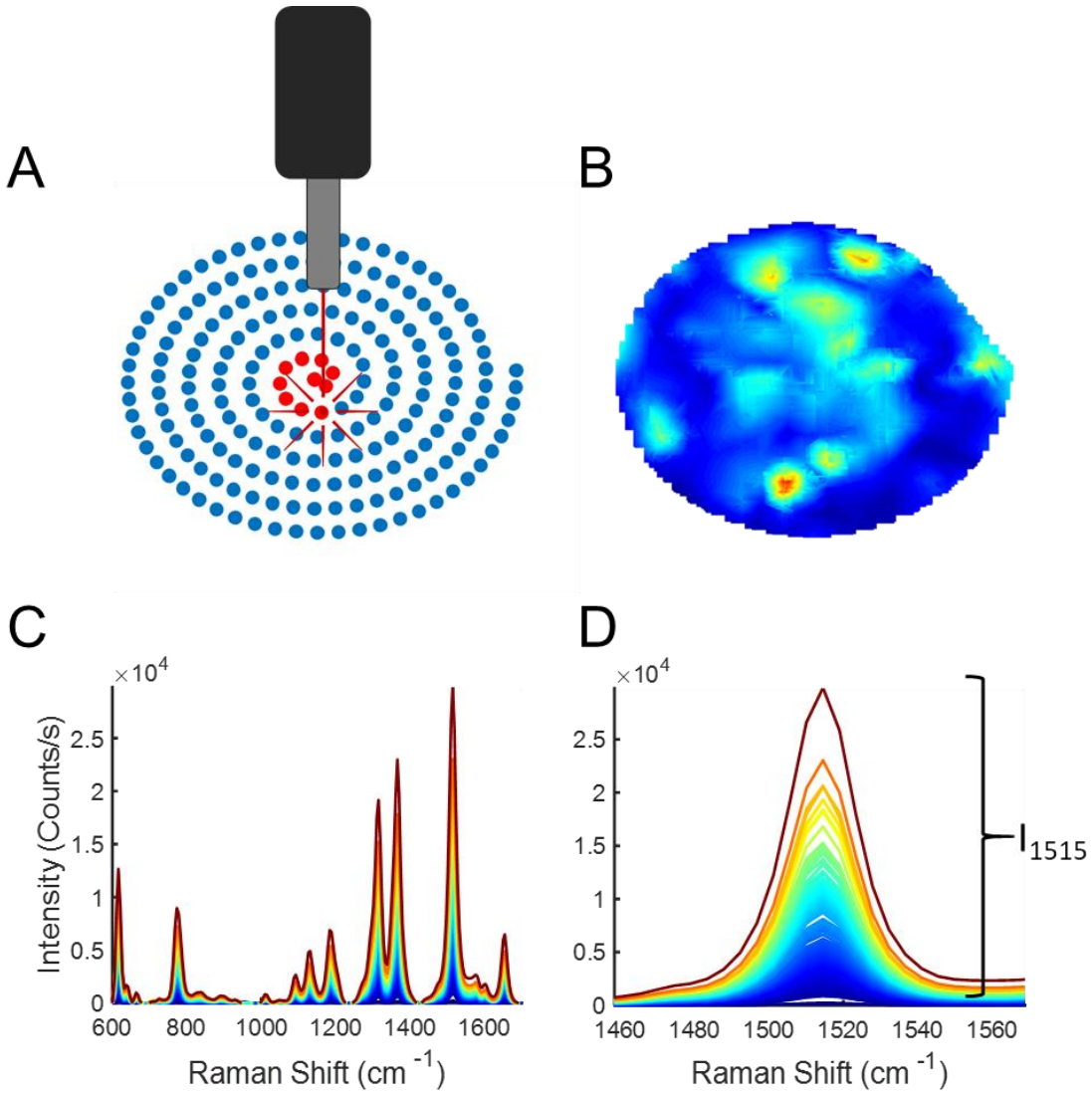

Figure 4.3: Illustration of data collection and analysis process. A: Raster pattern with highlighted movement path (Red) in a predefined spiral path (blue). B: Heat map demonstrating Raman intensity across a sensor surface based on a sample R6G concentration (10 μM); pixels are colored based on the intensity visible in plot C. C: Full spectra for data visible in plot B. D: Isolation of peak value at 1515cm^{-1}, used for quantification of R6G concentration.

4.2.7 SERS data analysis

All spectra were analyzed using a custom code in R2017A (Mathworks, Natick, MA) for analysis. The average spectrum from at least 200 spots per sponge was background-subtracted with a sextic fit. To quantify the spectra, the

1514 cm^{-1} peak was used for R6G, the 1175 cm^{-1} peak was used for MG, and the 1245cm^{-1} peak was used for cPyrene. The code quantified the intensity by finding the local maximum between the two immediate points above and below the indicated Raman shift. Throughout, we will refer to these as I_{1515}, I_{1175}, and I_{1245}, respectively. This intensity was averaged across three sponges unless otherwise noted, and the standard deviation measured across the three sponges. Standard curves were fit with least square linear regression lines. Detection limits were calculated through the linear fit by finding the first concentration above 3 times the standard deviation of the mean.

4.2.8 Concentrating of organic analytes with PDMS Sponges

To assess the ability of the porous PDMS sponges to uptake and retain organic analytes, two demonstrations were designed. First, 5mm sponges were inserted into a 1mL syringe (Becton Dickenson; Franklin Lakes, NJ), that was then loaded with a solution of 1 μM R6G. The syringe plunger was then used to force the solution through the sponge. The impact of sample volume on the amount of R6G retention was tested by loading 0, 1, 2, or 3 consecutive 1mL samples. As fluorescence of the dry R6G was not reliable, a color image was used to colorimetrically estimate the amount of retained R6G. Calculations were performed through isolation of the red channel in the RGB image; the white background was estimated as the mean of the blue and green channels which was

then subtracted from the red channel. The intensity of the sponge area within the monochromatic image was averaged and plotted.

Next, the potential for sponges to passively retain solvents that allow concentration of hydrophobic molecules was tested. We placed decanol-filled sponges in aqueous R6G or cPyrene and investigated the resulting concentration of each analyte. Sponges were soaked in decanol for 5 minutes and then centrifuged to allow the decanol to infiltrate the pores of the sponge. The decanol-filled sponges were then placed in the 1 mL aqueous analyte solutions and incubated on a nutating mixer for 90 minutes. After incubation, the sponges were placed on a glass slide, and the fluorescence was measured. For comparison, a standard curve was created by soaking the sponges in solutions of analyte in decanol. The samples were centrifuged to allow penetration of the analytes throughout the sponge. The fluorescence for all samples was read and quantified from a single image. Concentration factors were calculated based on a linear fit of the intensities obtained in the standard curve surrounding the tested concentration.

All fluorescence measurements were made using a BioSpectrum Chemi HR 410 W/LM-26 Transilluminator (UVP, Upland, CA) with 305 nm excitation and a SYBR Gold filter. The observed fluorescence was quantified using ImageJ

software (National Institutes of Health, Bethesda, MD). The mean pixel intensity value was obtained through a circular ROI on each sponge.

4.3 Results

In this work, we assess a novel flexible SERS substrate based on PDMS sponges. Data and visual demonstrations here illustrate that SERS sponges are able to integrate and improve upon many of the existing features of separate flexible SERS substrates. First, we demonstrate the controlled affinity of PDMS sponges to aqueous and organic solvents. Figure 4.4A and B show the selective uptake of an organic solvent (yellow, decanol) in the presence an aqueous solution (blue). Figure 4.4E provides a simple visual of the perfusion of the organic solvent into the sponge, while the aqueous solution remains on the sponge surface. The hydrophobicity of these sponges can be modified to enable uptake of any solvent through the use of a deposited surfactant (Triton X-100). Shown in Figure C and D, surfactant modified sponges readily uptake both the aqueous and organic phases. A fully saturated sponge with any solvent can, like traditional sponges, be compressed to eject its solution. (Figure 4.4F)

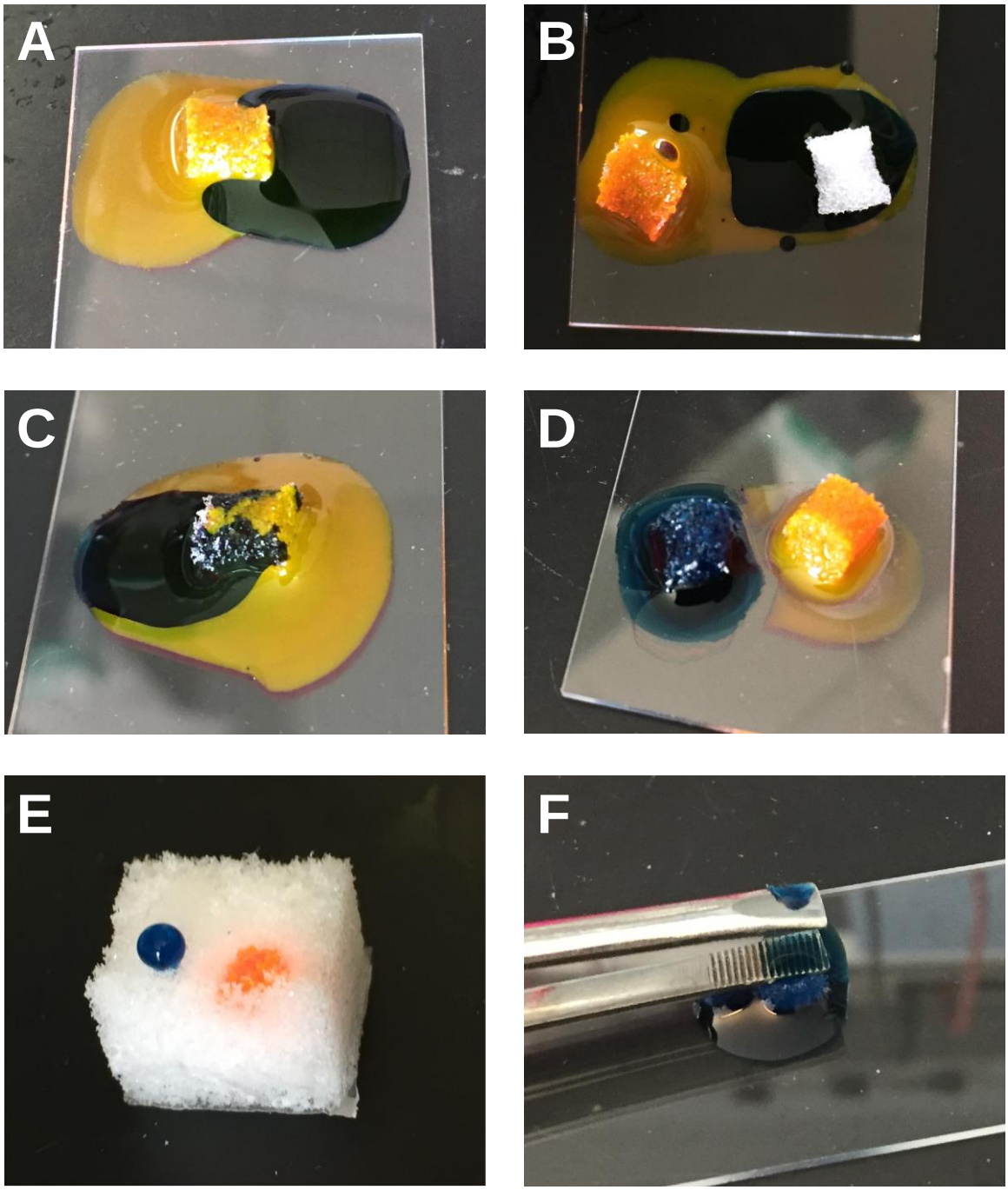

Figure 4.4: Photographs of phase preference for modified and unmodified sponges. A,B,&E: Specific uptake of organic phase (decanol, yellow) over aqueous phases (blue) in an unmodified PDMS sponge. C&D: Mixed and individual uptake of both organic and aqueous phases in a surfactant modified PDMS sponge. F: Ejection of absorbed liquid via sponge compression.

While these sponges can be utilized to directly acquire samples via sponge action, the shape customizability of the sponges allows simple integration with common assay hardware. To demonstrate this capability, we have taken four sponges and fit them to the inner diameter of a 1mL plastic syringe. The syringe was then loaded with a dye (R6G) which was forced through the sponge. Figure 4.5 shows the deposition of R6G on the surface of the sponge through an increasing volume of applied sample. The quantified pixel values of the isolated red channel of a color image are shown in Figure 4.5D. The pixel values show a relatively linear increase in concentration of R6G being deposited on the sponge from 0 to 2mL; a plateau is visible between 2mL and 3mL.

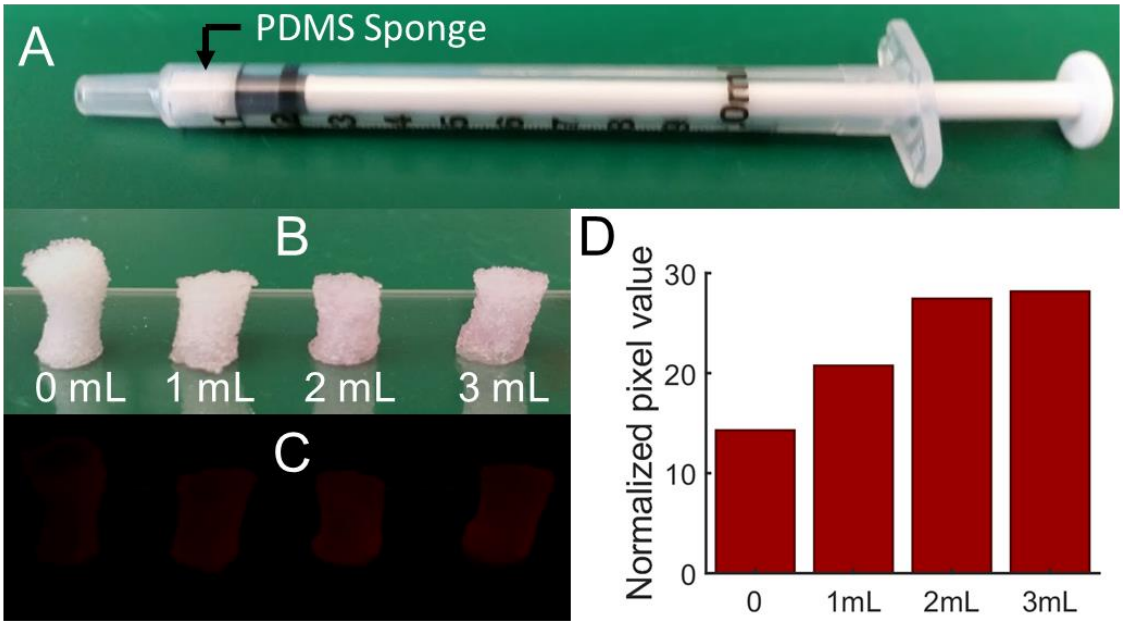

Figure 4.5: Extraction of an organic analyte (R6G) with a PDMS sponge. A: Image of sponge within a 1mL syringe. B: Images of sponges through which an increasing volume of R6G was forced through with a syringe. C: Background subtracted red channel of the image in B. D: Quantified pixel intensity as the average of the sponge area in C.

The porous nature of the PDMS sponge enables retention of solvents and potential concentration of organic molecules through affinity differences known as partition coefficients. PDMS sponges were loaded with an organic solvent (decanol) and placed in aqueous solutions of model analytes (R6G and cPyrene). After an incubation period the sponges were removed from the water and the fluorescence of dyes within the decanol was measured. Figure 4.6 illustrates the concentration process used as well as data obtained for concentration of both cPyrene and R6G. Figure 4.6B shows that for each model analyte, concentration factors are roughly 18 and 8-fold for R6G and cPyrene respectively.

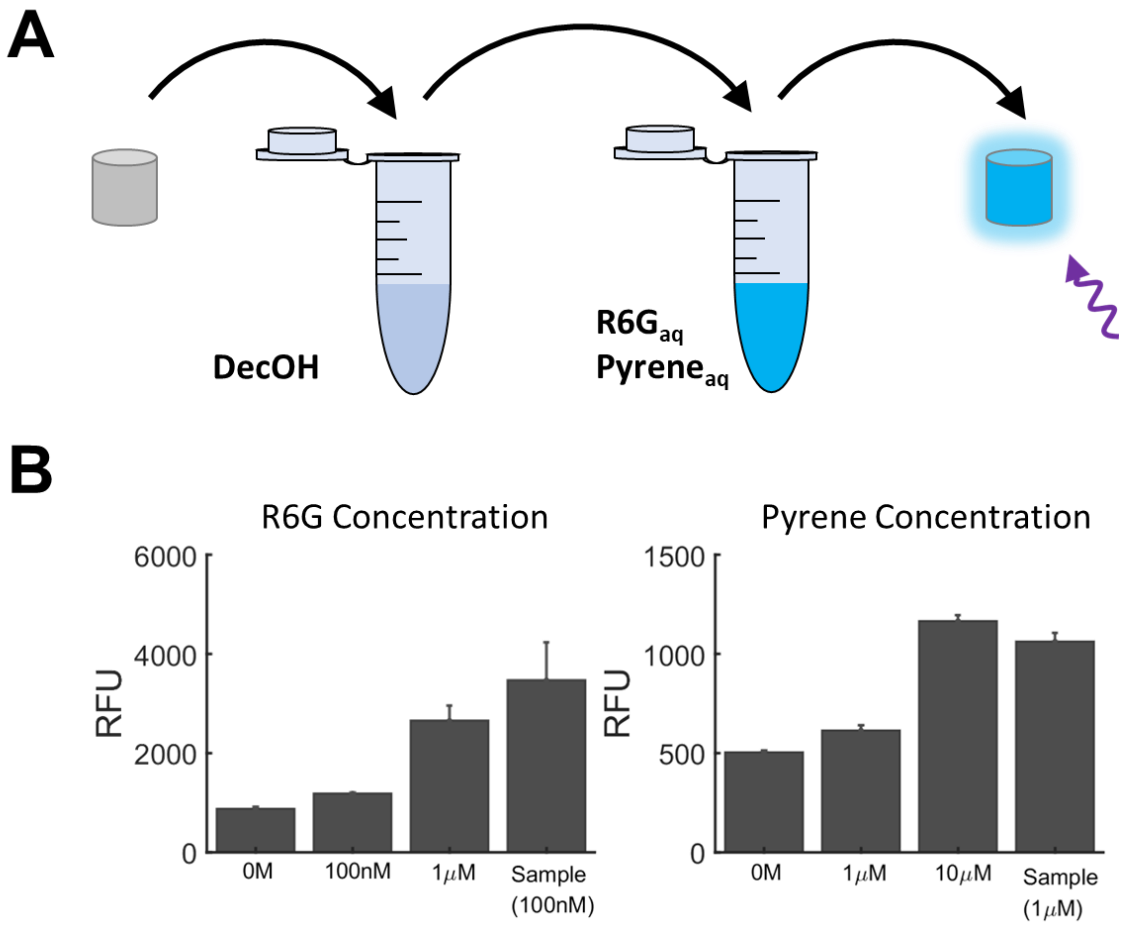

Figure 4.6: Illustration and data of phase based separation of organic analytes with PDMS sponges. A: Illustration of concentration process: decanol is loaded into sponges, which are then added to a sample solution containing either R6G (100 nM) or cPyrene (1 μM), after 90 minutes sponges are removed from the sample and fluorescence was recorded through UV transillumination. B: Quantified fluorescence intensity of dyes concentrated into sponges (Sample) and related concentrations of dyes.

In order to utilize the PDMS sponges as a SERS sensor, they were first decorated with silver nanoparticles. Nanoparticles were produced in a colloid through existing methodologies, applied to surfactant treated sponges twice and dried with heat. The surfactant provided enhanced wetting of the nanoparticle solution and aided deposition of the nanoparticles. SEM was used to visualize

the presence and distribution of nanoparticles on a representative sponge. Figure 4.7 shows three magnifications of the sponge surface and the visible presence of nanoparticles. The nanoparticles, visible as bright, amorphous areas, are seen in various sized aggregates throughout the sponge surface. Figure 4.7D shows superimposed EDS data on Figure 4.7C that illustrates the distribution of silver across the surface. Figure 4.7E shows a photograph of a representative SERS sponge used for further testing. The dark brown-black color is indicative of silver deposition.

Validation of SERS performance was accomplished through testing of three model analytes: R6G, cPyrene, and Malachite green. Tests were performed through raster scanning of the surface on which analyte samples were added. Figure 4.8 shows the summary of data collected for each analyte as well as the molecular structure. Spectra for each of the tested samples are also shown Figure 4.8 i and ii), and highlight the peaks used for quantification of each dye. The HCl treatment eliminates the citrate background from the R6G and MG signals, which dominates the visible field in the cPyrene spectra. The first subplot for each analyte (Ai, Bi, and Ci), shows the mean and standard deviations for the tested concentrations. The data follows a distinctly constant trend with each calculated Langmuir fit having an R^2 greater than 0.99. Notably, standard deviations below the highest concentrations are commonly low, indicating high

reproducibility. The theoretical detection limits were calculated to be 3.25nM, 41 nM, and 1.4 μM for R6G, MG, and cPyrene respectively.

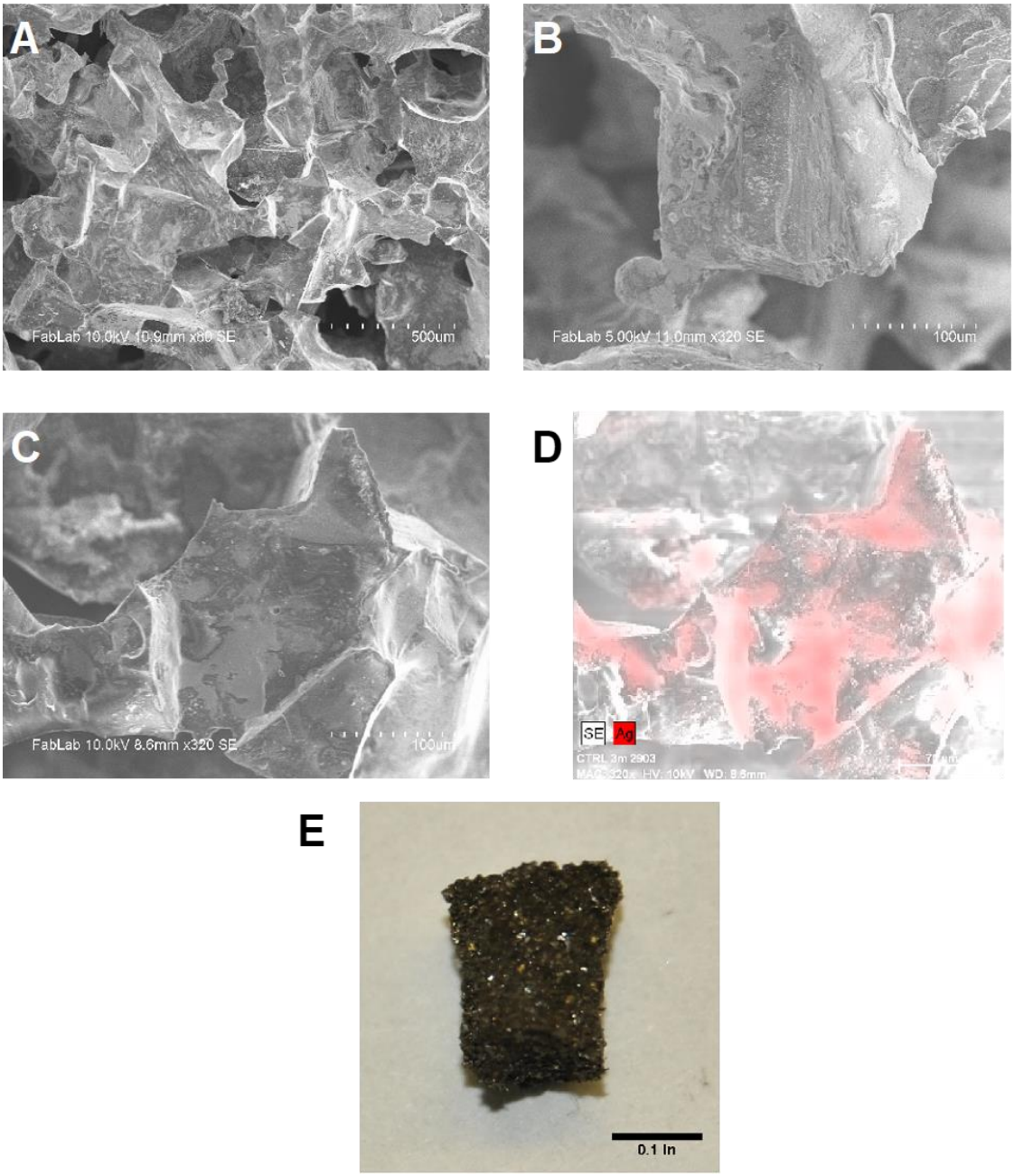

Figure 4.7: Scanning electron micrographs of nanoparticle decoration on SERS sponges. A: View (80x) of SERS sponges with lighter areas indicating silver nanoparticle deposits. B-C: Views (320x) of SERS sponges. D: EDS data superimposed on image C. Red color represents the presence of silver. These confirm the lighter areas as AgNPs. E: Photograph of nanoparticle decorated SERS sponge.

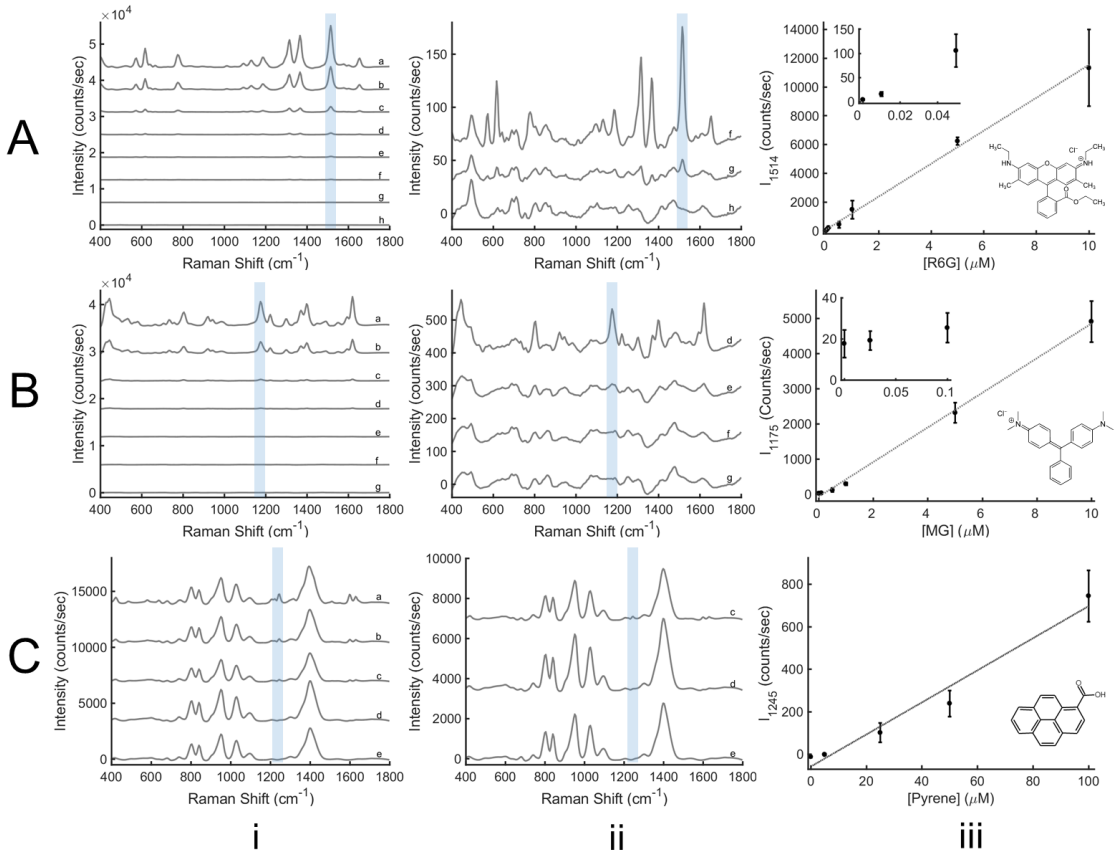

Figure 4.8: SERS sponge data summarizes detection and quantification of three model analytes: R6G, Malachite green, and Pyrene. A-C: SERS data collected via Raster scanning of sponge surfaces. Various concentrations were tested for each analyte. (i) Average spectra for 3 sensors at all tested concentrations. Blue highlighted area represents the peak chosen for quantification of signal intensity. I_{1515} for R6G, I_{1125} for MG, and I_{1245} for cPyrene. (ii) Zoomed view of data from (i). (iii) Concentration vs. Intensity plot based showing mean and standard deviation of the calculated mean peak intensity for each dye. A: Data collected from R6G samples, spectra labeled a-h represent averaged data from 10, 5, 1, 0.5, 0.1, 0.05, 0.01 and 0 μM R6G respectively. B: Data collected from MG samples, spectra labeled as a-g represent averaged data from 10, 5, 1, 0.5, 0.1, 0.025, and 0 μM respectively. C: Data collected from cPyrene samples, spectra labeled as a-e represent averaged data from 100, 50, 25, 5, and 0 μM respectively.

4.4 Discussion

Demonstrations for SERS as a portable sensing technology have successfully improved up on the rigid, lab-centric sensors with lower-cost, flexible substrates

with integrated sample handling functions. Though the diverse materials available for flexible SERS sensors have improved capabilities over rigid SERS substrates, they cannot fully replicate the functions required of lab-free sensing. Specifically, the ability to actively collect and eject samples is difficult with only passive flow in paper based devices and impossible with current elastomeric technologies. Additionally, the microliter sized samples commonly used for the sensors are adequate for certain conditions, but no volume scalability is afforded by 2-dimensional surfaces, and therefore severely limits the number of environmental applications. Lastly, SERS sponges provide a fully customizable platform for sensing that can readily deform or be fabricated to fit the shape and size requirements of any application. In this work, we demonstrate the fabrication and use of SERS sponges for the detection of model organic analytes (R6G, malachite green, carboxy pyrene) from aqueous solutions.

This work is divided into two independent demonstrations of the capabilities of SERS sponges: sample processing and SERS. Sample processing capabilities are illustrated by two examples of concentration of organic analytes. The hydrophobic surface of the PDMS combined with the high porosity provide the capability to extract organic analytes in either brief or prolonged exposures to samples. First, Figure 4.5 demonstrates how traditional assay hardware (i.e. a syringe) can be easily combined with PDMS sponges to allow simple extraction

and concentration of analytes. To a syringe, a single 5mm cylindrical sponge was added prior to loading a 1mL sample. The plunger of the syringe was then depressed fully, forcing the solution through the sponge, then out of the sponge as it was compressed by the plunger. This procedure was repeated on a single sponge up to 2 time for a final sample volume of 3 mL. Figure 4.5D shows an increasing red color coating the sponge surface, indicating R6G adsorption. A simple colorimetric analysis shows an increasing red color with increasing sample volume. This simple demonstration can easily be utilized outside the confines of a syringe through any technique that cyclically compresses and expands the sponge to intake and eject samples repeatedly. Many organic molecules may be similarly extracted from aqueous samples through the increased affinity of the sponge surface for organic molecules.

To highlight the combined benefits of the porous sponge structure and the hydrophobicity of the PDMS, an example of continuous environmental monitoring was devised. In many environmental samples, organic analytes exist at low concentrations or enter large water supplies in periodic bursts. As a result, continuous collection of a single sample may be more beneficial and cost-effective than regular sampling. [31] SERS sponges provide that capability through their ability to retain scalable volumes of water-immiscible organic solvents that can provide phase based separation and concentration of analytes of interest. We

demonstrate this capability through loading of decanol into the sponge pores and inserting them into an aqueous sample containing either R6G or cPyrene. After 90 minutes, the fluorescence of the decanol loaded sponge was compared with sponges directly loaded with dyes dissolved in decanol. The uptake of the dyes was quantified through fluorescence to enable simple quantification. Fluorescence results show not only extraction of the dyes, but concentration by 8 and 18-fold for cPyrene and R6G respectively. (see Figure 4.6) As with the syringe demonstration, this work illustrates a simple but expandable technique for analysis of organic molecules. Pure dye samples present an unlikely convenience in real world samples, however common contaminants such as particulate matter and proteins should be unlikely to enter pores of the sponge or the organic solution. As a particulate and molecular filter, the sponge and organic phase can enable concentration of small molecules and eliminate potential sensor fouling substances.

The highly functional PDMS sponges have been easily converted into high performing SERS sensors through a simple nanoparticle adsorption method. Alongside the obvious color change visible in Figure 4.7E, SEM and EDS images provide evidence of broad distribution of silver throughout the complex sponge structure. This method is simple and scalable to sponges of any size or

shape, and can therefore provide unprecedented control over the design of new SERS sensors.

Performance of SERS sponges to detect and quantify organic analytes was tested with varied concentrations of R6G, MG, and cPyrene. Each of these dyes was dissolved independently in water and applied to the SERS sponge surface. Raster scanning was used to densely evaluate the sensor surface and improve intra and inter-sensor variability. Figure 4.8 presents a summary of the SERS data collected from the three dyes as well as the spectra from which appropriate peak heights were extracted for quantification. Overall detection limits for each of the dyes indicates comparable performance of SERS sponges with existing techniques.[9,26,32] The R6G and MG exhibited drastically improved signals in the presence of HCl to displace the citrate cap present during synthesis of the AgNP colloid. The citrate background is the dominant signal present in the cPyrene spectra, and may ultimately impact the detection limit. Further, the citrate cap created difficulties when approaching phase based concentration techniques with SERS sponges as binding to the nanoparticles was impeded.

Ultimately, these sensors provide a range of potential functional benefits over existing SERS technologies as well as comparable SERS performance. Additional work is necessary to eliminate the adsorption method that requires a capped

colloid. In-situ methods are possible and would be an ideal alternative in future SERS sponge developments.

4.5 Conclusion

In this work, we present SERS sponges; these novel PDMS matrices introduce dynamic control over sensor shape and sample processing currently unavailable in existing SERS sensors. PDMS sponges are demonstrated here to provide sample processing in two potential applications and evaluated with SERS after decoration with AgNPs. First, the sponges rapidly and simply extracted an organic analyte (R6G) from aqueous samples through syringe filtration. The hydrophobic and porous nature of the sponges also enabled phase based separation for continuous sample extraction from aqueous samples; results showed up to 18-fold concentration of R6G in 90 minutes. Finally, successful adsorption of nanoparticles onto the sponge surface provided SERS performance comparable to existing sensors and was applied to detect R6G, Malachite Green, and cPyrene.

Chapter 5. Addressing variance and ambiguity in SERS through optimized sampling methods

5.1 Introduction

Ongoing developments in both academia and industry are positioning SERS as an affordable and simple alternative to existing laboratory techniques. As this approach continues, the nature and complexity of the samples tested with SERS will expand rapidly. Indeed, it is proposed in many publications that SERS is capable of immediate application as a sensitive analytical technique in a number of real-world scenarios.[113,117,118] However, SERS is still often criticized for poor reproducibility.[4–11] Empirical and computational recommendations have been proposed to improve the reproducibility of SERS, but consistent approaches have yet to be adopted.[4,9] Without standard, robust techniques for collecting and processing SERS measurements, SERS will continue to be touted as a "promising" technique instead of a "practical" one.

One of the most promising directions within the field of SERS is the use of low-cost, flexible substrates. Flexible sensors were introduced to replace rigid substrates designed around benchtop laboratory equipment. These new flexible systems augment SERS sensors with additional functions inherent in the substrate such as wicking in paper, which allows sample acquisition, purification,

and concentration.[108,113,117,118,130,179] Further, these sensors are commonly simple to manufacture through scalable processes. However, lower cost fabrication methods introduce nanostructures non-uniformly and increase spot-to-spot variance within and across sensors.

As a surface dependent mechanism, the production of signals is highly dependent on a number of potentially inconsistent factors. The most prominent source of signal variance in SERS stems from randomly oriented surface structures. Non-uniform nanostructures, such as those in colloids and most portable sensor designs, generate large signal disparities depending on the local field enhancements.[6,15] The impact of this on collected signals is shown in Table 5.1 and easily demonstrates the care that must be taken in applying SERS as a quantification technique. In particular, the incredibly small number of molecules necessary for large signal intensities one must strongly consider the impact of excitation locality on the meaning of signal intensity. Sensors that contain randomly aggregated, oriented, and distributed nanostructures must be properly sampled in order to ensure signals are collected from the full range of available enhancement sites. Without sufficient data, Raman intensities may not be representative of the number of analytes present. This effect has contributed, unsurprisingly, to the reputation of SERS as a poorly quantitative method.

Table 5.1: Distribution of SERS enhancement factors between tightly packed silver nanoparticles. (Reproduced with permission, Fang et al.[6])

Raman enhancement factor	Percentage of molecules	Percent contribution to SERS signal
$<2.8 \times 10^4$	0	0
2.8×10^4 to 1×10^5	61%	4%
10^5 to 10^6	33%	11%
10^6 to 10^7	5.1%	16%
10^7 to 10^8	0.7%	22%
10^8 to 10^9	0.08%	23%
10^9 to 10^{10}	0.006%	17%
$>10^{10}$	0.0003%	7%

Fortunately, work by our group and others has shown that the signal intensities produced across analyte dilutions of many orders of magnitude are concentration dependent and relatively reproducible.[108,110,111,180] As the impact of analyte concentration on signal intensity may be uncertain in SERS, it is important to examine the adherence of the produced signal to accepted adsorption behavior. The Langmuir isotherm represents a physically relevant model, because of its derivation from the kinetic process of surface-ligand interactions. Indeed, some groups have shown that SERS intensities readily fit the Langmuir model, indicating that the kinetics of deposition, and therefore signal, are predictably dependent on the analyte concentration. [1,13,16–22]

Despite the achievable adherence of SERS to the Langmuir isotherm, it is clear from the literature that methodological consistency between researchers is a significant concern. Common performance validation methodologies include collection of an arbitrary number of subjectively "random" points across a sensor. It is also common practice for researchers to state or display standard deviations of intra- and inter- sensor signals. However, analyses of the sources of variability are rare. Given the non-uniform distributions of enhancement factors between nanoparticle clusters, it is critical to objectively, consistently, and thoroughly scan sensor surfaces. Without multi-point averaging methods such as Raster scanning, recorded data has a high potential for biased or inconsistent results.

However, in a portable setting time is an integral component in any practical assay. Raster systems can enable automated collection of spectra over a broad sensor area, but at a severe time cost for samples with large exposure times that can exceed 20 seconds per spot. As a result, it is crucial that points be chosen in a manner that is optimized to reduce error with a minimum number of spots. Notably, the Raman probe company Snowy Range Instruments has already begun embedding Raster scanners in their instruments. Unfortunately, no data is available on their orbital scanning technique and any improvements or disadvantages of their chosen algorithm.

In this work, we explore the impact of spot to spot variability and optimization of the number of spots necessary to minimize both intra- and inter-sensor variance. Specifically, we utilized Raster scanning to densely sample surfaces of SERS sponges; from data sets consisting of 200 spots per sensor, we optimized the number of points selected as well as the method for algorithmically and objectively selecting points. Ultimately, we detail a suggested approach to collecting and processing SERS data that can improve spot to spot variability on inherently non-uniform sensors.

5.2 Materials and Methods

5.2.1 Materials

Polydimethyl siloxane (PDMS) was purchased as the Sylgard 184 two part kit (Dow Corning; Midland MI). Sugar cube templates were purchased as half teaspoon compressed cubes (Domino Sugar Baltimore, MD). Ethanol, methanol, and isopropyl alcohol were acquired through Pharmco-Aaper (Brookfield, CT). Sodium citrate tribasic dihydrate, silver nitrate, Triton X-100 were obtained from Sigma-Aldrich (St. Louis, MO). Rhodamine 6G (R6G, Rhodamine 590) was purchased as a chloride salt from Exciton (West Chester, OH).

5.2.2 Sensor Fabrication

Sensor evaluation was performed on SERS sponges as an example of a recent development within the expanding library of flexible substrates. Sponges were fabricated using sugar cubes as a sacrificial substrate following the protocol established in Chapter 4. First, PDMS was prepared in a standard 10:1 ratio of base to curing agent. PDMS was mixed thoroughly and placed in a vacuum desiccator for 20 minutes to eliminate air bubbles introduced through mixing. Sugar cubes were then added to the PDMS and placed under vacuum until the PDMS had fully penetrated the pores between the sugar crystals. Sponges were then place in an oven for 45 minutes at 80C to cure the PDMS. Once curing was complete, the sponges were placed in a water bath sonicator for 100 minutes. The water was then removed and replaced with IPA to improve pore penetration and enhance extraction of internal sugar crystals. Sponges were then squeezed to remove excess liquid and dried in an oven at 80C for two hours. Sponges were cut to useful cylindrical sizes via bisection of the cube and punching with a biopsy punch. Finally, the sponges were prepared for nanoparticle deposition through a surfactant coating. Triton X-100 was applied to the sponges through submersion for 5 minutes in a solution of 1% Triton in ethanol. The sponges were then dried in an oven for 2 hours and stored for future use.

Sensors were prepared through adsorption silver nanoparticles from a concentrated colloid. Silver nanoparticles (AgNP's) were generated through a modified Lee-Miesel method.[17] Briefly, 400mL of milli-Q water was brought to a vigorous boil followed by addition of 72 mg $AgNO_3$ and 80mg sodium citrate. The solution was allowed to boil for 10 minutes before the solution was removed from the heat and allowed to cool. Nanoparticles were then stored until use. To deposit the nanoparticles, they were first concentrated from their initial (1x) solution via centrifugation at 12000g for 20 minutes. The supernatant was then carefully decanted, leaving a 50x concentrated colloid. The sponges described above, were submerged in the nanoparticle solution and centrifuged to ensure full pore infiltration by the colloid. The sponges were then removed and dried for 2 hours at 80C. This process was repeated once more to produce the final tested sensors.

5.2.3 Raman spectrometry

A custom rastering system was built around a portable Ocean Optics QE65000 Raman system (Ocean Optics, Largo FL) at 785nm. Actuation was performed through use of two stepper motors powered through a Gecko motor driver (GeckoDrive; Santa Ana, CA) with stepping control by an Arduino UNO (Adafruit; New York, NY). The spectrometer and the arduino were coordinated with a custom LabVIEW interface. Data was collected from 200 points on the

circular sensor face of 5 sensors in a spiral pattern with constant angular separation and radial expansion from an estimated center point. In addition to the number of points chosen, analyses included different methods for selecting spots included in each subsample. Methods include:

1. Sequential sampling (SS): ordered sampling of points including each sequential point following the path of the laser from the center of the sensor towards the outer edge.

2. Reverse sequential sampling (RSS): ordered sampling of points including each sequential point following the reverse path of the laser from the endpoint at the edge of the sensor towards the center.

3. Linearly spaced sampling (LSS): ordered sampling of points separated by an equal number of unincluded points; for example, two points includes the first and last points, while the 100 points includes every other point from the first to last points.

4. Random sampling (RS): unordered sampling based on generation of random numbers from 1 to 200. Each point within a subsample is forced to be unique.

5. Maximum intensity sampling (HIS): unordered sampling based on peak intensity values. Within the 200 points on a single sensor, the highest signals are chosen based on the sample size.

6. Minimum intensity sampling (LIS): unordered sampling based on peak intensity values. Within the 200 points on a single sensor, the lowest signals are chosen based on the sample size.

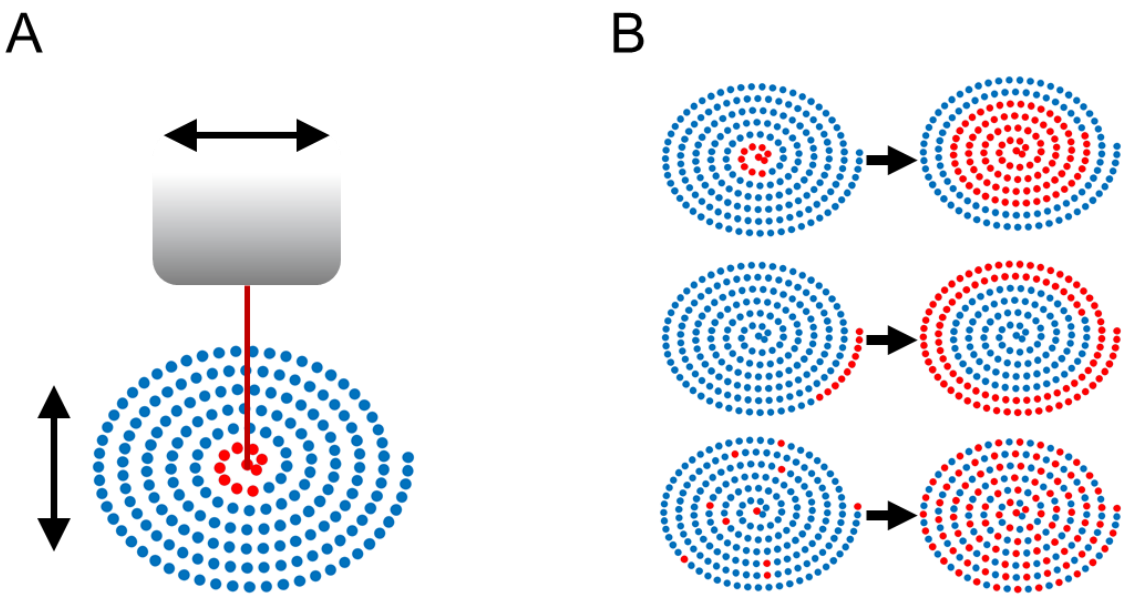

Figure 5.1: Illustration of Raster data collection and spot selection. A: Raster process in which motors are actuated in a cartesian coordinate system to move the Raman probe and SERS sensor independently, forming a spiral pattern. B: Example of 3 out 6 spot selection methods. Top, middle, and bottom, represent RS, RSS, and LSS respectively.

The common Raman dye R6G was use for characterization of all sensors. A pipette was used to evenly distribute 20 μL aqueous R6G samples, followed by 2% HCl to aid in adsorption to the silver. A single spectrum was collected at each point with a 1 second exposure time under a laser power setting of 0.365.

Recorded spectra for each point were stored independently and processed with custom scripts in MATLAB.

5.3 Results

The first goal of this work was to explore methods to highlight and reduce the impact of point to point variability within single a flexible Raman sensor. This is primarily accomplished through dense collection of data across the sensor surface through a Raster scanning approach. With dense surface sampling, it is possible to isolate the impact of various sampling scenarios, such as the number of points and objective point selection criteria.

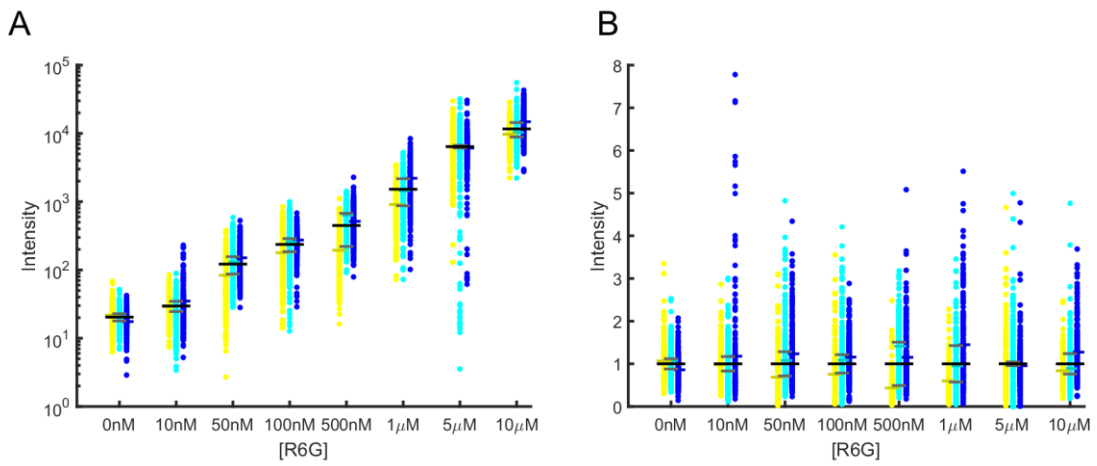

Figure 5.2: Data summary for 200 spots obtained from each of 3 sensors over 8 R6G concentrations. A & B: colors represent each of 3 sensors. Horizontal colored lines of each color represent the intra-sensor mean intensity for each sensor. Horizontal black and grey lines represent inter-sensor mean and standard deviation respectively. A: Peak intensity (Raman Shift: 1515cm^{-1}) values for background subtracted spectra plotted on a log scale. B: Peak intensity normalized to the inter-sensor mean for each concentration.

Figure 5.2 is a summary of the data collected for analysis. Eight concentrations of R6G were applied to three sensors (including a negative

control). Each set of 200 points per sensor is displayed, in addition to the intra- and inter- sensor means. Figure 5.2A displays the concentration dependent intensities on a log scale, while Figure 5.2B shows all data points normalized to the inter-sensor mean. From the normalized data it is immediately apparent that the data represents a non-normal set, skewed upwards. The inter-sensor means for each concentration are visibly distinct down to the minimum 10nM concentration. However, the variation in intensity within a single concentration is high and overlaps signals from neighboring concentration samples through multiple orders of magnitude. Robust analyses from these data require a representative sample from each sensor that cannot be acquired through few randomly chosen points.

5.3.1 Number of Spots

To determine the impact of the number of spots on concentration dependent SERS signals, the average and standard deviation was calculated over an increasing number of randomly chosen spots. Each new set of spots was objectively selected by through a random number generator in Matlab. It can be seen from Figure 5.3A that both the mean and standard deviations can vary substantially until a large enough number of spots is accumulated (around 50). Figure 5.3B expands this visually through three additional randomly chosen sets at spot numbers from 0 to 50 spots. Each sample mean and standard deviation

can differ significantly from each other and from the population mean that is achieved at large spot numbers.

The degree to which each concentration is varying from its mean was calculated as the standard error (SE) and is shown (Figure 5.4) for four runs representing 200 independent samples of 0 to 200 spots. The SE was averaged over all spots, sensors, and concentrations included in each run. SE values for each sample from the parent set range from as high as 45% to as low at 15% before settling at 18%. While concentration dependent signals become relatively stable and distinct near 50 points, the SE can be seen to vary by up to 2% or more with spot numbers less than 150 spots.

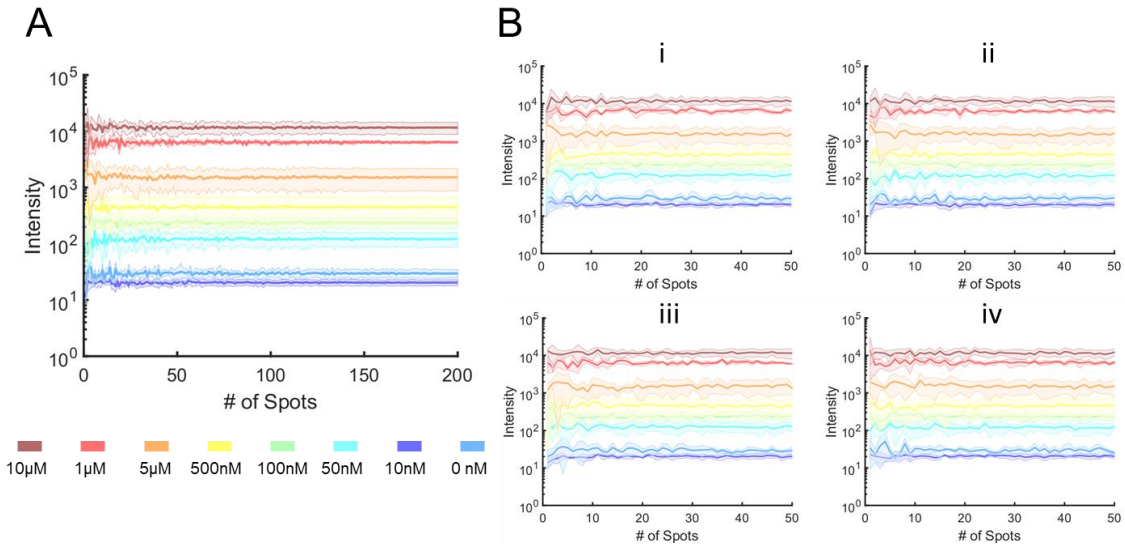

Figure 5.3: Change in concentration dependent Raman intensities based on number of spots selected via RS (random) sampling. A: Signal change over 200 independent spot selection sets, with sample spot numbers increasing from 1-200 respectively.. B: Signal variability over 50 indpendent spot selection sets with spot numbers increasing from 1 to 50 respectively. Subplots i-iv represent additional variability through additional test sets over the same spot numbers.

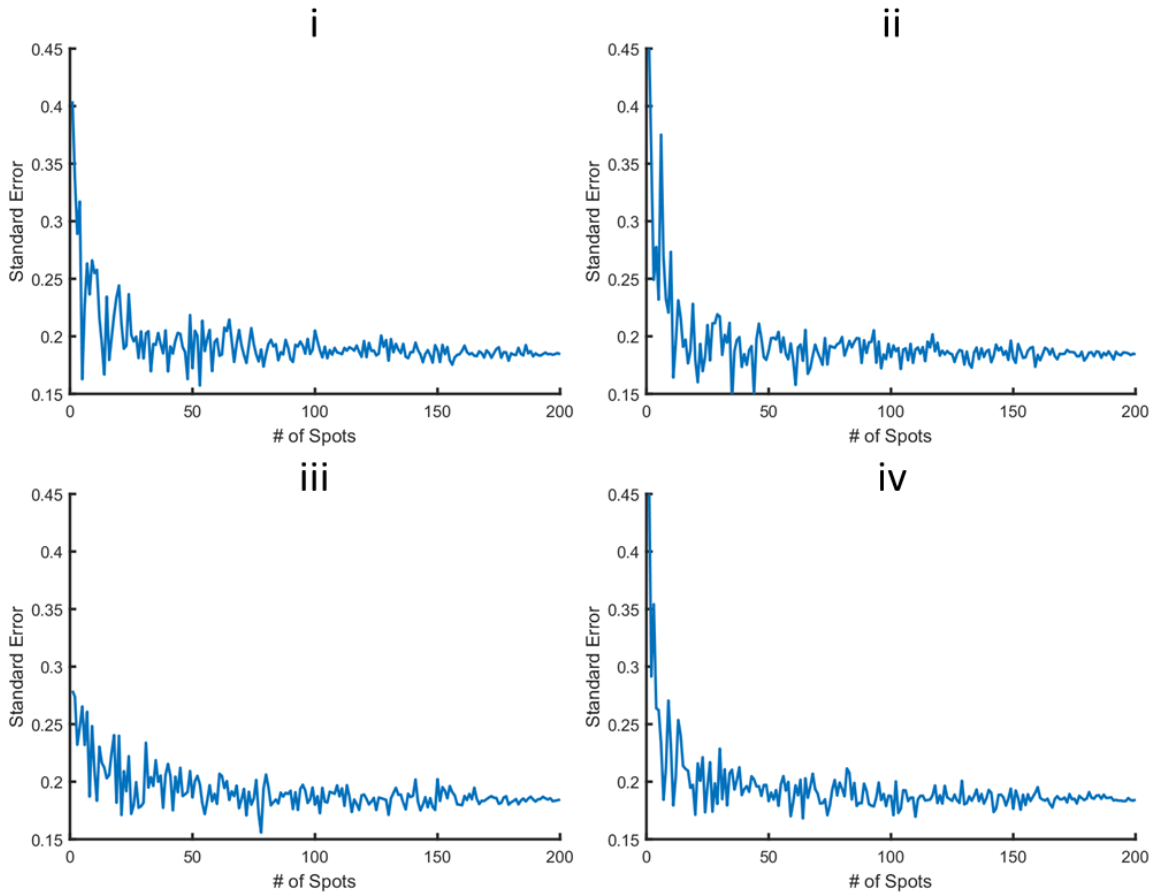

Figure 5.4: Standard error calculated as an average error over all 8 concentrations using RS (random) sampling of 1-200 spots. Subplots i-iv show four collections of independent sample sets, with each subset being an independent randomly sampled set from each sensor.

5.3.2 Spot selection criteria

Though it is common practice in SERS literature to choose "random" spots across a sensor, no work was found that evaluates the obvious potential for subjective effects. Our group and others eliminate subjectivity through the use of few, but consistent locations to minimize error; however, evidence has yet to be published that explores the impact of these sampling patterns and their fitness as a globally representative data set.

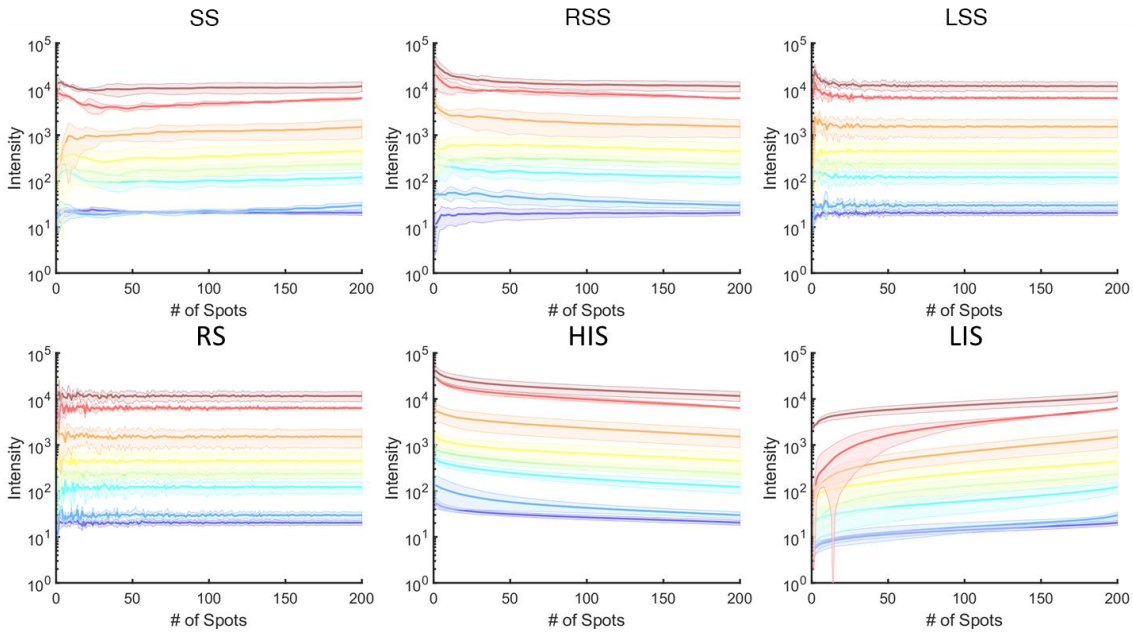

Figure 5.5: Concentration dependent signal intensities collected from an increasing sample size with 6 spot selection criteria. SS: Sequential sampling; RSS: Reverse sequential sampling; LSS: Linearly spaced sampling; RS: Random sampling; HIS: Maximum intensity sampling; LIS: Minimum intensity sampling

Figure 5.5 illustrates the impact of six spot selection algorithms on the mean SERS signal intensity for each concentration tested. Each spot selection technique is described in the methods. Each algorithm produced distinct effects on the mean, though a slow drop in the mean as the number of points increases is a common feature; the LIS method obviously produces the opposite effect.

Random spot selection (RS) produces nearly immediate convergence on the mean with significant variation depending on run and spot number. Regular spacing in chosen samples through the LSS method appears to produce some mean variation with increasing spot numbers, but variations appear generally less intense than random sampling and the sample data rapidly converges on the

population mean. Similar to the standard error of the RS method discussed above, the standard error of LSS samples drops to within 2% of the minimum 18% SE by 50 points.

As geographic selection criteria, SS and RSS produce means with complex behavior as the number of points increases. Unlike many of the other methods, the means for each concentration behave inconsistently, though they are generally able to converge on the population mean within 50 points. These effects are reflected in the standard error (Figure 5.6), that appears to show random and broad deviations from the 18% minimum during a slow convergence towards the minimum.

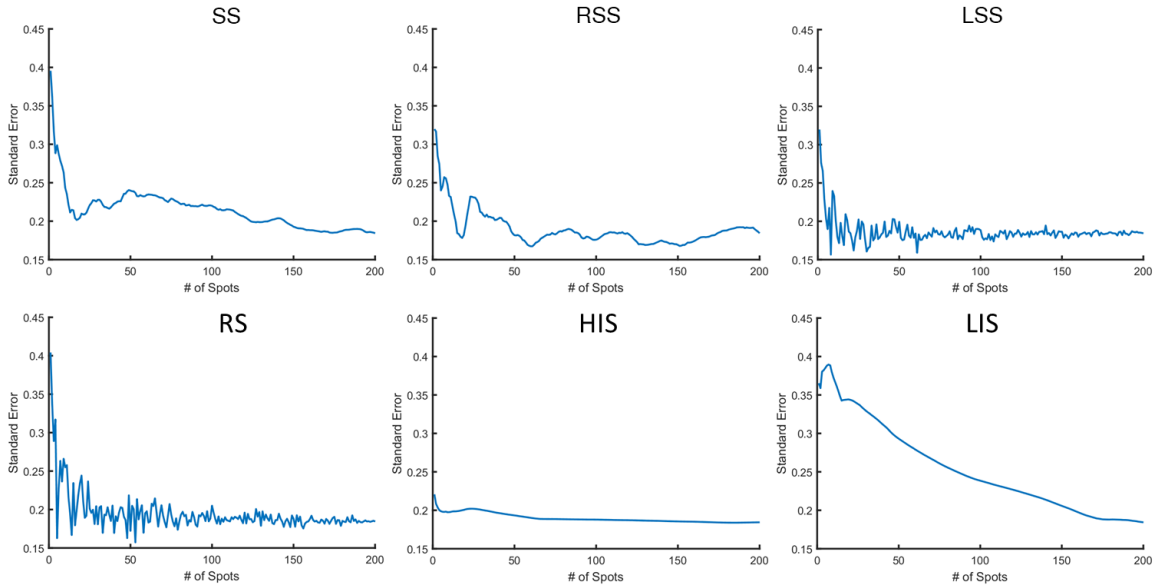

Figure 5.6: Standard error calculated as an average error over all 8 concentrations using 6 sampling criteria to generate sets of 1-200 spots.

The HIS and LIS methods produce data with somewhat expected results; interestingly, the standard deviations appear higher with the LIS method at low sample numbers. Between the tested R6G concentrations the SS and RSS methods produce the most inconsistent mean separations and occasionally produce overlapping data. Each of the other methods generally maintain consistent signal separation between concentrations. The standard error of the HIS method exhibits an almost immediate and permanent convergence on the minimum 18%. Conversely, the LIS method shows the slowest convergence rate as the number of spots increases.

5.3.3 Langmuir Fit

Adherence of Raman data to a physically relevant adsorption model helps defend the concentration dependent signals amidst varied signal intensities from inconsistent hot-spot distributions. Figure 5.7 shows the result of Langmuir fits to RS sample sets with increasing spot number. While it is possible to, again, visualize convergence of the means and reduction in the standard deviation, little disturbance in the quality of the Langmuir fit is visible. This is supported through Figure 5.8 which shows the sample size dependent change in the coefficient of determination (R^2) value, which is consistently high for all spot selection criteria with trends predictably similar to the standard error. The norm of the residuals for each Langmuir fit also exhibits similar trends.

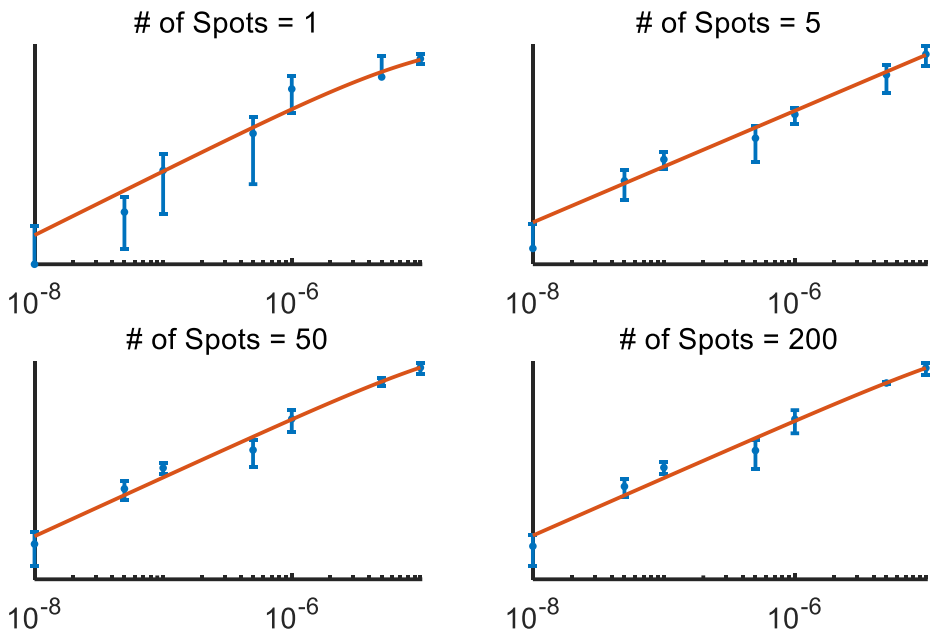

Figure 5.7: Langmuir fit to concentration dependent data from an increasing number of randomly selected points. Each of the four plots represents an independent, randomly (RS) sampled set of 1, 5, 50, or 200 spots. Both x- and y- axes are logarithmic.

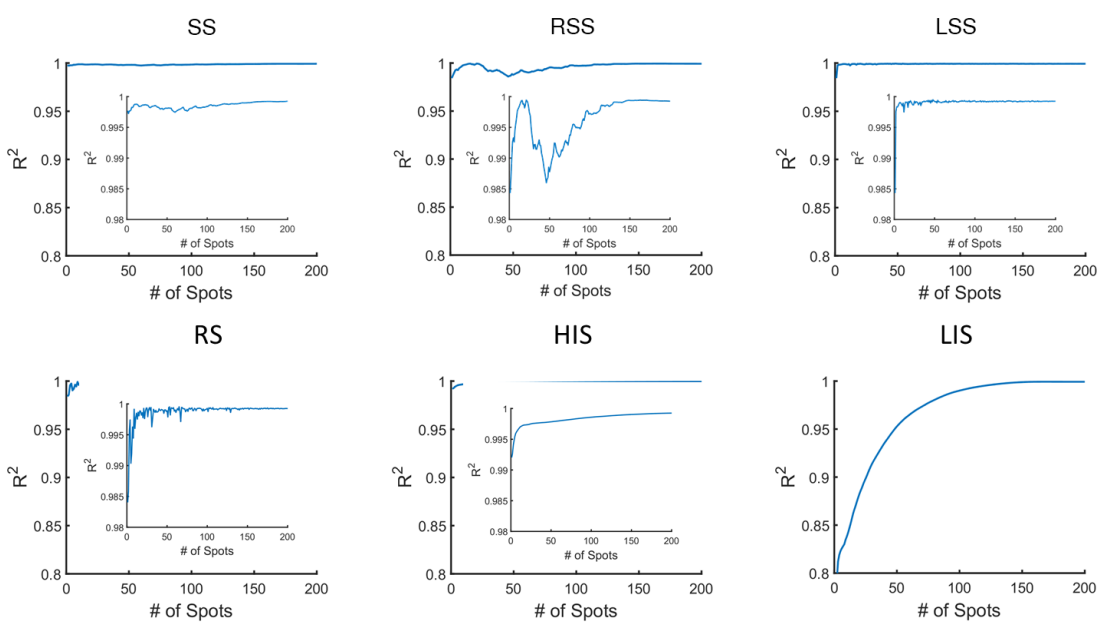

Figure 5.8: Quality of Langmuir fit calculated for an increasing number of points chosen through 6 sampling methods. Fit quality is defined as the coefficient of determination (R^2). Subplots represent a shifted y-axis representation of the parent plot.

5.4 Discussion

Development of novel SERS technologies and applications is rapidly progressing, but translation into practical sensors is rare. One of the primary hinderances in advancement of SERS as a robust technique is the reputation of poor reproducibility and quantitative potential. The push towards lower cost SERS substrates has simplified many problems, but only exacerbates the non-uniformities in SERS hot-spots that lead to inconsistent signal intensities. It is feasible that high density sampling of sensor surfaces can smooth and collectively reduce the sensor to sensor variation, but thus far little work has been done to confirm this. Instead, an arbitrary number of "random" points are commonly chosen to represent the signals across the entire sensor surface. Here we seek to utilize a single large data set as a platform to illustrate the impact of small sample size on SERS signals across a portable substrate.

The data, collectively presented in Figure 5.2, can be seen to densely pack around and below the mean with fewer, but drastically higher intensities above the mean. It is difficult to assign a single cause to the intensity distributions on a complex sensor surface, but the existence of few high intensity points supports the presence of non-uniform hot-spot generation.[6,7,15] It is assumed that, if the surface features of the sponge played a significant role (e.g. surface height), the intensity distribution would exist uniformly around the mean.

The existence of a non-normal distribution does not invalidate calculated means and, indeed, Figure 5.3 illustrates that even with a single randomly chosen point concentrations can be visibly differentiated across the tested range. However, Figure 5.4 also illustrates the danger of randomly sampling only a few spots. Below 50 points, the collective standard error begins as high as 45% but varies wildly to values well above and below the population error. It is clear that random sampling must be utilized with a sufficiently large number of points to provide reliable data. Further, these points were chosen objectively, while many groups may compound error through subjective choice of "random" spots.

Alternatives to random sampling were studied that can simplify the spot selection criteria. (see Figure 5.5) Interestingly, the most obvious sampling methods that follow the raster pattern in forward (SS) and reverse (RSS) directions provide the least predictable behavior in the means and standard deviation as spot number increases. The concentration dependent means can be seen to have inconsistent separation as the spot numbers increase, unlike the other techniques where this difference is largely consistent. This can be seen again in the standard errors (Figure 5.6), where sensor regions may create islands of high or low signals that actually disturb the coordination between intra-sensor means.

The most promising technique is the LSS method that samples the entire surface at regular intervals defined by the number of spots. While the initial standard error is high (Figure 5.6), the error rapidly converges to the minimum error. This method likely benefits from a more global approach that is not impacted by the existence of localities across the sensor surface as the increasing number of points simply increases the number of points in each locale. Though this method would still require up to 50 points to minimize error, the benefits of comprehensive surface sampling is clearly crucial to collect robust SERS data.

Of the techniques tested, the most effective sampling method to reduce error was the choice of the highest intensity points (HIS). Though the locations of the presumed hot-spots are unpredictable, their existence and signal intensities appear to be comparable between sensors. Though it is obviously necessary to sample the surface completely to discover the spots, once located these spots can provide high concentration separation and low error between sensors. With proper controls and sufficient sampling, this may be a reliable technique to increase detection limits of analytes with well-defined spectra.

With improved methods for sampling data, SERS will ideally provide a simple platform for a variety of biosensing techniques. In portable diagnostic applications, sensor readings cannot simply supply technicians with a peak intensity value, but must provide a reliable conversion to a meaningful analyte

concentration. The Langmuir isotherm provides a physically relevant model to predict the adsorption characteristics of analytes on surfaces and can be used as a fit for concentration dependent SERS data. The ability to predict adsorption, and signal intensity by extension, can provide automated conversion from a well calibrated spectrometer and sensor pair. Unfortunately, sufficiently robust procedures are necessary to obtain reproducible results.

Here we have tested the impact of spot number and choice on the quality of the Langmuir fit. Trends in the quality of the fit as the spot number increases and with the spot choice method (Figure 5.7 and Figure 5.8) largely mirror the standard error plots (Figure 5.6). Similar conclusions can therefore be drawn. Specifically, LSS is an efficient method for broad surface sampling that rapidly improves the fit parameters and therefore predictive power. The most efficient method is, again, the HIS method that utilizes the surprisingly well correlated high intensity sites in each sensor.

5.5 Conclusion

Surface enhanced Raman spectroscopy will continue to be studied as an alternative to existing lab and portable diagnostic techniques. Unfortunately, the potential reproducibility concerns with SERS largely prevent it from achieving broad success as a practical sensing method. Here we have studied methods for improving the reproducibility in SERS by establishing improved sampling

methods for portable SERS sensors. Specifically, we identified a linearly spaced sampling (LSS) method that when combined with high density sampling (50 points per sensor) provides consistent error reduction between sensors. Interestingly, comprehensive sampling allows the potential for quantification with relatively few high-intensity points that have higher means overall and drastically reduced error.

Chapter 6. Conclusion

6.1 Summary of findings

This work details the development of technologies and techniques to simplify portable biosensors and enable rapid and reliable on-site diagnostics. Specifically, this work centers around the use of surface enhanced Raman spectroscopy as a highly promising technique to simplify the hardware and technical expertise required to run complex assays and chemical analytics at the point-of-care. Current implementations of SERS in bioassays maintain inconvenient techniques that limit its readiness as a deployable alternative to existing transduction mechanisms, such as fluorescence. Specific limitations include increased numbers of steps, limited sensor functionality, and questionable reproducibility. Chapters 3-5 address each of these limitations independently and present novel solutions that advance SERS as a practical technology for portable biosensing.

Chapter 3 details the development of a novel thermoplastic device that, for the first time, allows use of SERS to quantify the output of multiplexed PCR reactions in real-time. Existing technologies require additional post-processing steps to introduce the PCR product to the SERS enhancement surface. In this work, we have developed a device that utilizes a dialysis membrane to provide size based separation of the dye liberated from a common probe based PCR

assay. The dialysis membrane was embedded in a laser cut and thermally bonded PMMA device that successfully isolated the PCR reaction well from a SERS active silver colloid. The novel vertical separation scheme introduced a unique thermal profile that was evaluated through a finite element model to ensure adequate temperature control throughout the PCR cycles. Under controlled isothermal and thermocycling conditions the membrane was then shown to allow specific passage of PCR produced free dyes, while restricting passage of unreacted PCR probes. Finally, PCR reactions were successfully run on chip allowing for the independent and simultaneous detection of multiple dyes from a single well. This method was applied to the detection of *Staphylococcus Aureus* and the drug resistance gene MecA. As a diagnostic, this technique will allow rapid identification of both species and drug resistance for pathogenic bacteria in a low-cost platform capable of simple application to the sample site.

Chapter 4 describes the development of a novel SERS substrate: PDMS sponges. These new highly customizable substrates are shown to provide flexible 3-dimensional manipulation and simple liquid handling on a complex matrix with controlled hydrophilicity. The inherently hydrophobic silicone surface provides the potential for organic phase and single step affinity separation of organic molecules. First, syringe filtration was tested as a simple demonstration of the immediate compatibility with common laboratory techniques. Using the syringe

plunger to force samples through the PDMS sponge, resulted in visible extraction of the model analyte (R6G) onto the surface of the sponge. Next, the porous and scalable nature of the sponge enables monitoring of aqueous environments through passive filtration by liquid phase extraction of small molecules into a retained organic phase within the sponge. Results show 8 and 18-fold concentration of carboxy-pyrene and R6G respectively over a 90-minute incubation. Finally, silver nanoparticles were simply dried onto the sponge surface to provide comparable SERS performance to existing flexible substrates. SERS performance was tested for the potential to detect and quantify model analytes: R6G, Malachite Green, and cPyrene.

Chapter 5 introduces a new concept for flexible SERS sensors: variance reduction through optimized spot selection criteria. The majority of methods for collecting signals across a flexible SERS substrate rely on unproven and seemingly subjective methods to select representative spots for analyte quantification. This work seeks to eliminate the subjectivity in common "random" spot selection methods and critically evaluate the impact of spot selection criteria on concentration dependent SERS signals. Using a custom rastering system built around a portable Raman spectrometer, 200 points were acquired on three sensors for each of seven concentrations of the dye R6G. Six spot selection algorithms were compared and contrasted for their independent

impacts on the intra and inter-sensor means from a single data set. The number of points used with each spot selection method was increased from a single point to the full 200 points. From these analyses, we are able to recommend that the most efficient method for collecting data from an arbitrary number of points is through a linear separation of points across the entire sensor surface. Interestingly, with a sufficiently large data set, we found that it is possible to selectively choose the highest intensity points within each sensor and effectively increase signal intensity while reducing intra-sensor variance.

6.2 Contributions to the field and potential impact

The often promised potential for SERS as a revolutionary technique has largely failed to produce a widely accepted practical sensor technology. The long history of development of SERS in both chemical and biological assays has led to many advancements that remain underutilized due to the remaining limitations in simplicity, functionality, and reproducibility in SERS technologies. This work has produced advancements in SERS techniques to address these three limitations and presents applications for their use in commercial and clinical settings.

Chapter 3 details the development of a SERS-PCR device that allows simultaneous separation and detection of the product of an ongoing reaction. This device is directly applied to improve the portability of molecular diagnostics.

However, the underlying technologies can be generalized to independently useful advancements that can be applied broadly in many academic, clinical, and commercial applications:

1. A salt and temperature stable colloid of aggregated AgNP's that are cationically modified to promote binding and enhancement of anionic polymers.
2. Immobilization and thermal sealing of a separatory membrane in a low-cost thermoplastic chip. The chip allows vertical size separation of solutes from one well to another at temperatures up to 95°C.
3. Two phase filter SERS method for quantification of analytes with colloidal SERS, while maintaining complete isolation of potentially fouling macromolecules from nanoparticles.

Chapter 4 details the development of a novel SERS substrate that enables new sample handling functionality for portable SERS assays. Specifically, nanoparticle functionalized PDMS foams are demonstrated to allow sponge-like sample acquisition and ejection as well as hydrophobic phase based separation and concentration of organic molecules. This technique is described for use as a method for quantifying the polycyclic aromatic hydrocarbon pyrene as well as the fungicide malachite green. PDMS sponges, however, present a platform for

future development based on core functionality not present in existing SERS sensors:

1. Flexible, hydrophobic material for single step isolation and concentration of arbitrary organic compounds from aqueous solutions on a sensor substrate.
2. Large volume flexible SERS sensor that allows simple fluid manipulation via sponge-like activity.
3. Soft-lithography of a SERS sensor allows formation of sensors with arbitrary, three-dimensional shapes to fit application dependent specifications.
4. Two-dimensional, cartesian Raman rastering system for automated data collection on arbitrary Raman sensors.

Chapter 5 details development and evaluation of methods to eliminate subjectivity and inconsistencies in signal acquisition from portable SERS substrates. These techniques are specifically applied to a single flexible SERS technology, but can be more broadly applied to any SERS technology. In addition to the medical and regulatory applications proposed in Chapter 5, improving the reproducibility in SERS data is an application agnostic necessity; current reproducibility concerns, prevent SERS from wide acceptance as a

practical alternative to more established techniques. The following novel observations and recommendations can improve the reproducibility, and therefore the dependability, of new SERS sensors and in academic and commercial evaluation of new SERS technologies.

1. Illustration of the increased variance from of random selection of few points across a non-uniform surface.
2. Introduction of the linearly spaced spot selection method to simultaneously minimize the number of points and inter-sensor variance.
3. Introduction of the maximum intensity sampling technique that allows simultaneous improvements in signal intensities and inter-sensor variance.

6.3 Future work

The technologies presented here establish readily accessible solutions for limitations in portable diagnostic and SERS technologies. Each individual technology also presents a platform for improvement and expansion to new applications.

Chapter 3 presents a novel method to apply SERS to PCR and allows a real-time readout with SERS for the first time. This method also successfully allows

amplification and detection of multiple genomic targets simultaneously. Unfortunately, this work presents a limited capability for quantification of the starting genome concentration. The non-linear trend that shows a slowing signal development rate as the target concentration decreases, is a crucial aspect of the device that must be evaluated in future iterations. While two diagnostically relevant MRSA genes were simultaneously detected, the multiplexing promise of SERS was not fully explored and future works should evaluate the potential to quantify many targets simultaneously. Expansion of the scope of this work beyond PCR can also simplify its translation into a portable diagnostic. The temperature requirements for PCR have a limiting effect on practical implementations in sample locations where power accessibility is a concern. Isothermal amplification methods are an appropriate next step to expand the usability of this technique. A new nuclease dependent method will be required, as existing isothermal techniques are incapable of fully digesting a fluorophore labelled probe.

Chapter 4 presents SERS Sponges, a novel flexible SERS substrate that allows improved sample handling functionality as well as simple phase based separation and concentration of organic molecules. This technology represents a promising new platform for development of new SERS applications. The work detailed in Chapter 4 focuses primarily on initial testing and performance evaluation of the

SERS sponges. Many directions are possible to continue development of SERS sponges including additional characterization, improved synthesis methods, improved functional demonstrations, and expanded applications.

Additional characterization work should explore the effect of sponge pore size on sample handling and SERS activity as well as the interactions with organic analytes and the PDMS or nanoparticle surface. The nanoparticle soaking method leads to impermanent adsorption onto the PDMS and can lead to nanoparticle loss with vigorous sample handling. A new synthesis method, based on in-situ synthesis using dimethyl formamide as both the solvent and reducing agent, has been tested but should be fully explored for the next iteration of SERS sponges.

This technology is perhaps the most promising solution for a SERS probe that integrates a SERS sensor into a Raman probe. The flexible and inorganic nature of PDMS sponges creates a dynamic substrate that can be easily refreshed for multiple uses. The relatively inert PDMS surface can be cleaned using harsh chemical that would destroy organic alternatives such as cellulose and its derivatives. The flexibility of the sponge allows simple liquid handling that can easily uptake and eject cleaning solutions.

One of the primary promises of SERS as a technique is the potential to identify arbitrary analytes through their Raman spectra. Unfortunately, the

surface dependent nature requires spontaneous interactions of the analyte with the Raman surface. The most important advancements in SERS will be exploration of the forces that drive molecule-nanoparticle interactions and leveraging those forces to expand the library of detectable analytes. This work is crucial regardless of the substrate used, but would provide unprecedented usability for the SERS sponges.

Chapter 5 describes new methods to improve the reproducibility of data collected from flexible SERS sensors. These methods were applied to a set of data for a single analyte on a single sensor type. To fully establish the impact of these techniques, work should be done to apply the recommended methods (LSS and HIS) to additional substrate types, such as the array of paper based devices. Further, the simplicity of the single component solutions used presents a starting point for evaluation of complex solutions that are closer to realistic samples. For instance, these techniques should also be evaluated for their potential to improve the reproducibility and detection limits of serum or whole blood samples that can easily obscure the signals from analytes of interest. With increasingly complex samples, future work should also evaluate the benefits of multivariate statistical approaches (e.g. partial least squares or principal component analysis) to improve discrimination of signals from complex samples.

Bibliography

1. Nayak, S., Blumenfeld, N. R., Laksanasopin, T. & Sia, S. K. Point-of-Care Diagnostics: Recent Developments in a Connected Age. *Anal. Chem.* **89,** 102–123 (2017).

2. Banerjee, R. & Humphries, R. Clinical and laboratory considerations for the rapid detection of carbapenem-resistant Enterobacteriaceae. *Virulence* **8,** 427–439 (2017).

3. Timbrook, T. T. *et al.* The Effect of Molecular Rapid Diagnostic Testing on Clinical Outcomes in Bloodstream Infections: A Systematic Review and Meta-analysis. *Clin. Infect. Dis. Off. Publ. Infect. Dis. Soc. Am.* **64,** 15–23 (2017).

4. Peeling, R. W. & Mabey, D. Point-of-care tests for diagnosing infections in the developing world. *Clin. Microbiol. Infect.* **16,** 1062–1069 (2010).

5. Jain, S. *et al.* Community-Acquired Pneumonia Requiring Hospitalization among U.S. Adults. *N. Engl. J. Med.* **373,** 415–427 (2015).

6. Drain, P. K. *et al.* Diagnostic point-of-care tests in resource-limited settings. *Lancet Infect. Dis.* **14,** 239–249 (2014).

7. Hislop, J. *et al.* Systematic review of the clinical effectiveness and cost-effectiveness of rapid point-of-care tests for the detection of genital chlamydia infection in women and men. *Health Technol. Assess. Winch. Engl.* **14,** 1–97, iii–iv (2010).

8. Zumla, A. *et al.* Rapid point of care diagnostic tests for viral and bacterial respiratory tract infections—needs, advances, and future prospects. *Lancet Infect. Dis.* **14,** 1123–1135 (2014).

9. Sano, T., Smith, C. L. & Cantor, C. R. Immuno-PCR: very sensitive antigen detection by means of specific antibody-DNA conjugates. *Science* **258,** (1992).

10. Adler, M., Wacker, R. & Niemeyer, C. M. Sensitivity by combination: immuno-PCR and related technologies. *The Analyst* **133,** 702–18 (2008).

11. Barletta, J., Bartolome, A. & Constantine, N. T. Immunomagnetic quantitative immuno-PCR for detection of less than one HIV-1 virion. *J. Virol. Methods* **157,** 122–32 (2009).

12. Niemeyer, C. M., Adler, M. & Wacker, R. Immuno-PCR: high sensitivity detection of proteins by nucleic acid amplification. *Trends Biotechnol* **23,** (2005).

13. Ikebukuro, K., Kiyohara, C. & Sode, K. Novel electrochemical sensor system for protein using the aptamers in sandwich manner. *Biosens. Bioelectron.* **20,** 2168–2172 (2005).

14. Pinto, A., Bermudo Redondo, M. C., Ozalp, V. C. & O'Sullivan, C. K. Real-time apta-PCR for 20 000-fold improvement in detection limit. *Mol. Biosyst.* **5,** 548–553 (2009).

15. Furdui, V. I. & Harrison, D. J. Immunomagnetic T cell capture from blood for PCR analysis using microfluidic systems. *Lab. Chip* **4,** 614–8 (2004).

16. Liu, P., Li, X., Greenspoon, S. A., Scherer, J. R. & Mathies, R. A. Integrated DNA purification, PCR, sample cleanup, and capillary electrophoresis microchip for forensic human identification. *Lab. Chip* **11,** 1041–8 (2011).

17. Waters, L. C. *et al.* Microchip device for cell lysis, multiplex PCR amplification, and electrophoretic sizing. *Anal. Chem.* **70,** 158–62 (1998).

18. Petralia, S. & Conoci, S. PCR Technologies for Point of Care Testing: Progress and Perspectives. *ACS Sens.* **2,** 876–891 (2017).

19. Notomi, T. *et al.* Loop-mediated isothermal amplification of DNA. *Nucleic Acids Res.* **28,** e63–e63 (2000).

20. Fu, S. *et al.* Applications of loop-mediated isothermal DNA amplification. *Appl Biochem Biotechnol* **163,** (2011).

21. Mori, Y. & Notomi, T. Loop-mediated isothermal amplification (LAMP): a rapid, accurate, and cost-effective diagnostic method for infectious diseases. *J Infect Chemother* **15,** (2009).

22. Cao, H., Fang, X., Li, H., Li, H. & Kong, J. Ultrasensitive Detection of Mucin 1 Biomarker by Immuno-Loop-Mediated Isothermal Amplification. *Talanta* doi:10.1016/j.talanta.2016.07.018

23. Hua, X. *et al.* Development of Phage Immuno-Loop-Mediated Isothermal Amplification Assays for Organophosphorus Pesticides in Agro-products. *Anal. Chem.* **86,** 8441–8447 (2014).

24. Pourhassan-Moghaddam, M. *et al.* Protein detection through different platforms of immuno-loop-mediated isothermal amplification. *Nanoscale Res. Lett.* **8,** 1–11 (2013).

25. Guatelli, J. C. *et al.* Isothermal, in vitro amplification of nucleic acids by a multienzyme reaction modeled after retroviral replication. *Proc. Natl. Acad. Sci.* **87,** 1874–1878 (1990).

26. Walker, G. T. *et al.* Strand displacement amplification--an isothermal, in vitro DNA amplification technique. *Nucleic Acids Res.* **20,** 1691–1696 (1992).

27. Jung, C., Chung, J. W., Kim, U. O., Kim, M. H. & Park, H. G. Isothermal Target and Signaling Probe Amplification Method, Based on a Combination of an Isothermal Chain Amplification Technique and a Fluorescence Resonance Energy Transfer Cycling Probe Technology. *Anal. Chem.* **82,** 5937–5943 (2010).

28. Zhang, Z. & Zhang, C. Highly Sensitive Detection of Protein with Aptamer-Based Target-Triggering Two-Stage Amplification. *Anal. Chem.* **84,** 1623–1629 (2012).

29. Zhang, L., Zhu, G. & Zhang, C. Homogeneous and Label-Free Detection of MicroRNAs Using Bifunctional Strand Displacement Amplification-Mediated Hyperbranched Rolling Circle Amplification. *Anal. Chem.* **86,** 6703–6709 (2014).

30. Ness, J. V., Ness, L. K. V. & Galas, D. J. Isothermal reactions for the amplification of oligonucleotides. *Proc. Natl. Acad. Sci.* **100,** 4504–4509 (2003).

31. Zhang, Y., Hu, J. & Zhang, C. Sensitive Detection of Transcription Factors by Isothermal Exponential Amplification-Based Colorimetric Assay. *Anal. Chem.* **84,** 9544–9549 (2012).

32. Qiu, T. *et al.* Label-free, homogeneous, and ultrasensitive detection of pathogenic bacteria based on target-triggered isothermally exponential amplification. *RSC Adv.* **6,** 62031–62037 (2016).

33. Compton, J. Nucleic acid sequence-based amplification. *Nature* **350,** 91–92 (1991).

34. Fahy, E., Kwoh, D. Y. & Gingeras, T. R. Self-sustained sequence replication (3SR): an isothermal transcription-based amplification system alternative to PCR. *Genome Res.* **1,** 25–33 (1991).

35. Tsaloglou, M.-N., Bahi, M. M., Waugh, E. M., Morgan, H. & Mowlem, M. On-chip real-time nucleic acid sequence-based amplification for RNA detection and amplification. *Anal. Methods* **3,** 2127–2133 (2011).

36. Gulliksen, A. *et al.* Parallel nanoliter detection of cancer markers using polymer microchips. *Lab. Chip* **5,** 416–420 (2005).

37. Gulliksen, A. *et al.* Real-Time Nucleic Acid Sequence-Based Amplification in Nanoliter Volumes. *Anal. Chem.* **76,** 9–14 (2004).

38. Dimov, I. K. *et al.* Integrated microfluidic tmRNA purification and real-time NASBA device for molecular diagnostics. *Lab. Chip* **8,** 2071–2078 (2008).

39. Mader, A., Riehle, U., Brandstetter, T., Stickeler, E. & Ruehe, J. Universal nucleic acid sequence-based amplification for simultaneous amplification of messengerRNAs and microRNAs. *Anal. Chim. Acta* **754,** 1–7 (2012).

40. Zhao, X., Dong, T., Yang, Z., Pires, N. & Høivik, N. Compatible immuno-NASBA LOC device for quantitative detection of waterborne pathogens: design and validation. *Lab. Chip* **12,** 602–612 (2012).

41. Vincent, M., Xu, Y. & Kong, H. Helicase-dependent isothermal DNA amplification. *EMBO Rep.* **5,** 795–800 (2004).

42. Tang, D. *et al.* Low-Cost and Highly Sensitive Immunosensing Platform for Aflatoxins Using One-Step Competitive Displacement Reaction Mode and Portable Glucometer-Based Detection. *Anal. Chem.* **86,** 11451–11458 (2014).

43. Piepenburg, O., Williams, C. H., Stemple, D. L. & Armes, N. A. DNA Detection Using Recombination Proteins. *PLOS Biol* **4,** e204 (2006).

44. Babu, B. *et al.* A rapid assay for detection of Rose rosette virus using reverse transcription-recombinase polymerase amplification using multiple gene targets. *J. Virol. Methods* **240,** 78–84 (2017).

45. Loo, J. F. C., Lau, P. M., Ho, H. P. & Kong, S. K. An aptamer-based bio-barcode assay with isothermal recombinase polymerase amplification for cytochrome-c detection and anti-cancer drug screening. *Talanta* **115,** 159–165 (2013).

46. Watanabe, H., Hayazawa, N., Inouye, Y. & Kawata, S. DFT Vibrational Calculations of Rhodamine 6G Adsorbed on Silver: Analysis of Tip-Enhanced Raman Spectroscopy. *J. Phys. Chem. B* **109,** 5012–5020 (2005).

47. Ding, S.-Y., You, E.-M., Tian, Z.-Q. & Moskovits, M. Electromagnetic theories of surface-enhanced Raman spectroscopy. *Chem. Soc. Rev.* **46,** 4042–4076 (2017).

48. Campion, A. & Kambhampati, P. Surface-enhanced Raman scattering. *Chem. Soc. Rev.* **27,** 241–250 (1998).

49. Le Ru, E. C., Blackie, E., Meyer, M. & Etchegoin, P. G. Surface Enhanced Raman Scattering Enhancement Factors: A Comprehensive Study. *J. Phys. Chem. C* **111,** 13794–13803 (2007).

50. Albrecht, M. G. & Creighton, J. A. Anomalously intense Raman spectra of pyridine at a silver electrode. *J. Am. Chem. Soc.* **99,** 5215–5217 (1977).

51. Creighton, J. A., Blatchford, C. G. & Albrecht, M. G. Plasma resonance enhancement of Raman scattering by pyridine adsorbed on silver or gold sol particles of size comparable to the excitation wavelength. *J. Chem. Soc. Faraday Trans. 2 Mol. Chem. Phys.* **75,** 790–798 (1979).

52. Fleischmann, M., Hendra, P. J. & McQuillan, A. J. Raman spectra of pyridine adsorbed at a silver electrode. *Chem. Phys. Lett.* **26,** 163–166 (1974).

53. Jeanmaire, D. L. & Van Duyne, R. P. Surface raman spectroelectrochemistry: Part I. Heterocyclic, aromatic, and aliphatic amines adsorbed on the anodized silver electrode. *J. Electroanal. Chem. Interfacial Electrochem.* **84,** 1–20 (1977).

54. Kneipp, K. *et al.* Single Molecule Detection Using Surface-Enhanced Raman Scattering (SERS). *Phys. Rev. Lett.* **78,** 1667–1670 (1997).

55. Nie, S. & Emory, S. Probing single molecules and single nanoparticles by surface-enhanced Raman scattering. *Science* **275,** 1102–1106 (1997).

56. Willets, K. A. & Van Duyne, R. P. Localized Surface Plasmon Resonance Spectroscopy and Sensing. *Annu. Rev. Phys. Chem.* **58,** 267–297 (2007).

57. Weaver, M. J., Zou, S. & Chan, H. Y. H. Peer Reviewed: The New Interfacial Ubiquity of Surface-Enhanced Raman Spectroscopy. *Anal. Chem.* **72,** 38 A–47 A (2000).

58. Haes, A. J. *et al.* Plasmonic Materials for Surface-Enhanced Sensing and Spectroscopy. *MRS Bull.* **30,** 368–375 (2005).

59. Adrian, F. J. Charge transfer effects in surface- enhanced Raman scatteringa). *J. Chem. Phys.* **77,** 5302–5314 (1982).

60. Moskovits, M. Persistent misconceptions regarding SERS. *Phys. Chem. Chem. Phys.* **15,** 5301–5311 (2013).

61. Campion, A., Ivanecky, J. E., Child, C. M. & Foster, M. On the Mechanism of Chemical Enhancement in Surface-Enhanced Raman Scattering. *J. Am. Chem. Soc.* **117,** 11807–11808 (1995).

62. Valley, N., Greeneltch, N., Van Duyne, R. P. & Schatz, G. C. A Look at the Origin and Magnitude of the Chemical Contribution to the Enhancement Mechanism of Surface-Enhanced Raman Spectroscopy (SERS): Theory and Experiment. *J. Phys. Chem. Lett.* **4,** 2599–2604 (2013).

63. Tantra, R., Brown, R. J. C. & Milton, M. J. T. Strategy to improve the reproducibility of colloidal SERS. *J. Raman Spectrosc.* **38,** 1469–1479 (2007).

64. Darby, B. L. & Le Ru, E. C. Competition between Molecular Adsorption and Diffusion: Dramatic Consequences for SERS in Colloidal Solutions. *J. Am. Chem. Soc.* **136,** 10965–10973 (2014).

65. Barmi, M. R., Andreou, C., Hoonejani, M. R., Moskovits, M. & Meinhart, C. D. Aggregation Kinetics of SERS-Active Nanoparticles in Thermally Stirred Sessile Droplets. *Langmuir* **29,** 13614–13623 (2013).

66. Guerrini, L. & Graham, D. Molecularly-mediated assemblies of plasmonic nanoparticles for Surface-Enhanced Raman Spectroscopy applications. *Chem. Soc. Rev.* **41,** 7085–7107 (2012).

67. Wu, C.-Y., Lo, W.-Y., Chiu, C.-R. & Yang, T.-S. Surface enhanced Raman spectra of oligonucleotides induced by spermine. *J. Raman Spectrosc.* **37,** 799–807 (2006).

68. Xie, Y. *et al.* Sensing of polycyclic aromatic hydrocarbons with cyclodextrin inclusion complexes on silver nanoparticles by surface-enhanced Raman scattering. *Analyst* **135,** 1389–1394 (2010).

69. Guerrini, L., Garcia-Ramos, J. V., Domingo, C. & Sanchez-Cortes, S. Sensing Polycyclic Aromatic Hydrocarbons with Dithiocarbamate-Functionalized Ag Nanoparticles by Surface-Enhanced Raman Scattering. *Anal. Chem.* **81,** 953–960 (2009).

70. Jana, N. R. & Pal, T. Anisotropic Metal Nanoparticles for Use as Surface-Enhanced Raman Substrates. *Adv. Mater.* **19,** 1761–1765 (2007).

71. Fang, Y., Seong, N.-H. & Dlott, D. D. Measurement of the Distribution of Site Enhancements in Surface-Enhanced Raman Scattering. *Science* **321,** 388–392 (2008).

72. Kwon, K. *et al.* Controlled Synthesis of Icosahedral Gold Nanoparticles and Their Surface-Enhanced Raman Scattering Property. *J. Phys. Chem. C* **111,** 1161–1165 (2007).

73. Scarabelli, L., Coronado-Puchau, M., Giner-Casares, J. J., Langer, J. & Liz-Marzán, L. M. Monodisperse Gold Nanotriangles: Size Control, Large-Scale Self-Assembly, and Performance in Surface-Enhanced Raman Scattering. *ACS Nano* **8,** 5833–5842 (2014).

74. Rodríguez-González, B., Burrows, A., Watanabe, M., Kiely, C. J. & Marzán, L. M. L. Multishell bimetallic AuAg nanoparticles: synthesis, structure and optical properties. *J. Mater. Chem.* **15,** 1755–1759 (2005).

75. Liu & Guyot-Sionnest, P. Synthesis and Optical Characterization of Au/Ag Core/Shell Nanorods. *J. Phys. Chem. B* **108,** 5882–5888 (2004).

76. Ma, W. *et al.* A SERS active gold nanostar dimer for mercury ion detection. *Chem. Commun.* **49,** 4989–4991 (2013).

77. Fan, W. *et al.* Graphene oxide and shape-controlled silver nanoparticle hybrids for ultrasensitive single-particle surface-enhanced Raman scattering (SERS) sensing. *Nanoscale* **6,** 4843–4851 (2014).

78. Zhang, Q., Large, N., Nordlander, P. & Wang, H. Porous Au Nanoparticles with Tunable Plasmon Resonances and Intense Field Enhancements for Single-Particle SERS. *J. Phys. Chem. Lett.* **5,** 370–374 (2014).

79. Abalde-Cela, S. *et al.* Surface-enhanced Raman scattering biomedical applications of plasmonic colloidal particles. *J. R. Soc. Interface* **7,** S435–S450 (2010).

80. L. Kleinman, S., R. Frontiera, R., Henry, A.-I., A. Dieringer, J. & Duyne, R. P. V. Creating, characterizing, and controlling chemistry with SERS hot spots. *Phys. Chem. Chem. Phys.* **15,** 21–36 (2013).

81. Fernanda Cardinal, M. *et al.* Expanding applications of SERS through versatile nanomaterials engineering. *Chem. Soc. Rev.* **46,** 3886–3903 (2017).

82. Sharma, B. *et al.* High-performance SERS substrates: Advances and challenges. *MRS Bull.* **38,** 615–624 (2013).

83. Li, W., Zhao, X., Yi, Z., Glushenkov, A. M. & Kong, L. Plasmonic substrates for surface enhanced Raman scattering. *Anal. Chim. Acta* **984,** 19–41 (2017).

84. Nguyen, B. H., Nguyen, V. H. & Tran, H. N. Rich variety of substrates for surface enhanced Raman spectroscopy. *Adv. Nat. Sci. Nanosci. Nanotechnol.* **7,** 033001 (2016).

85. Hong Lee, Y. *et al.* Using the Langmuir–Schaefer technique to fabricate large-area dense SERS-active Au nanoprism monolayer films. *Nanoscale* **5,** 6404–6412 (2013).

86. Abu Hatab, N. A., Oran, J. M. & Sepaniak, M. J. Surface-Enhanced Raman Spectroscopy Substrates Created via Electron Beam Lithography and Nanotransfer Printing. *ACS Nano* **2,** 377–385 (2008).

87. Dai, Z. *et al.* Obviously Angular, Cuboid-Shaped TiO2 Nanowire Arrays Decorated with Ag Nanoparticle as Ultrasensitive 3D Surface-Enhanced Raman Scattering Substrates. *J. Phys. Chem. C* **118,** 22711–22718 (2014).

88. Lee, S. Y. *et al.* Dispersion in the SERS Enhancement with Silver Nanocube Dimers. *ACS Nano* **4,** 5763–5772 (2010).

89. Brolo, A. G., Arctander, E., Gordon, R., Leathem, B. & Kavanagh, K. L. Nanohole-Enhanced Raman Scattering. *Nano Lett.* **4,** 2015–2018 (2004).

90. Yu, Q. & Golden, G. Probing the Protein Orientation on Charged Self-Assembled Monolayers on Gold Nanohole Arrays by SERS. *Langmuir* **23,** 8659–8662 (2007).

91. Yu, Q. *et al.* Surface-enhanced Raman scattering on gold quasi-3D nanostructure and 2D nanohole arrays. *Nanotechnology* **21,** 355301 (2010).

92. Yu, Q., Guan, P., Qin, D., Golden, G. & Wallace, P. M. Inverted Size-Dependence of Surface-Enhanced Raman Scattering on Gold Nanohole and Nanodisk Arrays. *Nano Lett.* **8,** 1923–1928 (2008).

93. Choi, C. J., Xu, Z., Wu, H.-Y., Liu, G. L. & Cunningham, B. T. Surface-enhanced Raman nanodomes. *Nanotechnology* **21,** 415301 (2010).

94. Sivashanmugan, K., Liao, J.-D., Liu, B. H., Yao, C.-K. & Luo, S.-C. Ag nanoclusters on ZnO nanodome array as hybrid SERS-active substrate for trace detection of malachite green. *Sens. Actuators B Chem.* **207,** 430–436 (2015).

95. Wu, H.-Y., Choi, C. J. & Cunningham, B. T. Plasmonic Nanogap-Enhanced Raman Scattering Using a Resonant Nanodome Array. *Small* **8,** 2878–2885 (2012).

96. Cole, R. M. *et al.* Understanding Plasmons in Nanoscale Voids. *Nano Lett.* **7,** 2094–2100 (2007).

97. Mahajan, S. *et al.* Relating SERS Intensity to Specific Plasmon Modes on Sphere Segment Void Surfaces. *J. Phys. Chem. C* **113,** 9284–9289 (2009).

98. Tognalli, N. G., Fainstein, A., Calvo, E. J., Abdelsalam, M. & Bartlett, P. N. Incident Wavelength Resolved Resonant SERS on Au Sphere Segment Void (SSV) Arrays. *J. Phys. Chem. C* **116,** 3414–3420 (2012).

99. Kahraman, M., Mullen, E., Korkmaz, A. & Wachsmann-Hogiu, S. Fundamentals and applications of SERS-based bioanalytical sensing. *Nanophotonics* **6,** 831–852 (2017).

100. Cinel, N. A., Bütün, S., Ertaş, G. & Özbay, E. 'Fairy Chimney'-Shaped Tandem Metamaterials as Double Resonance SERS Substrates. *Small* **9,** 531–537 (2013).

101. Vo-Dinh, T., Hiromoto, M. Y. K., Begun, G. M. & Moody, R. L. Surface-enhanced Raman spectrometry for trace organic-analysis. *Anal. Chem.* **56,** 1667–1670 (1984).

102. Lee, C. H., Tian, L. & Singamaneni, S. Paper-based SERS swab for rapid trace detection on real-world surfaces. *ACS Appl. Mater. Interfaces* **2,** 3429–35 (2010).

103. Polavarapu, L., Porta, A. L., Novikov, S. M., Coronado-Puchau, M. & Liz-Marzán, L. M. Pen-on-Paper Approach Toward the Design of Universal Surface Enhanced Raman Scattering Substrates. *Small* **10,** 3065–3071 (2014).

104. Brayner, R. *et al.* Surface-Enhanced Raman Scattering on Silver Nanostructured Films Prepared by Spray-Deposition. *Langmuir* **26,** 17465–17469 (2010).

105. Li, B., Zhang, W., Chen, L. & Lin, B. A fast and low-cost spray method for prototyping and depositing surface-enhanced Raman scattering arrays on microfluidic paper based device. *ELECTROPHORESIS* **34,** 2162–2168 (2013).

106. Qu, L.-L. *et al.* Fabrication of bimetallic microfluidic surface-enhanced Raman scattering sensors on paper by screen printing. *Anal. Chim. Acta* **792,** 86–92 (2013).

107. Qu, L.-L. *et al.* Batch fabrication of disposable screen printed SERS arrays. *Lab. Chip* **12,** 876–881 (2012).

108. Wu, W. *et al.* Low-Cost, Disposable, Flexible and Highly Reproducible Screen Printed SERS Substrates for the Detection of Various Chemicals. *Sci. Rep.* **5,** srep10208 (2015).

109. Hoppmann, E. P., Yu, W. W. & White, I. M. Inkjet-Printed Fluidic Paper Devices for Chemical and Biological Analytics Using Surface Enhanced Raman spectroscopy. *IEEE J. Sel. Top. Quantum Electron.* **20,** 7300510–7300510 (2014).

110. Hoppmann, E. P., Yu, W. W. & White, I. M. Highly sensitive and flexible inkjet printed SERS sensors on paper. *Methods* **63,** 219–224 (2013).

111. W. Yu, W. & M. White, I. Inkjet-printed paper-based SERS dipsticks and swabs for trace chemical detection. *Analyst* **138,** 1020–1025 (2013).

112. Yu, W. W. & White, I. M. Inkjet printed surface enhanced Raman spectroscopy array on cellulose paper. *Anal. Chem.* **82,** 9626–9630 (2010).

113. Zhu, Y., Li, M., Yu, D. & Yang, L. A novel paper rag as 'D-SERS' substrate for detection of pesticide residues at various peels. *Talanta* **128,** 117–124 (2014).

114. Cheng, M.-L., Tsai, B.-C. & Yang, J. Silver nanoparticle-treated filter paper as a highly sensitive surface-enhanced Raman scattering (SERS) substrate for detection of tyrosine in aqueous solution. *Anal. Chim. Acta* **708,** 89–96 (2011).

115. Laserna, J. J., Campiglia, A. D. & Winefordner, J. D. Surface-enhanced Raman spectrometry on a silver-coated filter paper substrate. *Anal. Chim. Acta* **208,** 21–30 (1988).

116. Hoppmann, E. P., Yu, W. W. & White, I. M. Detection of deoxyribonucleic acid (DNA) targets using polymerase chain reaction (PCR)

and paper surface-enhanced Raman spectroscopy (SERS) chromatography. *Appl. Spectrosc.* **68,** 909–915 (2014).

117. W. Yu, W. & M. White, I. Chromatographic separation and detection of target analytes from complex samples using inkjet printed SERS substrates. *Analyst* **138,** 3679–3686 (2013).

118. Chen, J. *et al.* Flexible and Adhesive Surface Enhance Raman Scattering Active Tape for Rapid Detection of Pesticide Residues in Fruits and Vegetables. *Anal. Chem.* **88,** 2149–2155 (2016).

119. Kahraman, M., Daggumati, P., Kurtulus, O., Seker, E. & Wachsmann-Hogiu, S. Fabrication and Characterization of Flexible and Tunable Plasmonic Nanostructures. *Sci. Rep.* **3,** srep03396 (2013).

120. P. Singh, J., Chu, H., Abell, J., A. Tripp, R. & Zhao, Y. Flexible and mechanical strain resistant large area SERS active substrates. *Nanoscale* **4,** 3410–3414 (2012).

121. J. Chung, A., Suk Huh, Y. & Erickson, D. Large area flexible SERS active substrates using engineered nanostructures. *Nanoscale* **3,** 2903–2908 (2011).

122. Shiohara, A., Langer, J., Polavarapu, L. & Liz-Marzán, L. M. Solution processed polydimethylsiloxane/gold nanostar flexible substrates for plasmonic sensing. *Nanoscale* **6,** 9817–9823 (2014).

123. Alexander, K. D., Skinner, K., Zhang, S., Wei, H. & Lopez, R. Tunable SERS in Gold Nanorod Dimers through Strain Control on an Elastomeric Substrate. *Nano Lett.* **10,** 4488–4493 (2010).

124. J. Natan, M. Concluding Remarks Surface enhanced Raman scattering. *Faraday Discuss.* **132,** 321–328 (2006).

125. M. Jarvis, R. *et al.* Towards quantitatively reproducible substrates for SERS. *Analyst* **133,** 1449–1452 (2008).

126. Sackmann, M. & Materny, A. Surface enhanced Raman scattering (SERS)—a quantitative analytical tool? *J. Raman Spectrosc.* **37,** 305–310 (2006).

127. Erol, M. *et al.* SERS Not To Be Taken for Granted in the Presence of Oxygen. *J. Am. Chem. Soc.* **131,** 7480–7481 (2009).

128. Laurence, T. A., Braun, G. B., Reich, N. O. & Moskovits, M. Robust SERS Enhancement Factor Statistics Using Rotational Correlation Spectroscopy. *Nano Lett.* **12,** 2912–2917 (2012).

129. He, D., Hu, B., Yao, Q.-F., Wang, K. & Yu, S.-H. Large-Scale Synthesis of Flexible Free-Standing SERS Substrates with High Sensitivity: Electrospun PVA Nanofibers Embedded with Controlled Alignment of Silver Nanoparticles. *ACS Nano* **3,** 3993–4002 (2009).

130. Berger, A. G., Restaino, S. M. & White, I. M. Vertical-flow paper SERS system for therapeutic drug monitoring of flucytosine in serum. *Anal. Chim. Acta* **949,** 59–66 (2017).

131. Andreou, C., Hoonejani, M. R., Barmi, M. R., Moskovits, M. & Meinhart, C. D. Rapid Detection of Drugs of Abuse in Saliva Using Surface Enhanced Raman Spectroscopy and Microfluidics. *ACS Nano* **7,** 7157–7164 (2013).

132. Westley, C. *et al.* Absolute Quantification of Uric Acid in Human Urine Using Surface Enhanced Raman Scattering with the Standard Addition Method. *Anal. Chem.* **89,** 2472–2477 (2017).

133. Kneipp, K. *et al.* Detection and identification of a single DNA base molecule using surface-enhanced Raman scattering (SERS). *Phys. Rev. E* **57,** R6281–R6284 (1998).

134. Han, X. X., Zhao, B. & Ozaki, Y. Surface-enhanced Raman scattering for protein detection. *Anal. Bioanal. Chem.* **394,** 1719–1727 (2009).

135. Premasiri, W. R. *et al.* Characterization of the surface enhanced raman scattering (SERS) of bacteria. *J. Phys. Chem. B* **109,** 312–20 (2005).

136. Gracie, K. *et al.* Simultaneous detection and quantification of three bacterial meningitis pathogens by SERS. *Chem. Sci.* **5,** 1030–1040 (2014).

137. van Lierop, D., Faulds, K. & Graham, D. Separation Free DNA Detection Using Surface Enhanced Raman Scattering. *Anal. Chem.* **83,** 5817–5821 (2011).

138. Faulds, K., Jarvis, R., Smith, W. E., Graham, D. & Goodacre, R. Multiplexed Detection of Six Labelled Oligonucleotides Using Surface Enhanced Resonance Raman Scattering (SERRS). *Analyst* **133,** 1505–1512 (2008).

139. Harper, M. M., Robertson, B., Ricketts, A. & Faulds, K. Specific detection of DNA through coupling of a TaqMan assay with surface enhanced Raman scattering (SERS). *Chem. Commun.* **48,** 9412–9414 (2012).

140. Cao, Y. C., Jin, R. & Mirkin, C. A. Nanoparticles with Raman spectroscopic fingerprints for DNA and RNA detection. *Science* **297,** 1536–1540 (2002).

141. Yoo, S. M. *et al.* Combining a Nanowire SERRS Sensor and a Target Recycling Reaction for Ultrasensitive and Multiplex Identification of Pathogenic Fungi. *Small* **7,** 3371–3376 (2011).

142. Ye, S., Guo, Y., Xiao, J. & Zhang, S. A sensitive SERS assay of l-histidine via a DNAzyme-activated target recycling cascade amplification strategy. *Chem. Commun.* **49,** 3643–3645 (2013).

143. Lin, H.-Y. *et al.* On-line SERS Detection of Single Bacterium Using Novel SERS Nanoprobes and A Microfluidic Dielectrophoresis Device. *Small* **10,** 4700–4710 (2014).

144. Wang, Y. *et al.* Duplex Microfluidic SERS Detection of Pathogen Antigens with Nanoyeast Single-Chain Variable Fragments. *Anal. Chem.* **86,** 9930–9938 (2014).

145. Gao, R. *et al.* Fast and sensitive detection of an anthrax biomarker using SERS-based solenoid microfluidic sensor. *Biosens. Bioelectron.* **72,** 230–236 (2015).

146. Inzaule, S. C. *et al.* Affordable HIV drug-resistance testing for monitoring of antiretroviral therapy in sub-Saharan Africa. *Lancet Infect. Dis.* **16,** e267–e275 (2016).

147. Medalla, F. *et al.* Estimated Incidence of Antimicrobial Drug–Resistant Nontyphoidal Salmonella Infections, United States, 2004–2012. *Emerg. Infect. Dis.* **23,** 29–37 (2017).

148. M. Koo, K., H. Wee, E. J., Wang, Y. & Trau, M. Enabling miniaturised personalised diagnostics: from lab-on-a-chip to lab-in-a-drop. *Lab. Chip* **17,** 3200–3220 (2017).

149. Yazdi, S. H. & White, I. M. Multiplexed detection of aquaculture fungicides using a pump-free optofluidic SERS microsystem. *The Analyst* **138,** 100–103 (2013).

150. Andreou, C., Mirsafavi, R., Moskovits, M. & D. Meinhart, C. Detection of low concentrations of ampicillin in milk. *Analyst* **140,** 5003–5005 (2015).

151. Jaworska, A., Fornasaro, S., Sergo, V. & Bonifacio, A. Potential of Surface Enhanced Raman Spectroscopy (SERS) in Therapeutic Drug Monitoring (TDM). A Critical Review. *Biosensors* **6,** 47 (2016).

152. Jarvis, R. M. & Goodacre, R. Discrimination of bacteria using surface-enhanced Raman spectroscopy. *Anal. Chem.* **76,** 40–7 (2004).

153. Penn, M. A., Drake, D. M. & Driskell, J. D. Accelerated surface-enhanced Raman spectroscopy (SERS)-based immunoassay on a gold-plated membrane. *Anal. Chem.* **85,** 8609–17 (2013).

154. Song, C. *et al.* Highly sensitive immunoassay based on Raman reporter-labeled immuno-Au aggregates and SERS-active immune substrate. *Biosens. Bioelectron.* **25,** 826–31 (2009).

155. Lounsbury, J. A., Poe, B. L., Do, M. & Landers, J. P. Laser-ablated poly(methyl methacrylate) microdevices for sub-microliter DNA amplification suitable for micro-total analysis systems. *J. Micromechanics Microengineering* **22,** 085006 (2012).

156. Klank, H., P. Kutter, J. & Geschke, O. CO 2 -laser micromachining and back-end processing for rapid production of PMMA-based microfluidic systems. *Lab. Chip* **2,** 242–246 (2002).

157. Faulds, K., Smith, W. E. & Graham, D. Evaluation of surface-enhanced resonance Raman scattering for quantitative DNA analysis. *Anal. Chem.* **76,** 412–7 (2004).

158. Perozziello, G. *et al.* A microfluidic dialysis device for complex biological mixture SERS analysis. *Microelectron. Eng.* **144,** 37–41 (2015).

159. Scrimgeour, J., Kyu Cho, J., Breedveld, V. & Curtis, J. Microfluidic dialysis cell for characterization of macromolecule interactions. *Soft Matter* **7,** 4762–4767 (2011).

160. Christensen, T. B. *et al.* PCR biocompatibility of lab-on-a-chip and MEMS materials. *J. Micromechanics Microengineering* **17,** 1527 (2007).

161. Kodzius, R. *et al.* Inhibitory effect of common microfluidic materials on PCR outcome. *Sens. Actuators B Chem.* **161,** 349–358 (2012).

162. Cao, Y. C., Jin, R. & Mirkin, C. A. Nanoparticles with Raman Spectroscopic Fingerprints for DNA and RNA Detection. *Science* **297,** 1536–1540 (2002).

163. Moskovits, M. Surface roughness and the enhanced intensity of Raman scattering by molecules adsorbed on metals. *J Chem Phys* **69,** 4159–4161 (1978).

164. Qu, L.-L. *et al.* Batch fabrication of disposable screen printed SERS arrays. *Lab. Chip* **12,** 876–881 (2012).

165. Walsh, R. J. & Chumanov, G. Silver Coated Porous Alumina as a New Substrate for Surface-Enhanced Raman Scattering. *Appl. Spectrosc.* **55,** 1695–1700 (2001).

166. Qu, L.-L., Geng, Y.-Y., Bao, Z.-N., Riaz, S. & Li, H. Silver nanoparticles on cotton swabs for improved surface-enhanced Raman scattering, and its application to the detection of carbaryl. *Microchim. Acta* **183,** 1307–1313 (2016).

167. Gong, Z. *et al.* Fabrication of SERS Swab for Direct Detection of Trace Explosives in Fingerprints. *ACS Appl. Mater. Interfaces* **6,** 21931–21937 (2014).

168. Kumar, S., Goel, P. & Singh, J. P. Flexible and robust SERS active substrates for conformal rapid detection of pesticide residues from fruits. *Sens. Actuators B Chem.* **241,** 577–583 (2017).

169. W. Yu, W. & M. White, I. A simple filter-based approach to surface enhanced Raman spectroscopy for trace chemical detection. *Analyst* **137,** 1168–1173 (2012).

170. Choi, S.-J. *et al.* A Polydimethylsiloxane (PDMS) Sponge for the Selective Absorption of Oil from Water. *ACS Appl. Mater. Interfaces* **3,** 4552–4556 (2011).

171. Kim, K.-H., Jahan, S. A., Kabir, E. & Brown, R. J. C. A review of airborne polycyclic aromatic hydrocarbons (PAHs) and their human health effects. *Environ. Int.* **60,** 71–80 (2013).

172. Péron, O., Rinnert, E., Lehaitre, M., Crassous, P. & Compère, C. Detection of polycyclic aromatic hydrocarbon (PAH) compounds in artificial sea-water using surface-enhanced Raman scattering (SERS). *Talanta* **79,** 199–204 (2009).

173. Xie, Y. *et al.* Selective SERS detection of each polycyclic aromatic hydrocarbon (PAH) in a mixture of five kinds of PAHs. *J. Raman Spectrosc.* **42,** 945–950 (2011).

174. Samanta, S. K., Singh, O. V. & Jain, R. K. Polycyclic aromatic hydrocarbons: environmental pollution and bioremediation. *Trends Biotechnol.* **20,** 243–248 (2002).

175. Boffetta, P., Jourenkova, N. & Gustavsson, P. Cancer risk from occupational and environmental exposure to polycyclic aromatic hydrocarbons. *Cancer Causes Control CCC* **8,** 444–472 (1997).

176. Restaino, S. M., Berger, A. & White, I. M. Inkjet-Printed Paper Fluidic Devices for Onsite Detection of Antibiotics Using Surface-Enhanced Raman Spectroscopy. in *Biosensors and Biodetection* (eds. Prickril, B. & Rasooly, A.) **2,** 525–540 (Springer New York, 2017).

177. Luellen, D. R. & Shea, D. Calibration and Field Verification of Semipermeable Membrane Devices for Measuring Polycyclic Aromatic Hydrocarbons in Water. *Environ. Sci. Technol.* **36,** 1791–1797 (2002).

178. Fisk, H., Westley, C., Turner, N. J. & Goodacre, R. Achieving optimal SERS through enhanced experimental design. *J. Raman Spectrosc.* **47,** 59–66 (2016).

179. Marks, H., Schechinger, M., Garza, J., Locke, A. & Coté, G. Surface enhanced Raman spectroscopy (SERS) for in vitro diagnostic testing at the point of care. *Nanophotonics* **6,** 681–701 (2017).

180. Restaino, S. M., Berger, A. & White, I. M. Inkjet-printed paper fluidic devices for onsite detection of antibiotics using surface-enhanced Raman spectroscopy. in *Biosensors and Biodetection: Methods and Protocols* (eds. Rasooly, A. & Prickril, B.) (Springer, In Press).

181. Lucht, S., Murphy, T., Schmidt, H. & Kronfeldt, H.-D. Optimized recipe for sol–gel-based SERS substrates. *J. Raman Spectrosc.* **31,** 1017–1022 (2000).

182. Olson, L. G., Uibel, R. H. & Harris, J. M. C18-Modified Metal-Colloid Substrates for Surface-Enhanced Raman Detection of Trace-Level Polycyclic Aromatic Hydrocarbons in Aqueous Solution. *Appl. Spectrosc.* **58,** 1394–1400 (2004).

183. Tessier, P. M. *et al.* On-Line Spectroscopic Characterization of Sodium Cyanide with Nanostructured Gold Surface-Enhanced Raman Spectroscopy Substrates. *Appl. Spectrosc.* **56,** 1524–1530 (2002).